

RUTHENIUM K-EDGE X-RAY ABSORPTION SPECTROSCOPY
STUDIES OF RUTHENIUM COMPLEXES
RELEVANT TO OLEFIN METATHESIS

by

KENDRA JOYCE GETTY

A THESIS SUBMITTED IN PARTIAL FULFILLMENT
OF THE REQUIREMENTS FOR THE DEGREE OF

MASTER OF SCIENCE

in

THE FACULTY OF GRADUATE STUDIES
(Chemistry)

THE UNIVERSITY OF BRITISH COLUMBIA
(Vancouver)

April 2008

© Kendra Joyce Getty, 2008

ABSTRACT

Despite previous extensive study of the widely-employed ruthenium-catalysed olefin metathesis reaction, the finer mechanistic details have not been elucidated. An area that is noticeably lacking is spectroscopic exploration of the relevant complexes. In this work, organometallic ruthenium complexes of importance to olefin metathesis have been investigated using Ru K-edge X-ray absorption spectroscopy. The lowest energy feature in the Ru K-edge spectrum has been unambiguously assigned as due to Ru $4d \leftarrow 1s$ transitions. These electric-dipole-forbidden transitions are extremely sensitive to geometry. For centrosymmetric complexes, the pre-edge feature has very low intensity because it is limited by the weak electric quadrupole mechanism. By contrast, non-centrosymmetric complexes exhibit a substantial increase in pre-edge intensity because Ru $5p$ - $4d$ mixing introduces electric-dipole-allowed character to the Ru $4d \leftarrow 1s$ transitions. The energy of the edge feature in the Ru K-edge spectrum corresponds to ionisation of $1s$ electrons and is a good indicator of the charge on the metal centre. Unexpectedly, we found that the first-generation ($L = \text{PCy}_3$) Grubbs precatalyst (**1**) has a higher $1s$ ionisation energy than the second-generation ($L = \text{H}_2\text{IMes}$) complex (**2**). This effect provides a compelling rationale for the unexplained differences in phosphine dissociation kinetics for complexes **1** and **2**: the phosphine dissociation rate of **2** is slower than **1** because the metal centre is more electron-deficient in **2**. Density functional theory calculations confirm the charge differences and offer some insight into the nature of bonding in these complexes, particularly with regard to the N-heterocyclic carbene and trialkylphosphine ligands. On the basis of these results, we propose that, for this system, the NHC ligand is a weaker σ -charge donor than the phosphine ligand, and that the NHC accepts significant π -electron density from the metal; both interactions function to reduce the electron density on the ruthenium centre. An ultimate goal is to investigate reactive species in the olefin metathesis mechanism; accordingly, we have made considerable progress toward collecting XAS data for a metallacyclobutane species, and we are pursuing methods to trap the four-coordinate intermediate in the metathesis cycle.

TABLE OF CONTENTS

ABSTRACT	ii
TABLE OF CONTENTS	iii
LIST OF TABLES	vi
LIST OF FIGURES	vii
LIST OF SCHEMES	ix
LIST OF CHARTS	x
LIST OF EQUATIONS	xi
LIST OF SYMBOLS & ABBREVIATIONS	xii
ACKNOWLEDGEMENTS	xiv
DEDICATION	xvii
CO-AUTHORSHIP STATEMENT	xviii
CHAPTER 1: INTRODUCTION	1
1.1. Objectives and Scope	1
1.2. Olefin Metathesis	2
1.2.1. Description	2
1.2.2. Applications.....	4
1.2.3. Historical Perspective	6
1.2.4. First-Generation Ruthenium-Benzylidene Complexes and Olefin Metathesis Mechanism	8
1.2.5. Second-Generation Ruthenium-Benzylidene Complexes	11
1.2.6. Bispyridine Ruthenium-Benzylidene Complexes	12
1.2.7. Heppert Carbide Complexes.....	13
1.2.8. Piers Phosponium-Alkylidene Complexes.....	14
1.2.9. Four-Coordinate Intermediate.....	15
1.2.10. Olefin-Bound Intermediate.....	17
1.2.11. Ruthenacyclobutane Structure.....	19
1.2.12. Theoretical and Spectroscopic Investigations of Grubbs Complexes	20
1.3. Phosphine and N-Heterocyclic Carbene Ligands.....	23
1.3.1. Phosphine Ligands.....	23
1.3.2. N-Heterocyclic Carbene Ligands	26
1.4. X-ray Absorption Spectroscopy	32
1.4.1. General Information.....	32
1.4.2. Transition Metal K-Edge X-ray Absorption Near-Edge Structure.....	34
1.4.3. Extended X-ray Absorption Fine Structure	37
1.4.4. Experimental Set-up.....	41
1.4.5. Data Reduction and Analysis.....	42
1.5. Conclusion.....	46
1.6. References	47
CHAPTER 2: BISPYRIDINE RUTHENIUM BENZYLIDENE SYNTHESIS	52
2.1. Introduction.....	52

2.2. Results and Discussion	54
2.3. Conclusions	63
2.4. Experimental	63
2.4.1. General Considerations	63
2.4.2. Materials	64
2.4.3. [(PCy ₃)(py) ₂ (Cl) ₂ Ru=CHPh] (7)	64
2.4.4. [(PCy ₃)(3-Br-py) ₂ (Cl) ₂ Ru=CHPh] (9)	65
2.4.5. [(PCy ₃)(3-NO ₂ -py) ₂ (Cl) ₂ Ru=CHPh] (11)	66
2.4.6. [(PCy ₃)(4-OMe-py) ₂ (Cl) ₂ Ru=CHPh] (13)	66
2.4.7. [(H ₂ IMes)(py) ₂ (Cl) ₂ Ru=CHPh] (8)	67
2.4.8. [(H ₂ IMes)(3-Br-py) ₂ (Cl) ₂ Ru=CHPh] (10)	68
2.4.9. [(H ₂ IMes)(3-NO ₂ -py) ₂ (Cl) ₂ Ru=CHPh] (12)	68
2.4.10. [(H ₂ IMes)(4-OMe-py) ₂ (Cl) ₂ Ru=CHPh] (14)	69
2.4.11. Monopyridine Analogue	70
2.5. References	71
CHAPTER 3: PRE-EDGE FEATURES	72
3.1. Introduction	72
3.2. Results and Discussion	75
3.3. Conclusions	81
3.4. Experimental	82
3.4.1. General Considerations	82
3.4.2. Materials	82
3.4.3. XAS Sample Preparation	82
3.4.4. XAS Data Acquisition	83
3.4.5. XAS Data Processing and Analysis	84
3.5. References	88
CHAPTER 4: EDGE FEATURES	90
4.1. Introduction	90
4.2. Results and Discussion	95
4.3. Conclusions	108
4.4. Experimental	108
4.5. References	109
CHAPTER 5: CONCLUSIONS AND RECOMMENDATIONS	111
5.1. References	115
APPENDIX 1. METALLACYCLOBUTANE STRUCTURE	116
Appendix 1.1. Introduction	116
Appendix 1.2. Results and Discussion	117
A1.2.1. Synthesis in Dichloromethane	117
A1.2.2. Synthesis in Other Solvents	121
A1.2.3. Photodegradation in the X-ray Beam	123
Appendix 1.3. Conclusions	125
Appendix 1.4. Experimental	126

A1.4.1. General Considerations.....	126
A1.4.2. Materials.....	126
A1.4.3. Representative Synthesis of Complex 15 in Dichloromethane	126
A1.4.4. Synthesis of Complex 15 in Dibromomethane	127
A1.4.5. XAS Sample Preparation of Complex 15	127
A1.4.6. XAS Data Acquisition	128
A1.4.7. XAS Data Processing.....	128
Appendix 1.5. References.....	129
APPENDIX 2. INVESTIGATIONS OF LOW-TEMPERATURE REACTIONS WITH CO	130
APPENDIX 3. COMPUTATIONAL DETAILS	133
Appendix 3.1. References.....	134

LIST OF TABLES

Table 1.1	Structural properties and the EXAFS parameters that they affect.....	39
Table 1.2	Calculated and refined parameters in the EXAFS fitting routine	45
Table 2.1	Hammett substituent constants, benzylidene ¹ H NMR signals, and PCy ₃ ³¹ P NMR signals for complexes 7-14	56
Table 3.1	Complexes 1-14 with coordination number, approximate symmetry, pre-edge feature area and pre-edge energy position.....	76
Table 3.2	Initial motor configuration on SSRL beamline 7-3.....	84
Table 3.3	Results from least-squares fitting of pre-edge and edge features	87
Table 4.1	Experimental data for complexes containing L = PCy ₃ or L = H ₂ IMes	91
Table 4.2	Experimental olefin metathesis activity data for complexes 1 and 2	94
Table 4.3	Experimental pre-edge energies, ionisation energies, and DFT-calculated ruthenium charges for complexes 1-14	98
Table 4.4	Density functional computational results for complexes 1 and 2	106

LIST OF FIGURES

Figure 1.1	Approximate number of publications each year of the forty-year history of olefin metathesis with an inset showing the distribution of document types.....	5
Figure 1.2	Steric and electronic properties of phosphine ligands.....	24
Figure 1.3	XAS spectrum depicting XANES and EXAFS regions	34
Figure 1.4	Transition metal XAS spectrum with XANES region expanded (inset)	35
Figure 1.5	XANES region transitions and spectral features.....	37
Figure 1.6	Scattering interference and transition metal XAS spectrum with EXAFS region expanded (inset).....	38
Figure 1.7	Basic XAS experimental set-up.....	42
Figure 1.8	EXAFS data processing: spline function (A), k^3 -space (B) and R -space (B) plots	44
Figure 2.1	^1H NMR spectra of first-generation bispyridine ruthenium-benzylidene complexes.....	58
Figure 2.2	^1H NMR spectra of second-generation bispyridine ruthenium-benzylidene complexes.....	59
Figure 2.3	^1H NMR spectra of mixtures of bispyridine complex 10 and its monopyridine analogue before (A) and after (B) treatment under vacuum with an expanded view of the benzylidene region (inset)	61
Figure 3.1	Ru K-edge XAS spectra for first-generation complexes 1 , 3 , 5 , and 7 with pre-edge feature expanded (inset).....	77
Figure 3.2	Ru K-edge XAS spectra for second-generation complexes 2 , 4 , 6 , and 8 with pre-edge feature expanded (inset).....	77
Figure 3.3	Ru K-edge XAS spectra for first-generation bispyridine complexes 7 , 9 , 11 , and 13 with pre-edge feature expanded (inset)	78
Figure 3.4	Ru K-edge XAS spectra for second-generation bispyridine complexes 8 , 10 , 12 , and 14 with pre-edge feature expanded (inset)	78
Figure 3.5	Ru K-edge XAS experimental data and fit for complex 2	86
Figure 4.1	Near-edge Ru K-edge XAS spectra, fits to the data, and second-derivatives of the data (inset) for complexes 1 (L = PCy ₃) and 2 (L = H ₂ IMes).....	97
Figure 4.2	Near-edge Ru K-edge XAS spectra for complexes 3 (L = PCy ₃) and 4 (L = H ₂ IMes).....	99
Figure 4.3	Near-edge Ru K-edge XAS spectra for complexes 5 (L = PCy ₃) and 6 (L = H ₂ IMes)	99
Figure 4.4	Near-edge Ru K-edge XAS spectra for complexes 7 (L = PCy ₃) and 8 (L = H ₂ IMes).....	100
Figure 4.5	Near-edge Ru K-edge XAS spectra for complexes 9 (L = PCy ₃) and 10 (L = H ₂ IMes).....	100
Figure 4.6	Near-edge Ru K-edge XAS spectra for complexes 11 (L = PCy ₃) and 12 (L = H ₂ IMes).....	101

Figure 4.7	Near-edge Ru K-edge XAS spectra for complexes 13 (L = PCy ₃) and 14 (L = H ₂ IMes).....	101
Figure 4.8	Cl K-edge and Ru L _{2,3} -edge XAS spectra (A) and a rescaled view of the Ru L _{2,3} -edge XAS spectra (B) for complexes 1 and 2	103
Figure 4.9	Extended energy region of Ru K-edge XAS spectra for complexes 1 to 14	105
Figure A1.1	Ru K-edge XAS spectra of four separate samples of complex 15	120
Figure A1.2	XANES region of the Ru K-edge XAS spectra of complex 15 for six consecutive sweeps with pre-edge feature expanded (inset).....	124
Figure A1.3	EXAFS region of the Ru K-edge XAS spectra of complex 15 for six consecutive sweeps with oscillations expanded (inset)	124
Figure A2.1	NMR spectra of reaction of complex 1 and CO(g) with an expanded view of the benzylidene region (inset).....	124

LIST OF SCHEMES

Scheme 1.1	Chauvin's non-pair-wise mechanism illustrating productive cross-metathesis.....	7
Scheme 1.2	Generally-accepted olefin metathesis mechanism for ruthenium carbenes.....	11
Scheme 1.3	Synthesis of the bispyridine ruthenium-benzylidene complexes	13
Scheme 1.4	Synthesis of the Heppert carbide complexes	14
Scheme 1.5	Synthesis of the Piers phosphonium-alkylidene complexes.....	15
Scheme 1.6	Portion of olefin metathesis mechanism for cis- and trans-bound olefin pathways.....	18
Scheme 1.7	Synthesis of ruthenacyclobutane complex	19
Scheme 2.1	Synthesis of bispyridine ruthenium-benzylidene complexes by Grubbs and coworkers.....	52
Scheme 3.1	Ruthenium complexes listed in order of increasing pre-edge intensity	79
Scheme A1.1	Synthesis of ruthenacyclobutane complex	116

LIST OF CHARTS

Chart 1.1	Principal olefin metathesis reactions	2
Chart 1.2	List of complexes included in this work	3
Chart 1.3	Important complexes in the development of olefin metathesis	8
Chart 1.4	Four-coordinate intermediates and their analogues.....	17
Chart 1.5	Ruthenium-carbene complexes that have been studied spectroscopically.....	22
Chart 1.6	A variety of common N-heterocyclic carbenes.....	27
Chart 1.7	Electronic properties of N-heterocyclic carbene ligands	29
Chart 1.8	Experimental design from the Bielawski group.....	30
Chart 2.1	Bispyridine ruthenium-benzylidene complexes synthesised in this work	55
Chart 3.1	Complexes investigated in this study	74
Chart 4.1	List of complexes included in this study	94

LIST OF EQUATIONS

Equation 1.1 EXAFS single-scattering equation	39
Equation 1.2 Photoelectron wavenumber, k	40
Equation 1.3 Oscillatory fine structure, $\chi(E)$	44
Equation 3.1 Pre-edge: Voigt Amplitude Function.....	85
Equation 3.2 Ionisation edge: Cumulative Gaussian/Lorentzian Function	85

LIST OF SYMBOLS & ABBREVIATIONS

-	minus; covalent bond
=	equals; double bond
±	plus or minus
~	approximately
% V_{bur}	percent buried volume
←	to (indicates transition)
α	bonded atom designation
β	bonded atom designation
δ	chemical shift in ppm (NMR)
$\delta_a(k)$	absorber phase shift functions (EXAFS)
Δ	change in
ϵ_r	dielectric constant
σ	Hammett substituent constant
σ_i^2	mean-square deviation in R_i (EXAFS)
μ	absorption; dipole moment, D
$\mu(E)$	total absorption coefficient (XAS)
$\mu_0(E)$	smooth atomic background (spline function; XAS)
ν	frequency
θ	ligand cone angle in degrees
$\chi(E)$	chi = oscillatory fine structure (EXAFS)
$\lambda(k)$	photoelectron mean free path function (EXAFS)
$\phi(k)$	total EXAFS phase shift function (EXAFS)
$\psi_i(k)$	scatterer phase shift functions (EXAFS)
$A_i(k)$	backscattering amplitude function (EXAFS)
Ad	adamantyl group
ADMET	acyclic diene metathesis polymerisation
Anal.	Analysis
av	average
BDE	bond dissociation energies
BP86	Vosko-Wilk-Nusair local density approximation with exchange (Becke) and correlation (Perdew) corrections
br	broad signal
Calcd	calculated
CM	cross metathesis
cm^{-1}	wavenumber(s)
cod	cyclooctadiene
Cy	cyclohexyl group
d; d	doublet (NMR); deuterium labelling (NMR solvents)
D	Debye (dipole moment units)
DFT	density functional theory
e	elementary charge
eV	electronvolt(s)
E	incident photon energy (XAS)
E_0	ionisation (threshold) energy (XAS; see also I/E)
EXAFS	extended X-ray absorption fine structure
Fc	ferrocene
FEFF	ab initio code (EXAFS)
$f_i(k)$	EXAFS amplitude function (EXAFS)
h	Planck's constant
\hbar	$h/2\pi$

H ₂ Mes	1,3-bis(2,4,6-trimethylphenyl)-4,5-dihydroimidazol-2-ylidene
ΔH_{rxn}	heat of reaction
I_0	incident light
I_1	transmitted light (after sample; XAS)
I_2	transmitted light (after reference; XAS)
IE_{1s}	ionisation energy of 1s electrons
IFEFFIT	command line program (EXAFS)
IMes	1,3-bis(2,4,6-trimethylphenyl)-imidazol-2-ylidene
IR	infrared
J	coupling constant (NMR)
k	rate constant; force constant; photoelectron wavenumber
L	ligand
m	multiplet (NMR)
M	metal
MDC	multipole derived charges (DFT)
m_e	mass of the photoelectron
Me	methyl group
Mes	2,4,6-trimethylphenyl; mesityl group
min.	minute(s)
MLCT	Metal-to-ligand charge transfer
Mik	Mulliken (DFT)
N_i	number of atom i scatterers (EXAFS)
NHC	N-heterocyclic carbene
NMR	nuclear magnetic resonance
OTf	triflate anion = CF_3SO_3^-
PeakFit	software for fitting data
Ph	phenyl group
Pr	2,6-diisopropylphenyl
pK_a	-log of the acid dissociation constant
py	pyridine group
q	charge (on a metal centre)
R	generic ligand group; interatomic distance
R_i	absorber-backscatterer distance for atom i (EXAFS)
rel	relative
RCM	ring-closing metathesis
ROM	ring-opening metathesis
ROMP	ring-opening metathesis polymerisation
s	singlet (NMR)
S_0^2	total amplitude reduction factor (EXAFS)
$S_i(k)$	amplitude reduction function (EXAFS)
SIXPack	graphical user interface for XAS data processing and analysis
SSRL	Stanford Synchrotron Radiation Laboratory
STO	Slater-type orbital (DFT)
t	triplet (NMR)
^t Bu	<i>tert</i> -butyl group
Tol	4-methylphenyl (<i>p</i> -tolyl group)
TZP	triple zeta basis set with an additional set of polarization functions (DFT)
UBC	University of British Columbia
UV	ultra-violet
Vis	visible
XANES	X-ray absorption near-edge structure
XAS	X-ray absorption spectroscopy
Z	atomic number (atom identity for EXAFS)

ACKNOWLEDGEMENTS

First and foremost, I would like to express my sincere gratitude to Pierre for being a wonderful supervisor. Thank you for your guidance and for always having time to discuss our science as well as any other topic whether it be teaching, careers, personal issues, politics, or current events. Your support has been paramount in my experience as a graduate student.

Being a part of the Kennepohl group has been a great experience and I appreciate the time spent (which is substantial during beamtime!) with past and present group members: Mario, Vlad, Anusha, Alison, Chelsea, Stephanie, Max, Charles, Craig, Chris, Danielle, and Thamy. I am grateful to have worked so closely with Mario who has patiently explained concepts and diligently worked on our joint projects. Our common interests in learning new things and in skepticism have made for some very intriguing discussions! I especially want to thank Anusha for always helping me out in the lab and Vlad for trying to make sure I didn't work too hard! There are also plenty of little things for which to thank you guys, but above all, I thank you for your friendship.

I thank Prof. Warren Piers and his group at the University of Calgary for providing complexes **3**, **4**, **5** and **6** as part of our collaboration and for hosting me in Calgary. Special thanks to Patricio Romero and Edwin van der Eide for providing some samples of complex **15** and instruction on its synthesis.

I would like to express my appreciation to the staff at the Stanford Synchrotron Radiation Laboratory (SSRL) for technical and scientific support during data collection. Special thanks to Dr. Serena DeBeer George (SSRL) for

her assistance. I am grateful to Dr. Sam Webb (SSRL) for his help with the SIXPack software.

I thank Rob Thompson for teaching me valuable glove box and Schlenk line techniques. Thanks to Amy Douglas and Tim Kelly for miscellaneous equipment and supplies as well as for their friendship. I am grateful to Prof. Jennifer Love for helpful discussions during the course of this work. I also thank her group members for letting me use their glove box when mine was not working and for useful tips on various issues. I acknowledge Prof. Robert H. Grubbs for his interest in this work and for constructive comments.

I appreciate all of the hard work of the UBC Chemistry Department staff in the main office and all the shops and services. Your support was invaluable in success of my work. I especially thank the NMR staff for answering the phone on the weekend! I have had the pleasure of interacting with numerous faculty members as a student in their courses, on committees, through CGSS activities, and socially; all of which have been very rewarding.

For me, a major benefit of graduate school was participating in extracurricular activities and workshops. I am thankful to all the people I have been fortunate to meet through the Chemistry Graduate Student Society, Let's Talk Science, the Chemistry Department Safety Committee, and the Centre for Teaching and Academic Growth. I would like to express my gratitude to Sophia Nussbaum and Anka Lekhi for the positive impact they've had on my teaching skills.

From my undergraduate education, I owe thanks to numerous people; most notably, at the University of Saskatchewan: Prof. Bernie Kraatz, Roberta Šilerová, Jason Maley, Samuel Gyepi-Garbrah, Marian Landl, and, at Umeå University: Prof. Lage Pettersson, Ingegärd Andersson, and Andràs Gorzsàs.

I am indebted to my grandparents, parents, siblings, other family, and friends from around the world. Although their impact has been less direct, it is an essential part of my happiness and success. Special recognition to my sister and best-friend, Alana, for always saying the right thing to keep me motivated.

This research is funded by NSERC (Canada). Start-up funds and infrastructure support were provided by UBC. Portions of this research were carried out at SSRL, a national user facility operated by Stanford University on behalf of the United States Department of Energy, Office of Basic Energy Sciences. The SSRL Structural Molecular Biology Program is supported by the Department of Energy, Office of Biological and Environmental Research, and by the National Institutes of Health, National Center for Research Resources, Biomedical Technology Program.

To Jonathan

You show me what this life is for

CO-AUTHORSHIP STATEMENT

Pierre Kennepohl identified and designed the research program. The XAS data were collected by me or other members of the Kennepohl research group. As part of our collaboration with Warren Piers (University of Calgary), Edwin van der Eide taught me how to synthesise and prepare XAS samples of the ruthenacyclobutane (**15**); he helped me synthesise one batch and I synthesised the other samples. I synthesised all of the bispyridine ruthenium-benzylidene complexes, except for one batch of all eight complexes that was synthesised by Charles Au and Max Liu (summer students; University of British Columbia). I collected and analysed all of the NMR data. Minaz Lakha (University of British Columbia) performed the elemental analysis. I analysed all of the XAS data. Mario Ulises Delgado-Jaime performed all of the theoretical calculations. I wrote all of the chapters of this thesis with input from Pierre Kennepohl and Mario Ulises Delgado-Jaime.

CHAPTER 1: INTRODUCTION

1.1. Objectives and Scope

The goal of this work was to investigate the geometric and electronic structure of complexes relevant to ruthenium-catalysed olefin metathesis. Ru K-edge X-ray absorption spectroscopy (XAS) was the primary tool used.

Chapter 1 provides the background for understanding the work described in this thesis and its purposes. In Section 1.2, the olefin metathesis reaction and its history are described, which is followed by a review of research related to the geometric and electronic structure of ruthenium complexes relevant to olefin metathesis. Important to the work in this thesis is the role of the spectator L ligand where L = N-heterocyclic carbene or phosphine ligand; thus, Section 1.3 highlights the steric and electronic properties of these ligands as well as methods employed to measure those properties. Section 1.4 introduces the XAS technique and its application as a tool for the investigation of inorganic systems.

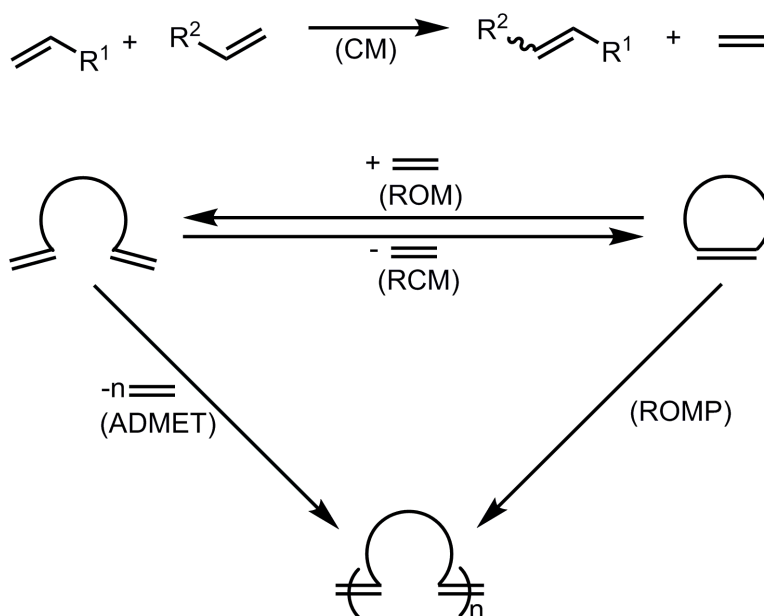
Chapter 2 describes the synthesis and characterisation of eight bispyridine ruthenium-benzylidene complexes (**7-14**). Chapter 3 explains the information gained from the pre-edge features in the Ru K-edge XAS spectra of complexes **1-14**. Chapter 4 highlights the ionisation edge features in the Ru K-edge XAS spectra of complexes **1-14**. Chapter 5 provides a conclusion of the work herein and considers future directions in this area. Appendix 1 describes the synthesis and preliminary XAS studies of the ruthenacyclobutane complex (**15**). Appendix 2 contains some initial work on reactions with small molecules.

1.2. Olefin Metathesis

1.2.1. Description

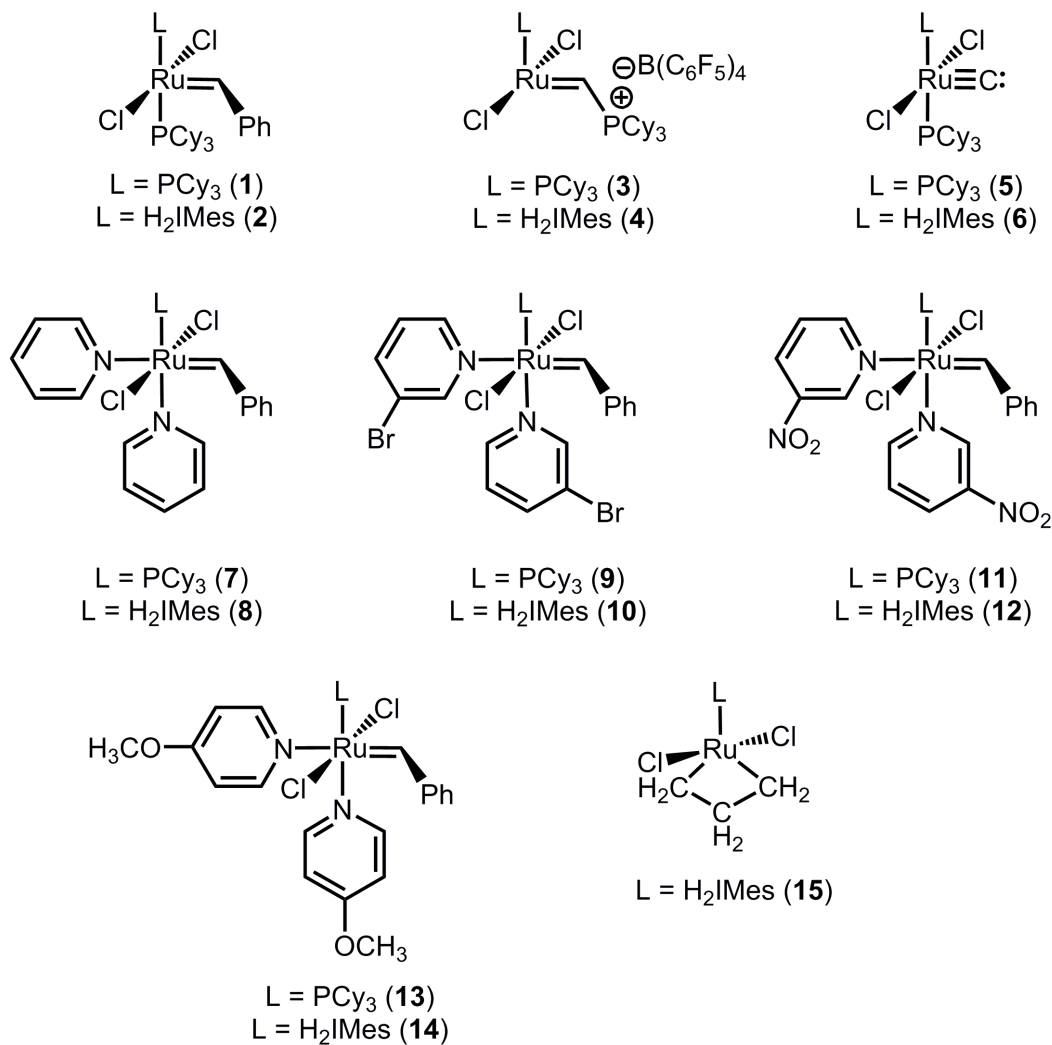
Olefin metathesis is an example of the rearrangement of carbon-carbon double bonds. Organometallic complexes catalyse this reaction, which can replace numerous traditional organic synthesis steps and generate new synthetic approaches. Several review articles and books relating to various aspects of olefin metathesis have recently been published.¹⁻⁵ There are a number of different types of metathesis (Chart 1.1); for example, cross metathesis (CM), ring-closing metathesis (RCM), ring-opening metathesis (ROM), ring-opening metathesis polymerisation (ROMP), and acyclic diene metathesis polymerisation (ADMET).² Despite the considerably different products of these reactions, each has the common feature of reorganising the olefinic bonds.

Chart 1.1 Principal olefin metathesis reactions



Grubbs-type ruthenium-carbene complexes are some of the most important olefin metathesis catalysts. For this work, fifteen ruthenium complexes of relevance to olefin metathesis were studied (Chart 1.2).

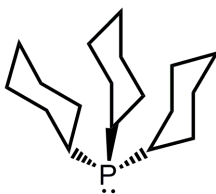
Chart 1.2 List of complexes included in this work



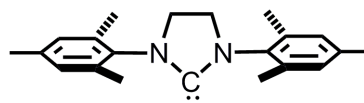
Where:



Ph = phenyl



PCy_3 = tricyclohexylphosphine



H_2IMes =
 1,3-bis(2,4,6-trimethylphenyl)-
 4,5-dihydroimidazol-2-ylidene

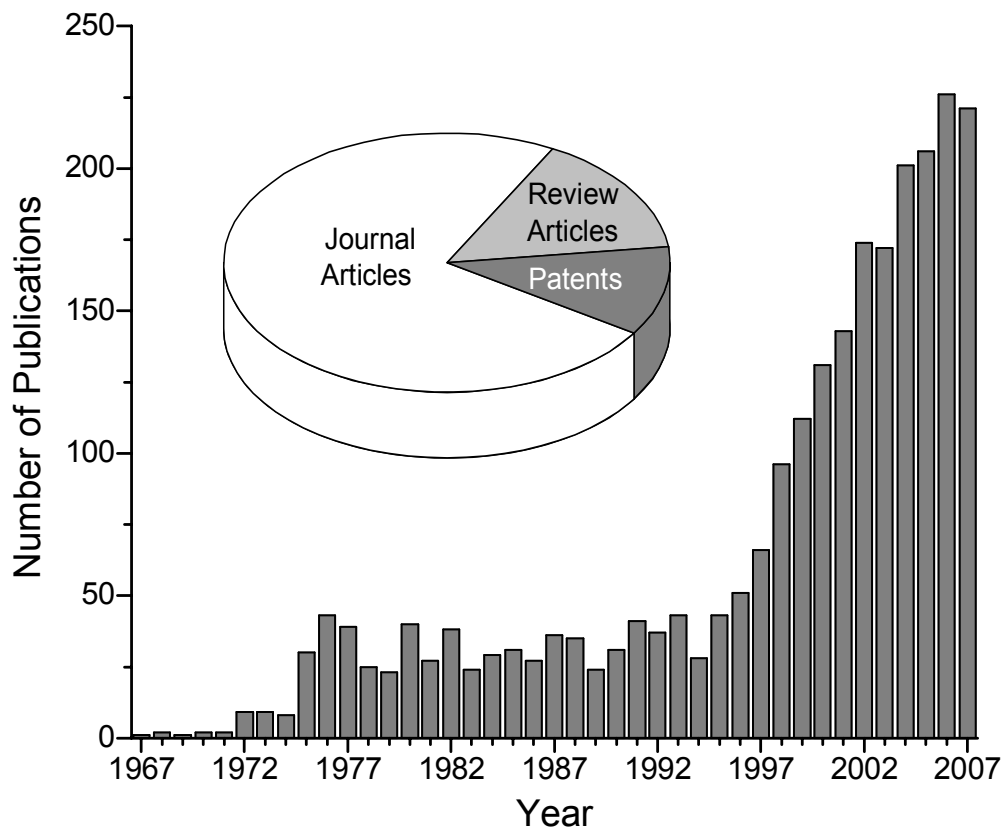
1.2.2. Applications

Olefin metathesis has become a widespread, versatile carbon-carbon bond-forming method with numerous applications. The importance of this reaction was recognised in 2005 when the Nobel Prize in Chemistry was awarded to Yves Chauvin, Robert Grubbs and Richard Schrock “for the development of the metathesis method in organic synthesis”.⁶ Metathesis catalysts are used to create bonds that would otherwise require several synthetic steps to achieve; this allows the synthesis of high-molecular-weight, highly-functionalised natural products.⁷ For this reason, large-scale synthesis of pharmaceuticals is being pursued: Boehringer-Ingelheim Pharmaceuticals has employed ruthenium-carbene catalysts for the ring-closing metathesis of a promising Hepatitis C medication.^{8,9} The viability of interesting polymer and materials applications of ruthenium catalysts has been investigated, such as self-healing polymers,^{10,11} catenanes and rotaxanes,¹²⁻¹⁴ and photolithography patterning.¹⁵ Recently, olefin metathesis has even been explored as a tool in inorganic synthesis.¹⁶ These applications exemplify the diverse potential of olefin metathesis, a field under intense continuing research and development. A simple literature search* for the term “olefin metathesis” results in over 2500 hits. The

* The literature search was performed with SciFinder Scholar 2007 on January 5, 2008 using CAPLUS and MEDLINE. The search phrase "olefin metathesis" was entered and duplicates were removed. The results were then analysed to establish the approximate number of references per year and in the categories of journal articles, review articles and patents. Other types of references include dissertations, books, and meeting abstracts. At the time of the literature search, not all of the publications for 2007 were entered in the database; therefore, the actual number is expected to be larger for that year. This information is provided as a qualitative description of the increasing importance of olefin metathesis and is not intended for quantitative analysis.

number of publications per year has risen substantially over the 40 year history of olefin metathesis with a more rapid increase since the mid-1990s (Figure 1.1).

Figure 1.1 Approximate number of publications each year of the forty-year history of olefin metathesis with an inset showing the distribution of document types



1.2.3. Historical Perspective

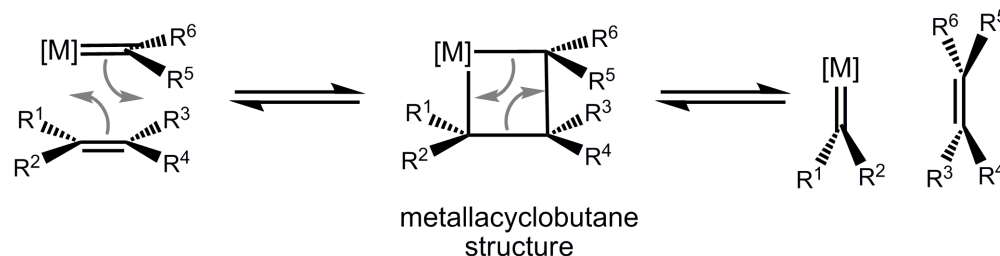
Ziegler's unexpected observations of metal-catalysed olefin polymerisation played an integral role in the development of olefin metathesis and the field of organometallic chemistry.^{1,5} The first olefin metathesis reactions were performed by Ziegler catalysts: early-transition-metal salts with main-group alkylating agents. One of the first reports came from Truett in 1960 and described an "unusual ring opening reaction" using norbornene and $\text{TiCl}_4/\text{LiAlR}_4$.¹⁷ Natta's group investigated several transition metals as Ziegler catalysts to achieve ring opening polymerisation and found that polymer stereochemistry changed with different catalysts.^{18,19} At around the same time, Fischer discovered the first isolable metal-carbon double-bonded complexes (metal carbenes) with tungsten (**16**; Chart 1.3);²⁰ however, the connection between this class of complexes and olefin metathesis was not yet known.

Over the next few years, Calderon and coworkers developed metathesis-catalysed systems and made important contributions to the mechanistic studies; most notably, they established that the reaction involved the cleavage of carbon-carbon double bonds.^{21,22} This led to several similar mechanistic proposals, all of which suggested a pair-wise interaction of carbon atoms in the intermediate steps.^{23,24} In 1971, in an effort to explain incompatible results, Chauvin and coworkers proposed a mechanism involving a [2+2] cycloaddition of an olefin to a transition metal alkylidene[†] to form a metallacyclobutane intermediate (Scheme

[†] The terms "carbene" and "alkylidene" are often used interchangeably and can be considered synonyms in this thesis. E.O. Fischer isolated the first metal-carbon double-bonded complexes, which were subsequently called "Fischer carbenes". These are characterised by a singlet-state

1.1),²⁵ which can then break apart to give the original species (non-productive) or a new olefin and metal alkylidene (productive). Katz also proposed this type of non-pair-wise mechanism and was able to further rationalise inconsistent observations.²⁶ Studies by Grubbs and Katz and their coworkers offered additional support for this mechanism,²⁷⁻²⁹ and it remains the generally-accepted mechanism today.

Scheme 1.1 Chauvin's non-pair-wise mechanism illustrating productive cross-metathesis



The Chauvin mechanism suggested that metal-carbene complexes may catalyse the reaction;⁵ at the time, the only known metal-carbene species were low-oxidation-state Fischer-type complexes such as pentacarbonyl (methoxyphenylmethylene)tungsten²⁰ (**16**; Chart 1.3). This and a related pentacarbonyl (diphenylmethylene)tungsten compound³⁰ were investigated³¹⁻³³ and shown to catalyse olefin metathesis although the activity was quite low.⁴

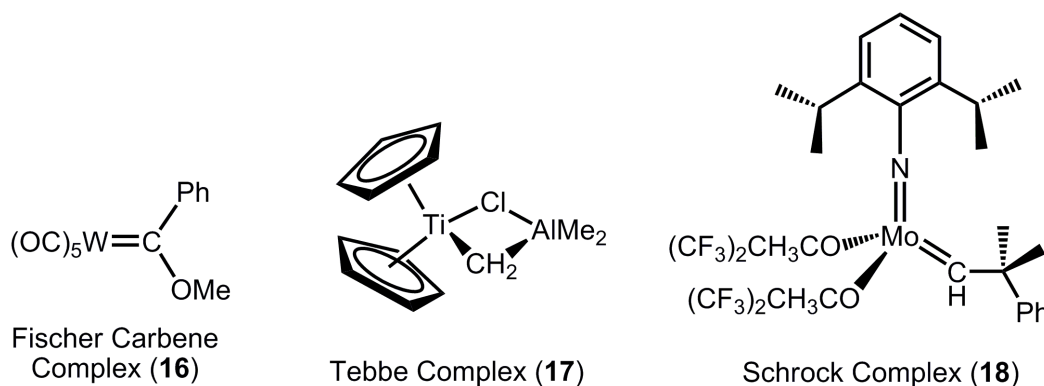
With the improved understanding of the mechanism, rational catalyst design of metal-carbene complexes led to better-defined catalytic systems. The titanium based Tebbe catalyst (**17**; Chart 1.3)³⁴ was not very active, but proved

carbene carbon bonded to a heteroatom; they react as electrophiles. R. R. Schrock discovered different types of metal-carbon double-bonded complexes, which are often referred to as "Schrock alkylidenes" (or carbenes); these are triplet-state carbene carbons that are not bonded to a heteroatom and react as nucleophiles. Because some carbenes do not behave strictly as nucleophiles or electrophiles, the distinction is not always clear.

useful for mechanistic investigations because it was possible to isolate the metallacycle.³⁵

Schrock and coworkers introduced tantalum and later tungsten and molybdenum catalysts;^{36,37} one of the most successful of these complexes is a four-coordinate molybdenum alkylidene³⁸⁻⁴¹ (**18**; Chart 1.3). The higher oxidation state complexes showed much greater activity, performed several new types of metathesis reactions and had higher stereoselectivity with certain ligand environments than known catalysts.^{1,39,40} These complexes are sensitive to air, moisture and some functional groups, making them somewhat difficult to use;^{1,39,40} limitations that were improved by ruthenium-based catalysts (see Sections 1.2.4 & 1.2.5).

Chart 1.3 Important complexes in the development of olefin metathesis



1.2.4. First-Generation Ruthenium-Benzylidene Complexes and Olefin

Metathesis Mechanism

Ruthenium halides for strained olefin polymerisation had been used in the mid-1960s,⁴² and, with this in mind, Grubbs and coworkers began using ruthenium to catalyse olefin metathesis in the late 1980s. They found that ruthenium(II) was very active and they highlighted key benefits of late-transition-

metal complexes: they have greater environmental and functional group stability than early transition metals.^{43,44} Because ruthenium(II) is a softer Lewis acid than the high-oxidation-state early transition metals, it prefers softer Lewis bases, which provides ruthenium complexes with greater selectivity for olefins over other functional groups. These properties allow ruthenium complexes to be handled in air and used with highly-functionalised molecules in a range of solvents. The Grubbs group went on to develop the 16-electron, five-coordinate ruthenium(II) carbenes with the general formula: $(PR_3)_2X_2Ru=CHR'$. These complexes have a simpler synthetic preparation than previously isolated tungsten and molybdenum catalysts.^{45,46}

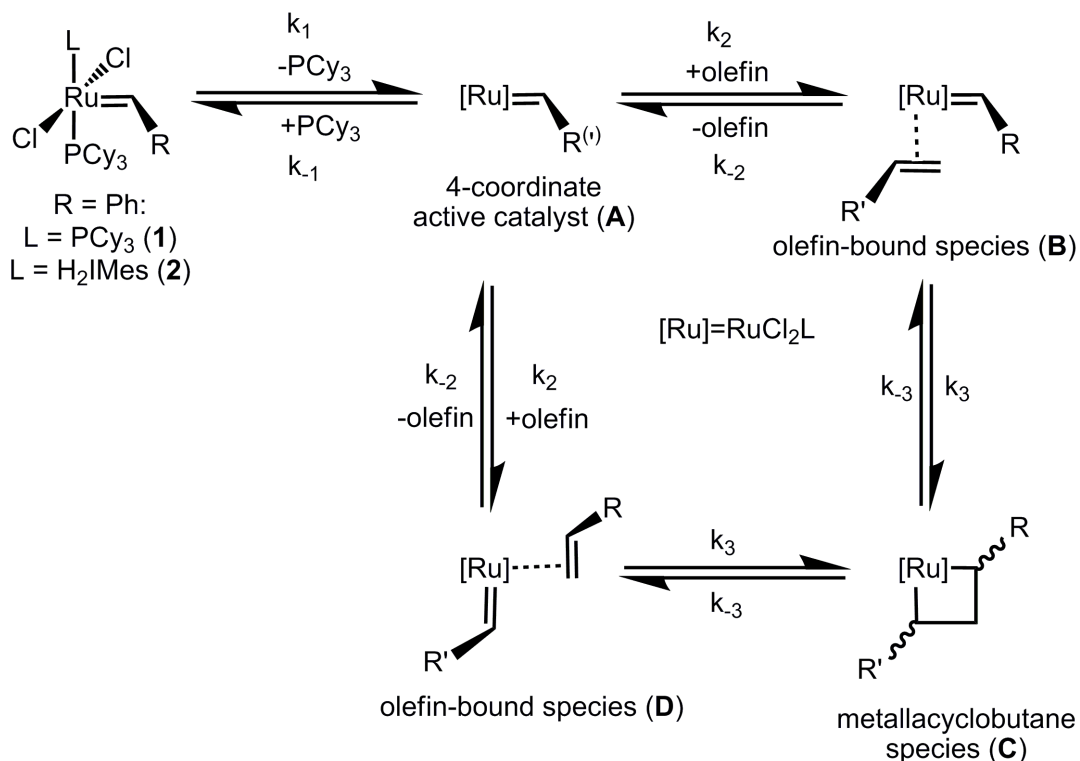
Unlike early-transition-metal catalysts, the activity of the more electron-rich ruthenium complexes increases when the PR_3 ligand (see Section 1.3.1 for additional background on phosphine ligands) is more electron-donating, as observed when the original triphenylphosphine (PPh_3) ligands were replaced with tricyclohexylphosphine (PCy_3) donors. This was presumed to be due to a stabilisation of the metallacyclobutane intermediate, which is formally ruthenium(IV).⁴⁶ As well, the activity increased due to faster initiation when the vinylalkylidene ($=CHCH=CPh_2$) ligand was exchanged for an alkylidene ($=CHR$; R = alkyl, aryl) group.⁴⁷ The synthesis was improved⁴⁸ and scaled up[‡] in 1995, allowing the first-generation Grubbs catalyst ($(PCy_3)_2Cl_2Ru=CHPh$; **1**) to become commercially available shortly after these accomplishments.⁵ Accessibility, along

[‡] Mike Giardello developed most of the methodology for the scale up of complex **1**, but this work was not published.⁵

with high stability and activity, led to extensive use of complex **1** for olefin metathesis in organic synthesis.

Mechanistic studies⁴⁹⁻⁵¹ were carried out to identify the differences between ruthenium(II) complexes and previously studied catalysts. These investigations established that the five-coordinate complexes were actually precatalysts to the four-coordinate active species in which a neutral PR_3 ligand had dissociated. The mechanism of the reaction (Scheme 1.2) involves the initial dissociation of a phosphine ligand to form the four-coordinate active catalyst (**A**). This species can then recoordinate phosphine and return to the dormant five-coordinate precatalyst (**1** or **2**) or it can bind an olefin (**B**). A ruthenacyclobutane structure is then formed (**C**) and collapsed, followed by olefin dissociation to regenerate a four-coordinate species (**A**) that repeats the reaction. In productive metathesis, the metallacyclobutane species (**C**) collapses into the olefin-bound species **D**, such that the olefins are rearranged into new species. Conversely, non-productive metathesis can also occur where the metallacyclobutane breaks apart in the reverse reaction going through the olefin-bound species **B** to re-form **A**.^{50,51}

Scheme 1.2 Generally-accepted olefin metathesis mechanism for ruthenium carbenes



1.2.5. Second-Generation Ruthenium-Benzylidene Complexes

First-generation Grubbs catalysts were not as active as some of the Schrock catalysts,⁵ and catalyst design continued with the exploration of a newer class of tuneable two-electron donors: N-heterocyclic carbenes (NHCs). Theoretical and experimental studies had indicated that NHC ligands are stronger σ -donors than phosphines (see Sections 1.3.1 and 1.3.2).⁵²⁻⁵⁷ The replacement of one phosphine group with an N-heterocyclic carbene was achieved by three independent research groups at about the same time.⁵⁸⁻⁶⁷ These complexes proved to have generally much higher activity while maintaining stability and preference for olefins in what are called the second-generation Grubbs catalysts of the form: $(\text{PR}_3)\text{LX}_2\text{Ru}=\text{CHR}'$. The commercially

available complex (**2**) contains the saturated N-heterocyclic carbene, H₂IMes, and has the formula: (PCy₃)(H₂IMes)Cl₂Ru=CHPh.⁶²

The second-generation complexes were expected to have faster phosphine dissociation than first-generation complexes due to the stronger σ -donor trans to the leaving phosphine ligand; however, these complexes have slower phosphine dissociation by about two orders of magnitude.^{50,51,68} The increased activity is instead due to a higher rate of catalyst turnover and it was proposed that the more electron donating and bulky NHC ligands result in more active catalysts because they have higher selectivity for the olefin over the phosphine.^{50,51,69} A recent computational study suggested that the faster dissociation rate in **1** as compared to **2** is due to specific steric congestion and not electronic in nature.⁷⁰ The basis for slower phosphine dissociation in the NHC-containing complexes has not been established experimentally.

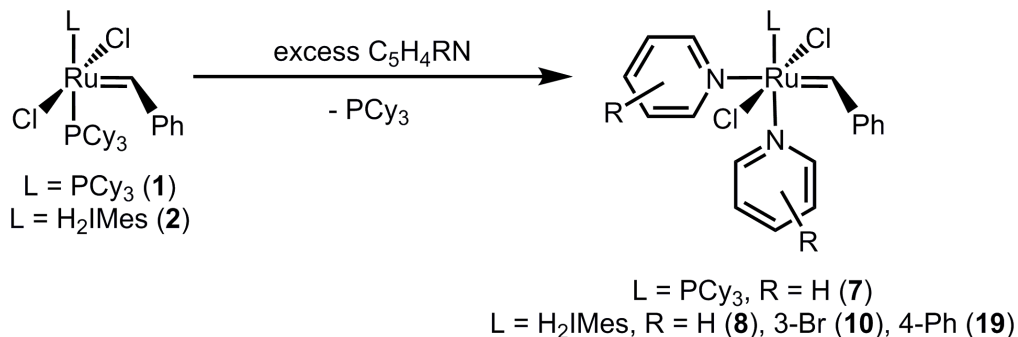
1.2.6. Bispyridine Ruthenium-Benzylidene Complexes

Further developments in the Grubbs group established that when an excess of unsubstituted or monosubstituted pyridine is added to **1** or **2**, one neutral phosphine ligand is replaced with two more labile pyridine ligands, resulting in the six-coordinate bispyridine complexes[§] of the form L(C₅H₄RN)₂Cl₂Ru=CHPh where L = PCy₃ or H₂IMes and R = H, 3-Br, or 4-Ph (**7,8,10,19**).⁷¹⁻⁷³ The facile room-temperature reaction results in cis geometry of the pyridines, with one pyridine trans to the L ligand and one pyridine trans to the

[§] The NHC-containing bispyridine complexes, especially complex **10** where R = 3-Br, are often referred to as "third-generation Grubbs catalysts"; however, in this thesis, complexes **7-14** are referred to as "first-" or "second-generation (Grubbs) bispyridines" to highlight the presence of L = phosphine or L = NHC, respectively.

benzylidene (Scheme 1.3). Both first- and second-generation complexes have also been observed as the five-coordinate monopyridine adducts.^{71,73}

Scheme 1.3 Synthesis of the bispyridine ruthenium-benzylidene complexes



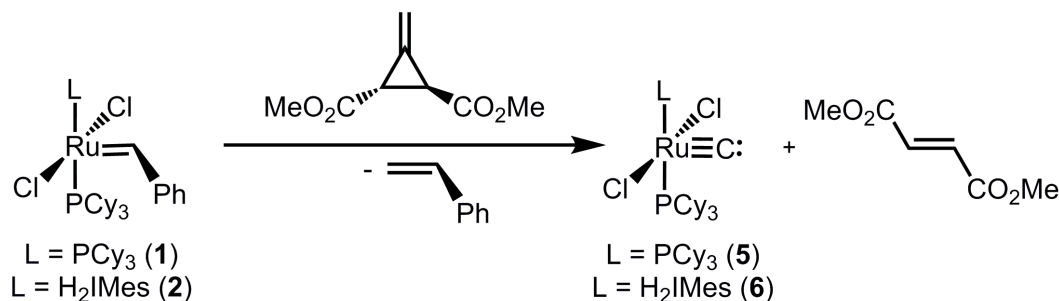
The Grubbs bispyridines have been useful precursors for new catalysts due to faster, cleaner reactions to form novel ruthenium benzylidenes.⁷¹ The catalytic activity of complexes with L = H₂IMes and three different substituted pyridines (R = H (**8**), 3-Br (**10**), or 4-Ph (**19**)) was studied and initiation rates were found to be extremely fast.⁷² The 3-bromopyridine complex (**10**) has the highest overall catalytic activity.⁷² Although these complexes initiate quickly, they are less stable to heat, air, and moisture than the precursor catalysts **1** and **2**.⁷⁴

1.2.7. Heppert Carbide Complexes

Heppert and coworkers unexpectedly formed terminal ruthenium-carbide complexes, L(PCy₃)Cl₂Ru≡C: (**5** & **6**), from the stoichiometric reaction of ruthenium-carbene complexes **1** and **2** with *trans*-2,3-dicarbomethoxymethylene cyclopropane (Scheme 1.4).⁷⁵ The complexes have an extremely short Ru-C_{carbide} bond indicative of a Ru-C triple bond. The other metrical data, such as Ru-P and Ru-Cl bond lengths, are similar to those of the analogous complexes **1** and **2**.⁷⁵ These complexes are not metathesis active,⁷⁶ but have been implicated

as decomposition products for some metathesis catalysts.^{76,77} They have also been valuable as precursors for the Piers complexes⁷⁸ (**3** & **4**; see Section 1.2.8) and as a structural variant for our studies.

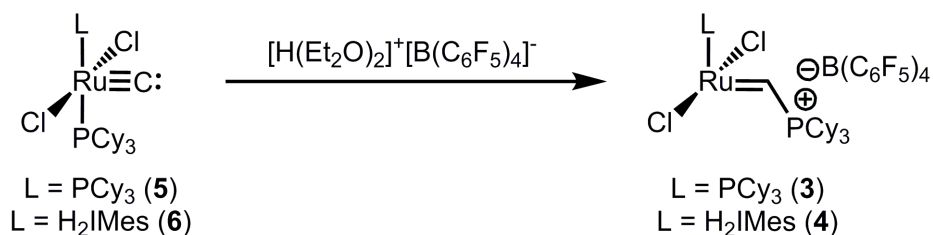
Scheme 1.4 Synthesis of the Heppert carbide complexes



1.2.8. Piers Phosponium-Alkylidene Complexes

In another serendipitous discovery, Piers and coworkers synthesised the ruthenium phosphonium alkylidenes $[\text{LCI}_2\text{Ru}=\text{CHPCy}_3]^+[\text{B}(\text{C}_6\text{F}_5)_4]^-$ (**3** & **4**) from the Heppert carbides by protonation with $[\text{H}(\text{OEt}_2)_2]^+[\text{B}(\text{C}_6\text{F}_5)_4]^-$ (Jutzi's acid), leading to phosphine ligand transfer to the carbide (Scheme 1.5).⁷⁸ The second generation complex (**4**) has slightly shorter $\text{Ru}-\text{C}_{\text{alkylidene}}$ and $\text{Ru}-\text{C}_{\text{NHC}}$ bonds, but the surroundings of the metal centre are structurally similar to the parent compound (**2**) except that one coordination site is vacant.⁷⁸ Crystallographic studies of this phosphonium alkylidene with three additional counter ions (BF_4^- , OTf^- , BPh_4^-) indicate that the cation is structurally unchanged and that the ruthenium centre does not interact with the anion in each complex.⁷⁹ The four complexes also have very similar catalytic activity for RCM in dichloromethane at 0°C .⁷⁹

Scheme 1.5 Synthesis of the Piers phosphonium-alkylidene complexes



These four-coordinate complexes are excellent olefin metathesis catalysts that initiate faster than Grubbs bispyridines and exceed the high conversion and speed of Schrock alkylidenes.⁷⁸ This high catalytic activity is largely attributed to circumventing phosphine dissociation, which drastically accelerates initiation and prevents the catalyst from being trapped by excess dissociated phosphine.⁷⁸ Initiation is presumed to be the much lower-barrier olefin-binding step⁷⁸ although there may also be a structural rearrangement required.

The Piers complexes are the closest structural analogues of the four-coordinate phosphine-dissociated intermediates formed in the initiation step of Grubbs catalyst-mediated olefin metathesis (see section 1.2.9).⁷⁸ Importantly, the second-generation phosphonium alkylidene (**4**) can be used to synthesise ruthenacyclobutane complexes relevant to the metathesis mechanism (see Section 1.2.11).

1.2.9. Four-Coordinate Intermediate

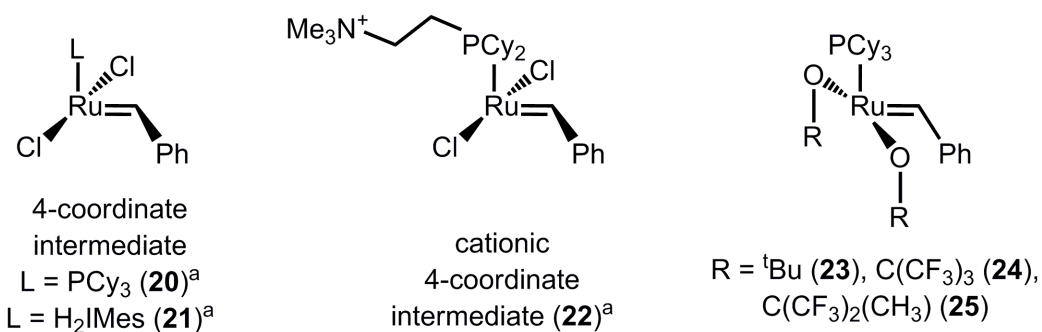
The proposed active species in ruthenium-catalysed olefin metathesis (Chart 1.4; **20** & **21**) are coordinatively unsaturated complexes.⁸⁰ The experimental observation of the gas-phase four-coordinate intermediate was achieved by Chen and coworkers via mass spectrometry of a cationic ruthenium-carbene (Chart 1.4; **22**).⁸¹⁻⁸³ The mass spectrometric investigations indicate that

gas phase ruthenium-catalysed olefin metathesis reactions closely parallel, and thus are relevant to, the corresponding solution-phase reactions.⁸¹ Although important in terms of the intermediacy and gas-phase lifetime of the four-coordinate species, these studies offer no indication of the geometric or electronic structure of these intermediates.

Interestingly, Vogler and coworkers reported that the first-generation Grubbs complex (**1**) undergoes photodissociation of a phosphine ligand upon irradiation at 546 nm due to ligand field excitation.⁸⁴ Thus far, this information has not been utilised to generate quantities of the four-coordinate complex sufficient for spectroscopic investigation.

Indeed, the solution-phase four-coordinate intermediate has proven to be an elusive species. Three four-coordinate, 14-electron ruthenium-alkylidenes (Chart 1.4; **23**, **24** & **25**) were isolated by Grubbs and coworkers.⁸⁰ These complexes have limited metathesis activity and the enhancement upon addition of HCl is thought to result from formation of the active catalyst (**20**), which then proceeds with olefin metathesis.⁸⁰ These findings indicate that the bulky complexes are poor analogues for the elusive active catalyst. Piers and coworkers have provided the best model complexes so far with their highly-active phosphonium alkylidene complexes (see Section 1.2.8; **3** & **4**); however, even these catalysts must have important differences from the four-coordinate intermediate because they are extremely stable and require initiation.

Chart 1.4 Four-coordinate intermediates and their analogues

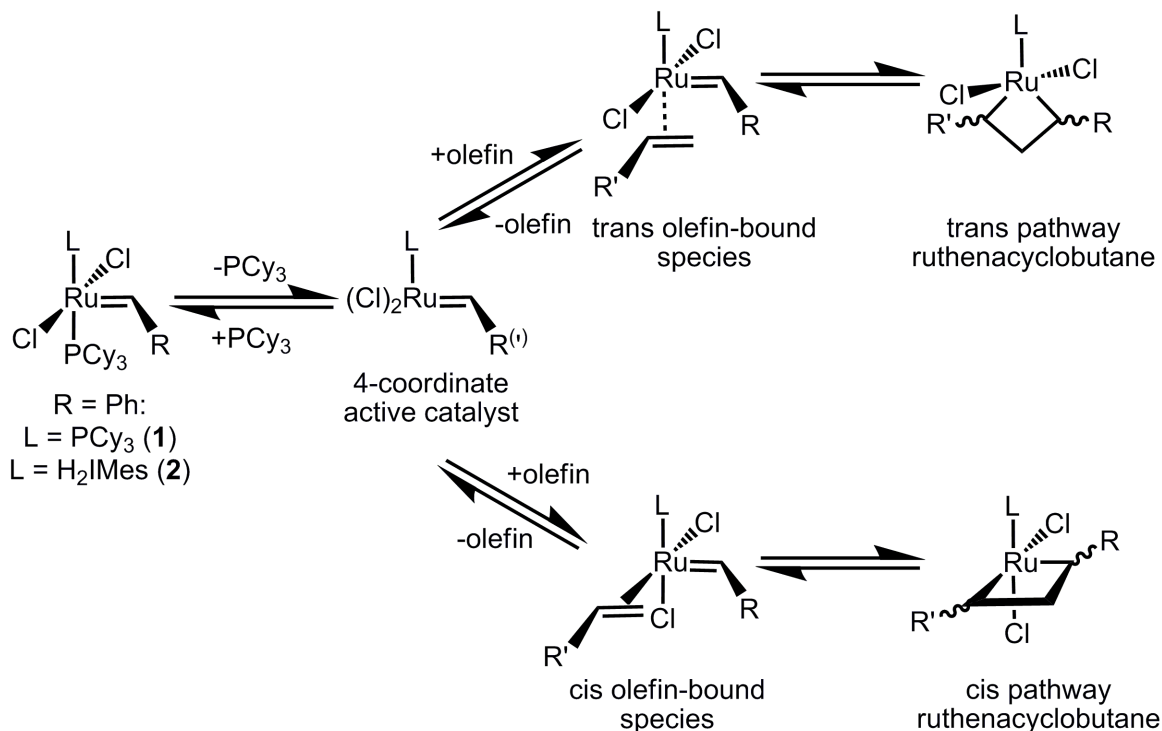


^a These intermediates have unknown geometry; they are shown here with the same geometry as the parent compound with one phosphine ligand dissociated.

1.2.10. Olefin-Bound Intermediate

The orientation of the olefin-bound intermediate in the olefin metathesis mechanism is expected to influence the geometry of the metallacyclobutane intermediate and control the stereoselectivity of the olefin metathesis reaction. Experimental work has conflicted on this point with some studies suggesting side-bound (cis to L)^{85,86} and some indicating bottom-bound (trans to L)⁸⁵⁻⁸⁸ olefin coordination in the ruthenium-carbene metathesis mechanism (Scheme 1.6).

Scheme 1.6 Portion of olefin metathesis mechanism for cis- and trans-bound olefin pathways

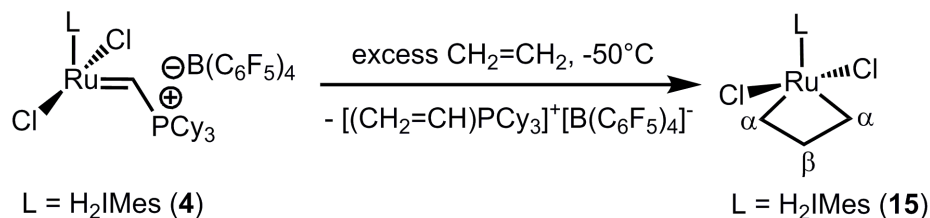


Grubbs and coworkers isolated a complex that was suggestive of cis-bound olefin in 2001.⁸⁵ In a recent report, they reacted **8** with 1,2-divinylbenzene to form a mixture of two isomers.⁸⁶ They considered three possible structural isomers: one trans-bound and two variations of cis-bound olefin and found evidence for only the two cis-bound products. By contrast, Snapper and coworkers isolated a metathesis-active ruthenium complex with a tethered trans olefin formed from a stoichiometric ROM reaction of **1** with functionalised cyclobutenes.⁸⁷ Additionally, NMR studies of ruthenacyclobutanes also provide support for trans coordination (see Section 1.2.11).⁸⁸⁻⁹⁰ A recent computational study by Correa and Cavallo concluded that for complex **2** the trans-bound olefin is usually favoured due to steric factors, but that steric, electronic, and solvent effects are all important and it is possible for one factor to overcome the others.⁹¹

1.2.11. Ruthenacyclobutane Structure

It remains uncertain whether the metallacyclobutane is a transition state or an intermediate in the ruthenium olefin metathesis mechanism. A preliminary theoretical report suggested that it is a transition state,⁸² however, subsequent computational studies have generally concluded that the ruthenacycle is an intermediate.⁹²⁻⁹⁴ Additionally, the observation of the second-generation ruthenacyclobutane (**15**) in 2005⁸⁸ suggests that it is an observable intermediate at least for catalysts where L = H₂IMes. This complex is formed by addition of ethene gas to a dichloromethane solution of the second-generation Piers catalyst (**4**) at -50°C with the formation of the ruthenacyclobutane ((H₂IMes)Cl₂Ru(CH₂CH₂CH₂), **15**) and a vinyl phosphonium salt, such as [(CH₂=CH)PCy₃]⁺[B(C₆F₅)₄]⁻ (Scheme 1.7).⁸⁸ The reaction has only been successful for second-generation complexes, but it proceeds similarly with different anions and for a small range of olefins.⁸⁸⁻⁹⁰ Intramolecular exchange of C_α and C_β (Scheme 1.7; **15**) of the ring as well as intermolecular exchange of these carbons atoms with free ethene was observed experimentally⁸⁹ and supported computationally.⁹⁵

Scheme 1.7 Synthesis of ruthenacyclobutane complex



Examination of **15** via low-temperature NMR spectroscopy indicates C_{2v} symmetry with trigonal bipyramidal geometry where the chlorides are in the axial

positions and the metallacycle ring is planar with respect to the imidazole ring.^{89,90} The NMR data suggest that there is a significant $M\cdots(C_{\alpha}-C_{\beta}-C_{\alpha})$ agostic interaction in **15**, which is supported by calculations.⁹³ Computational studies propose that agostic interactions stabilise the formally 14-electron metallacyclobutane structure so that it is lower in energy than the 16-electron olefin-coordinated species.⁹³ The $M\cdots C_{\beta}$ distance has been calculated as just slightly longer than the $Ru-C_{\alpha}$ bond (1.974 Å) at 2.271 Å, indicating a flat ring geometry.^{89,93} Because **15** cannot be isolated in the solid state, one of the only methods available to experimentally-determine the details of its geometry is Ru K-edge X-ray absorption spectroscopy, which can be performed on frozen solutions.

1.2.12. Theoretical and Spectroscopic Investigations of Grubbs

Complexes

Numerous computational studies have been performed on Grubbs-type complexes to help better understand the mechanism.^{70,91-105} These reports have offered support for experimental findings as well as explanations for unanswered questions. They have confirmed that both the first (**1**) and second-generation (**2**) Grubbs precatalysts undergo initial phosphine dissociation to form a four-coordinate intermediate.^{96,99,100} Also, several reports have considered the nature of the increased activity of **2** compared to **1** despite the increased barrier to phosphine dissociation for **2**.^{70,92,97,98} Although these studies differ in their assessment of whether steric or electronic factors are more important, they

generally conclude that **2** has a higher barrier to phosphine dissociation, but a lower metathesis reaction barrier.

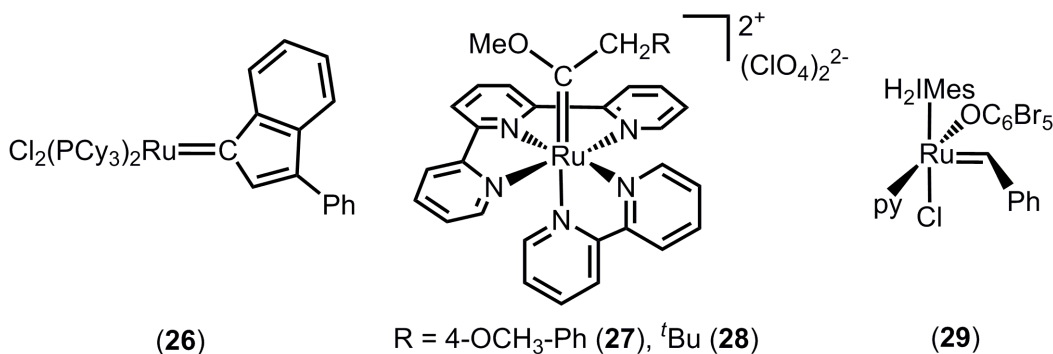
Curiously, there have been very few spectroscopic investigations^{84,106-108} into ruthenium-carbene complexes, which are required to verify the theoretical work. Vogler and coworkers assigned the UV-Vis absorption spectra of complexes **1** and **20** based on computational data and made suggestions about the geometric changes, which lead to the ligand field triplet that initiates the photolysis (see also Section 1.2.9).⁸⁴ In a more recent report, this group has described a MLCT transition ($\pi^*_{\text{carbene}} \leftarrow \text{Ru}^{\text{II}}$) that results in unique carbene dissociation from the complex $\text{Ru}(\text{PI})(\text{PCy}_3)_2\text{Cl}_2$ where PI = 3-phenylindenylidene (**26**; Chart 1.5).¹⁰⁸

Che and coworkers assigned the UV-Vis absorption and emission bands for methoxyalkylcarbenerruthenium(II) complexes supported by the terpyridine-bipyridine ligand set (**27** & **28**; Chart 1.5).¹⁰⁶ These complexes are not metathesis-active, but are of interest for applications such as light-emitting devices and photosensitisers because they display interesting photophysical and photochemical properties.¹⁰⁶

A previous report by our group, in collaboration with Deryn Fogg, examined the Cl K-edge X-ray absorption spectra of complexes **1** and **2**.¹⁰⁷ This preliminary study established the methodology to determine Ru-Cl covalency using XAS. The covalency was found to be very similar for the first- and second-generation Grubbs complexes, but different for a complex containing a pseudohalide and pyridine ligand in place of one chloride and phosphine ligand

(29; Chart 1.5).¹⁰⁷ This suggests that the nature of the Ru-Cl bond is sensitive to different ligation around the ruthenium centre, but that replacing the phosphine in **1** with an NHC in **2** does not affect the Ru-Cl covalency.

Chart 1.5 Ruthenium-carbene complexes that have been studied spectroscopically



The structure-activity relationships for ruthenium metathesis catalysts are not well understood, and information about the geometric and electronic structure of all the relevant species is essential for rational catalyst design. Spectroscopic studies are necessary to corroborate computational findings and to determine the nature of the metal-ligand bonds as they progress throughout the metathesis cycle.

1.3. Phosphine and N-Heterocyclic Carbene Ligands

Phosphine and N-heterocyclic carbene ligands are both important ligands, not only for olefin metathesis, but for organometallic chemistry in general. In this thesis, the distinction between the first-generation ($L = PR_3$) and second-generation ($L = NHC$) complexes is significant; therefore, this section outlines some of the background and common methods for determining the electronic and steric properties of these two ligand classes.

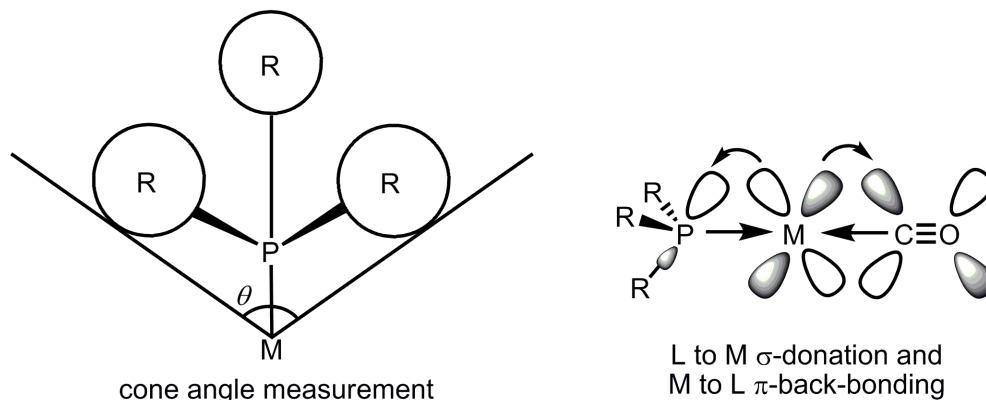
1.3.1. Phosphine Ligands

Phosphines are neutral two-electron donor ligands of the form PR_3 (where $R = H$, alkyl, aryl, halide or mixed). They are ubiquitous in organometallic chemistry largely because they can be predictably tuned to optimise the desired properties of a complex.⁵⁶ Tolman carried out many of the important investigations of the steric and electronic properties of phosphine ligands and he developed parameters to approximate both properties.¹⁰⁹⁻¹¹¹

The principal steric parameter is the cone angle, θ , which begins at the metal (assuming an M-P distance of 2.28 Å based on Ni-P complexes) and encloses the van der Waals surface of all the ligands over all rotational orientations about the M-P bond (Figure 1.2).^{110,111} Cone angles can be a useful indicator of reactivity; for example, phosphine dissociation rates have been shown to increase with increasing cone angle in some systems.^{110,111} Conversely, studies of second-generation Grubbs-type complexes exhibit the opposite trend; for example, PCy_3 ($\theta = 170^\circ$) dissociates 58 times slower than

PPh_3 ($\theta = 145^\circ$), which indicates that electronic factors may play a more important role in phosphine dissociation of those compounds because PCy_3 is thought to be a better σ -donor than PPh_3 .⁶⁸

Figure 1.2 Steric and electronic properties of phosphine ligands



The Tolman electronic parameter is based on the a_1 vibrational frequency of a carbonyl ligand in the complex, ν_{CO} , initially measured for a series of $\text{Ni}(\text{CO})_3\text{L}$ complexes.^{109,111} The rationale is that if the donation from the phosphine to the metal increases, there will be a proportional increase in the back-donation of the metal to the carbonyl carbon (and no increased back-donation to the phosphorus), which will subsequently reduce the donation from the oxygen to the carbon and weaken the C-O bond (Figure 1.2). The C-O stretching frequency is a good estimate of C-O bond strength because it is related to the force constant, k , which correlates to the bond's resistance to displacement of its atoms.¹¹² Therefore, ν_{CO} values were proposed as a useful measure of phosphine donation; the experimental values correlated well with the electron-donating ability of the ligands.¹⁰⁹ Although this measure is still widely employed today, it should be noted that force constants are generally not calculated. In using the stretching frequencies directly, assumptions are often

made; for example, that there is invariant or no coupling between vibrational modes and that correction for anharmonic effects is not required.¹¹² Other factors may also affect ν_{CO} , such as electrostatic interactions¹¹³ and steric perturbations.¹¹¹

Importantly, this electronic parameter indirectly assesses electron donor-acceptor properties and only considers net donation, without separating σ - and π -effects or considering electrostatic interactions. Changes to ν_{CO} upon ligand replacement may be due to differences in electrostatics, σ -donation, π -acceptance, or a combination of these; specific interactions are likely to depend on the particular complex rather than simply on the ligand itself. Other experimental measures of ligand electronic properties include heats of reaction ($-\Delta H_{\text{rxn}}$) or relative bond dissociation energies (BDE), crystallographic bond distances, $\text{p}K_{\text{a}}$ values, reduction potentials, and various NMR shifts and coupling constants. It was shown with pyrrolyl phosphines that an increase in π -back-bonding significantly increased ν_{CO} and had variable effects on $-\Delta H_{\text{rxn}}$.

Phosphines bind to transition metals through σ -donation of their lone pairs while π -back-bonding most likely occurs from a filled metal d-orbital to empty ligand σ^* orbitals (Figure 1.2).^{114,115} Separation of σ -donation, π -donation, and π -acceptance has been investigated using electrochemical data and it was shown that back-bonding increases with more electron-withdrawing substituents on the phosphine, such as PF_3 , but that π -effects may have little impact on reactivity.^{116,117} Other work has correlated NMR coupling constants, $J_{\text{Pt-P}}$, to

Hammett substituent constants^{118**} and emphasised that the π -accepting capability of phosphines increases with more electron-rich metal centres.¹¹⁹ Large trialkylphosphines, such as PCy₃, are generally considered pure σ -donors with negligible π -interactions.

There has been extensive discussion and disagreement in the literature regarding the measures or combinations of measures that provide the most accurate information about ligand parameters and the nature of metal-phosphine bonds.¹²⁰⁻¹²⁷ Despite the debate, relatively simple models, such as Tolman electronic and steric parameters have been employed with considerable experimental success.

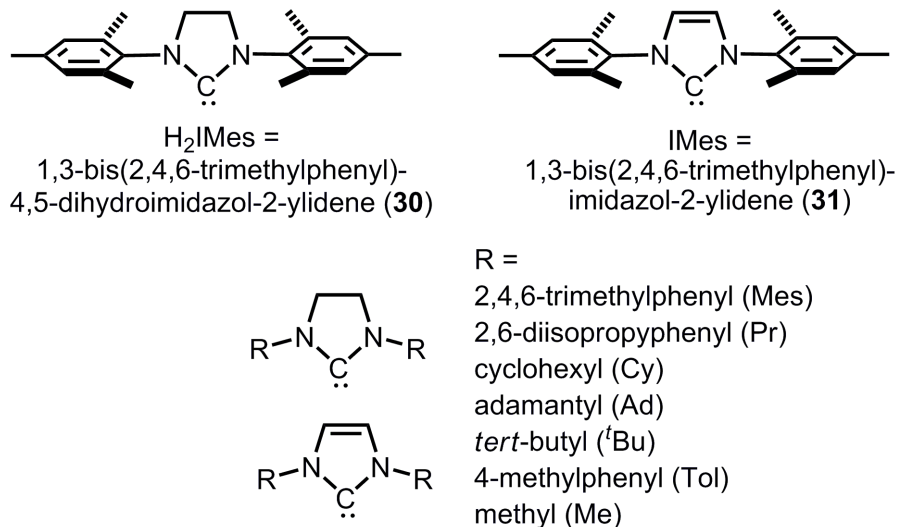
1.3.2. N-Heterocyclic Carbene Ligands

Öfele and Wanslick discovered N-heterocyclic carbene (NHC) containing complexes in 1968,^{128,129} but it was not until 1991 that Arduengo and co-workers isolated a stable free NHC that would coordinate to transition metals.¹³⁰ Since isolation, NHCs have become widely used in transition metal catalysis where they often replace phosphines as spectator ligands with generally positive effects on catalytic activity.^{131,132} A variety of NHCs have been synthesised and the most relevant ligands for ruthenium-catalysed olefin metathesis are the saturated H₂IMes (**30**; also called SIMes) and unsaturated IMes (**31**) (Chart 1.6). Because of their utility as phosphine replacements, the steric and electronic properties of

** The Hammett substituent constant, σ , indicates the electron donating or withdrawing effect of *meta*- and *para*-substituents based on the ionisation constants of appropriately substituted benzoic acids.

NHCs have been of great interest; however, straightforward trends have been much more elusive for NHCs than for phosphine ligands.⁵⁶

Chart 1.6 A variety of common N-heterocyclic carbenes



A steric measure has been developed for NHC and PR_3 ligands that is analogous to the Tolman cone angle, but more appropriate for the asymmetric NHCs; this permits a more direct comparison of steric requirements.¹³³ The method is based on the percent volume of a sphere centred on the metal that is buried by overlap with atoms of the particular ligand ($\%V_{\text{bur}}$).¹³³ The volume of the sphere represents the space around the metal centre that must be shared by other ligands. PCy_3 has a percent buried volume similar to those of IMes and H_2IMes .⁵⁷

Arduengo found that NHCs do not require steric bulk to form stable complexes and inferred that they must be stabilised electronically.¹³⁴ NHCs were soon labelled as strong σ -donors similar to trialkylphosphines with no need for back-donation from the metal centre; this was partly based on calculations of beryllium(II) carbene complexes where π -back-bonding is not possible.¹³⁵ Further

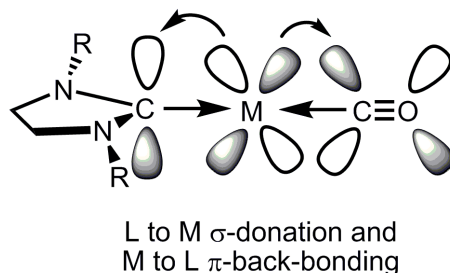
experimental and theoretical reports suggested negligible π -acceptor character for NHC ligands.^{54,136-145} The experimental studies of the electronic properties of NHCs primarily use the techniques that were previously employed for phosphines.^{146,147}

Some research has directly compared phosphine and NHC ligands,⁵²⁻⁵⁷ concluding that NHCs form stronger bonds (based on experimental and theoretical BDEs) than phosphines because they are better electron donors than even the most basic tertiary phosphines (based on ν_{CO} values).^{57,148} The groups of Nolan⁵⁷ and Herrmann¹⁴⁹ have compared ν_{CO} values for a variety of NHCs to each other and found very small differences between NHCs and especially between the unsaturated and saturated forms. It is worth noting that, as with phosphines, ν_{CO} is an indirect estimate of net donation from a ligand because σ - and π -effects both contribute to the intensity in opposite ways (Chart 1.7). Additionally, it is expected that electrostatic interactions may affect these measures.

The issue of net donation seems to be underemphasised in the literature, often based on the assumption that NHC ligands are pure σ -donors, which is an increasingly challenged assertion. Potentially incorrect assumptions have led to the application of ν_{CO} values as good measures of σ -donation: the additional electron density that is back-bonded to the carbonyl must be coming from L; L must have negligible or the same π -accepting character as every other L ligand being investigated; every ligand besides CO must have the same electron donor-

acceptor properties and electrostatic interactions after a change in L; and the metal centre must have the same effective charge in all complexes.

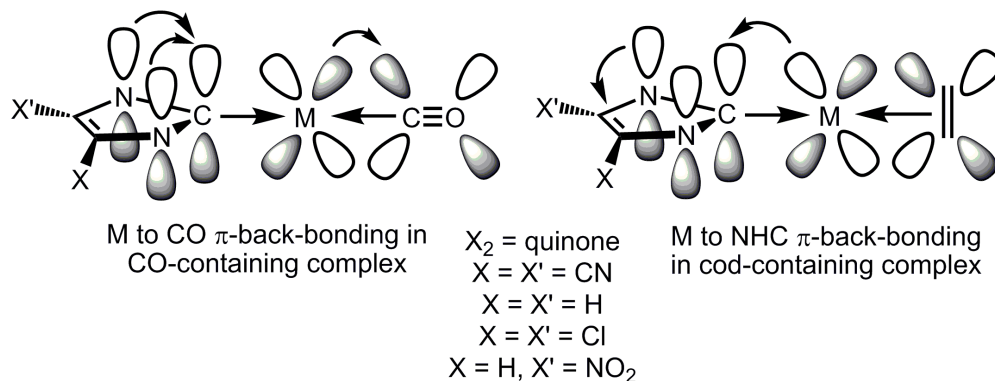
Chart 1.7 Electronic properties of N-heterocyclic carbene ligands



Recently, a number of studies have indicated that NHCs have flexible bonding capabilities. These have included the ability to donate^{133,147,150-152} as well as accept^{133,146,147,153-160} π -electron density. Bielawski and coworkers have experimentally shown good evidence for metal to NHC π -back-bonding with molecules specifically designed to probe this property. One such system employs a quinone-annulated NHC coordinated to a RhL_2Cl fragment where L_2 = two carbonyl ligands or one cyclooctadienyl (cod) ligand (Chart 1.8).¹⁵⁹ They found that when changing the π -accepting CO ligands to the cod ligand with little π -accepting ability, the quinone CO stretching frequencies decreased and the reduction potentials increased. These results suggest that, in the cod containing complex without a strong π -withdrawing carbonyl ligand, there may be significant π -donation to the NHC ligand, resulting in both weaker CO bonds on the quinone and a more electron-rich NHC ligand. A second report from the Bielawski group employs NHCs with and without electron-withdrawing substituents in the 4,5 positions of the unsaturated imidazole ring of $(\text{NHC})\text{RhL}_2\text{Cl}$ where, again, L_2 = 2CO or cod (Chart 1.8).¹⁶⁰ IR data of the CO

complexes and ^1H NMR data of the cod complexes both follow the trend of less back-donation to the L ligand(s) as the π -acidity of the 4,5 substituents on the NHC increases (π -acidity: $\text{H} < \text{Cl} < \text{CN}$).

Chart 1.8 Experimental design from the Bielawski group



An experimental and theoretical investigation by Nolan and coworkers in 2007 has utilised computational analysis with ^{13}C and ^{195}Pt NMR data for $(\text{NHC})\text{Pt}(\text{dmsO})\text{Cl}_2$ complexes to show that saturated NHCs donate and accept more electron density than unsaturated NHCs, which leaves the metal centre more electron-rich.¹⁴⁶ The coupling constants for platinum and the carbene carbon ($J_{\text{Pt-C}}$) are expected to be proportional to the electron density of the σ -orbital of the bond thereby allowing separation of σ and π effects. $J_{\text{Pt-C}}$ is lower for saturated complexes, suggesting that there is less σ -character in the bond. Nolan and coworkers also found that the Pt signal shifts upfield, indicating more electron density at the Pt centre for saturated NHCs. They used computational analysis to verify and facilitate explanation of these findings as due to a synergistic effect between σ -donation and π -acceptance in NHCs.

Recent computational studies showing non-negligible π -acceptance have estimated the π -contribution to the bond from 10 to 30%.^{156,158} Frenking and

coworkers approximated the π -contribution at 20% for M-NHC complexes¹⁵⁷ and they also investigated the electrostatic stabilisation of M-L bonds for a variety of ligands.^{113,157,161} They concluded that electrostatic rather than covalent interactions are the major contributor to M-L bond strength for both phosphines and NHCs.^{††} Additionally, covalent contributions to bond energies are generally larger for phosphine ligands (35-44%)¹¹³ than for NHC ligands (22-32%).¹⁵⁷ These results illustrate – and the authors emphasise – that bonding interactions must be understood before drawing conclusions about a particular component because any observable property results from the overall molecular interactions.¹⁶¹

There is significant experimental and computational evidence for the possibility of both π -donation and π -acceptance of N-heterocyclic carbene ligands. Additionally, electrostatic interactions likely play an important role in both M-NHC and M-PR₃ bonding; thus, these bonding components cannot be ignored when attempting to rationalise structure-activity relationships. There appears to be a trade-off between the accuracy and the applicability of ligand parameter measures or combinations of measures. Although high accuracy is an ultimate goal, the specific objectives of individual research may benefit from less accurate, but easily applicable measures of parameters. Perhaps the main issue here is careful attention to what each technique is actually measuring and the assumptions required to extend the analysis to specific properties.

^{††} The M-PR₃ complexes studied are M(CO)₅PR₃ where R = H, CH₃, F, Cl and M = Cr, Mo, W. The M-NHC complexes studied are [M(NHC)₂]⁺ or M(NHC)X where NHC = imidazol-1-ylidene, M = Cu, Ag, Au, and X = F, Cl, Br, I.

1.4. X-ray Absorption Spectroscopy

1.4.1. General Information

X-ray absorption spectroscopy (XAS) is a technique that measures the absorption, μ , by a sample as a function of photon energy, E (usually in units of electronvolts^{‡‡162}). At the appropriate energies, core level electrons are promoted to empty or partially-empty bound states; at higher energies, the electrons are completely ionised to the continuum of unbound states.¹⁶³ XAS transitions are named according to the initial state with the principal quantum number as an uppercase letter and the specific absorption line (when more than one line is possible) as a subscript number. For example, 1s = K; 2s = L₁; 2p_{1/2} = L₂; 2p_{3/2} = L₃; 3s = M₁; and so on; thus, a K-edge spectrum spans the photon energy for the ionisation of electrons from the 1s orbital whereas an L_{2,3}-edge spectrum corresponds to the 2p electron ionisation region.^{164,165}

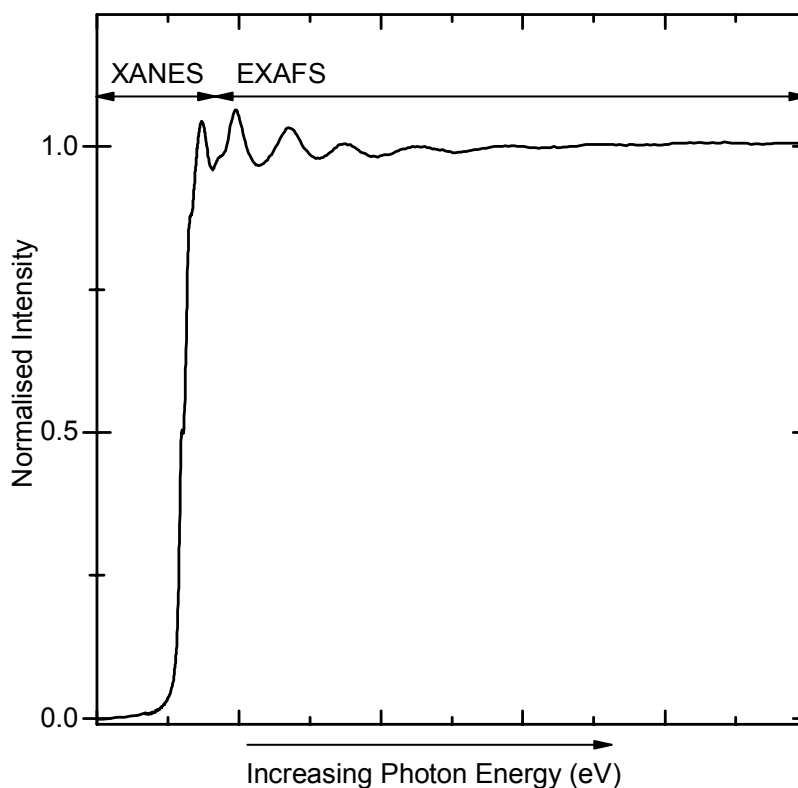
XAS is an element-specific technique because the ionisation energies of core electrons are generally well-separated from their nearest neighbour. For example, the Ru K-edge occurs at approximately 22117 eV, whereas the Tc and Rh K-edges are at 21044 eV and 23220 eV, respectively.¹⁶⁴ XAS is also versatile because it can be applied to almost any element and is sensitive to, but not limited by, oxidation state, coordination number, or geometry. A key benefit of XAS is that it can be used for dilute, non-crystalline samples.¹⁶³

^{‡‡} The electronvolt, eV, is a commonly-used non-SI unit defined as the energy acquired by a particle containing one unit of charge through a potential difference of one volt; it is equal to the elementary charge, e ($1.602\ 177\ 33(49) \times 10^{-19}$ C) multiplied by 1 V, so 1 eV is approximately 0.160 aJ, which is ≈ 96.485 kJ/mol.

There are two main regions of an XAS spectrum: X-ray absorption near-edge structure (XANES)^{§§} and extended X-ray absorption fine structure (EXAFS) (Figure 1.3). When the incident X-ray energy reaches the ionisation energy of a core electron, the corresponding spectral feature is a sharply rising edge that then plateaus (often approximated as an arctangent function). At lower energies, core electrons can undergo bound-state transitions, which can be observed as features called pre-edge peaks.^{165,166} This region containing the pre-edge and edge features is known as the XANES. Above the edge energy, the ejected photoelectron wave interacts with nearby atoms that backscatter the wave. The interference of the emitted and backscattered photoelectrons creates oscillations in the region called EXAFS.¹⁶⁵ The XANES region provides electronic structure as well as some geometric structure information whereas EXAFS provides further geometric information. Because both regions can be collected in the same XAS experiment, it is often convenient and useful to examine their different, but complementary, information.

^{§§} XANES is occasionally defined as X-ray absorption near-edge spectroscopy; another acronym is sometimes used: NEXAFS which represents “near-edge X-ray absorption fine structure”; these terms can be considered synonymous.

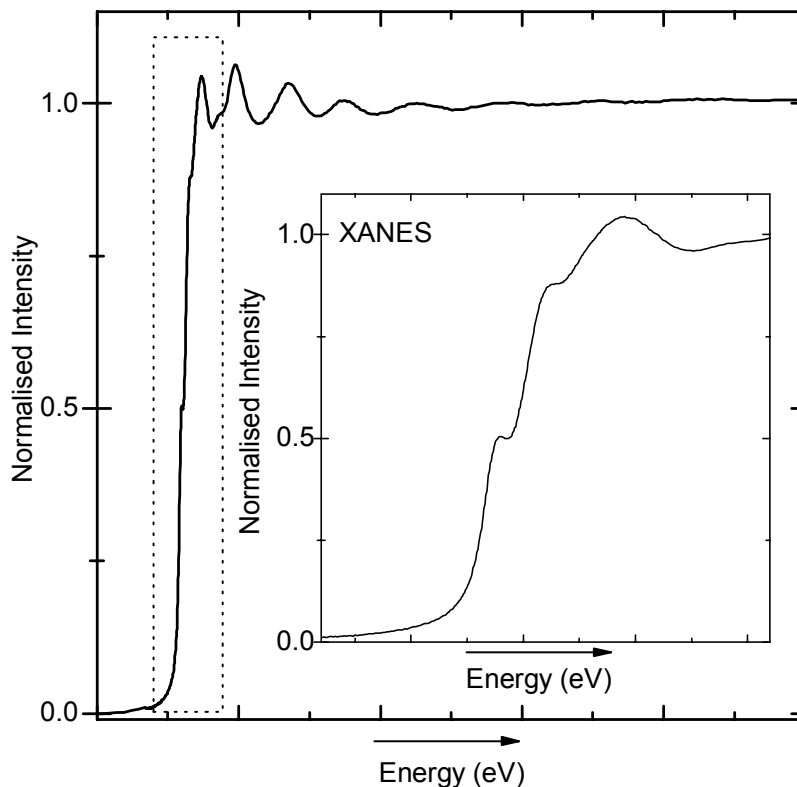
Figure 1.3 XAS spectrum depicting XANES and EXAFS regions



1.4.2. Transition Metal K-Edge X-ray Absorption Near-Edge Structure

The XANES region of a metal K-edge spectrum results from bound-state transitions and ionisation of 1s electrons. Figure 1.4 shows an example of a transition metal K-edge XAS spectrum with an inset of the expanded XANES region.

Figure 1.4 Transition metal XAS spectrum with XANES region expanded (inset)

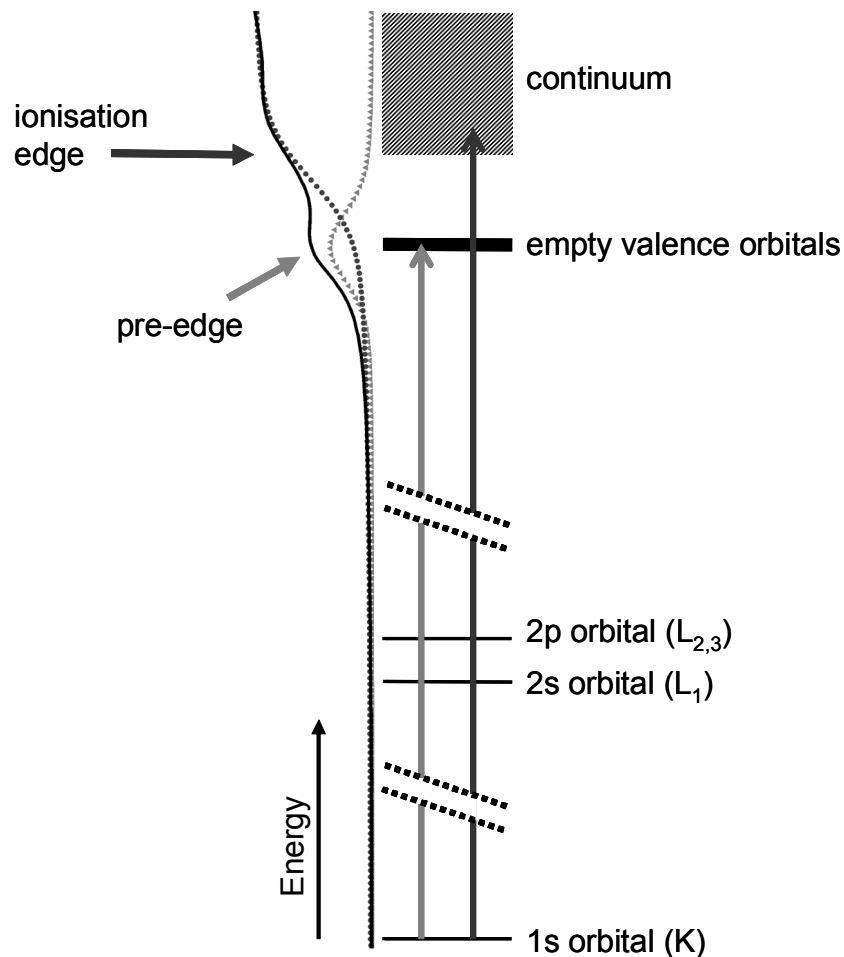


The pre-edge features in first-row transition metal XAS spectra are usually attributed to metal $3d \leftarrow 1s$ or $4p \leftarrow 1s$ transitions (Figure 1.5).¹⁶³ For centrosymmetric compounds, $nd \leftarrow 1s$ transitions are formally electric dipole forbidden, but as that symmetry is broken they become partially allowed due to contributions of np character to nd orbitals. Some minor $nd \leftarrow 1s$ intensity is expected for centrosymmetric complexes owing to electric quadrupole-allowed character,¹⁶⁷ but this has been estimated at 100 times weaker than electric dipole contributions.^{168,169} This means that centrosymmetric compounds, such as octahedral or square planar geometries, have very low-intensity $nd \leftarrow 1s$ transition pre-edge features whereas lower symmetry complexes can have higher-intensity pre-edge features. Therefore, $nd \leftarrow 1s$ transition pre-edge edge

features are good indicators of coordination number and ligand geometry around the metal centre; this relationship is particularly well-established for iron complexes.^{166,170-172}

The edge jump is an intense step-like feature attributable to the ionisation of K-shell electrons from the metal centre ($\infty \leftarrow 1s$) (Figure 1.5); these features often overlap with dipole-allowed transitions to valence p-orbitals ($np \leftarrow 1s$) or to more diffuse orbitals.^{163,173} The ionisation energy of 1s electrons (IE_{1s}) is directly proportional to the charge at the metal centre (q_M). This relationship is often used to correlate the energy of the rising edge of metal K-edge spectra to the oxidation state of the metal centre; these determinations are relative, requiring standard samples for comparison.^{163,173,174} IE_{1s} is sensitive to even small changes in local charge, that is, alterations that do not constitute an oxidation state change, such as differences in ligation.¹⁶³

Figure 1.5 XANES region transitions and spectral features

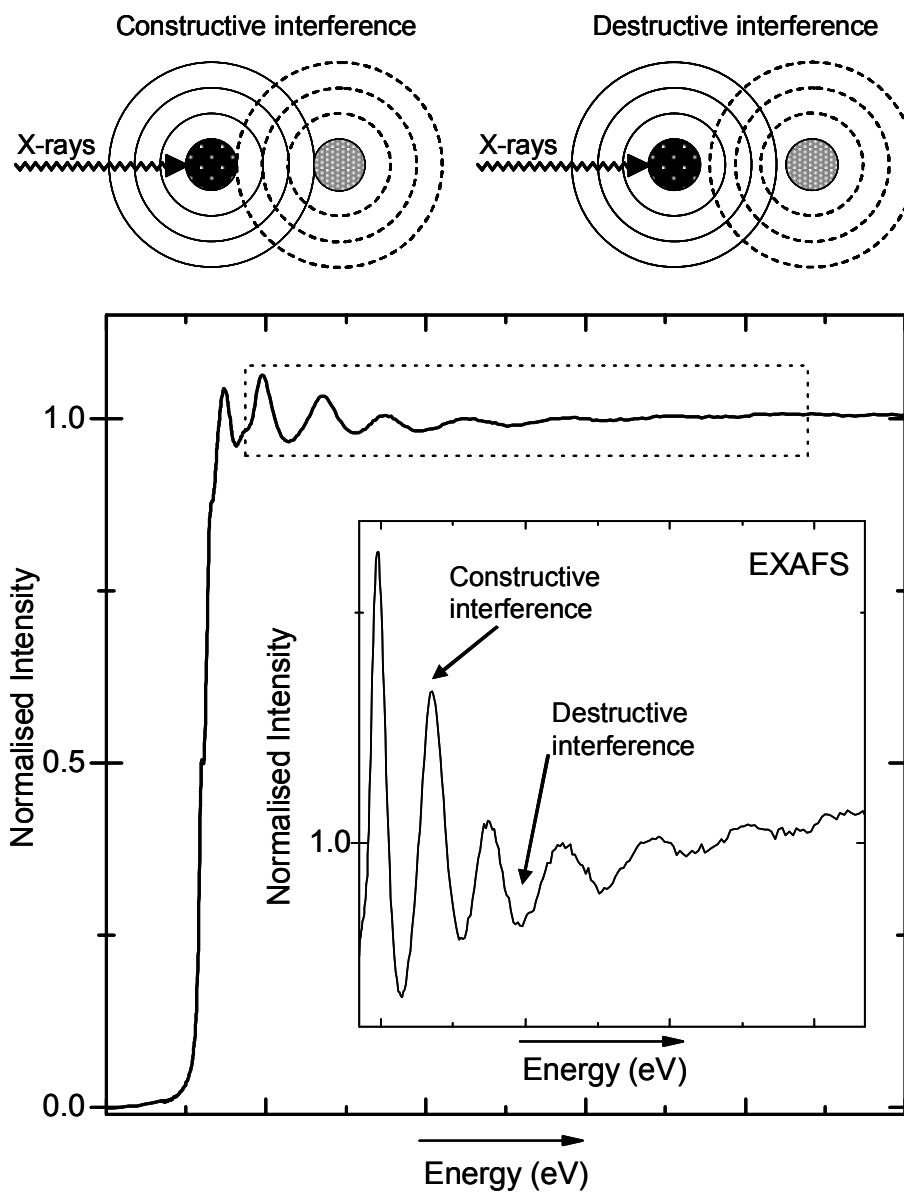


1.4.3. Extended X-ray Absorption Fine Structure

The EXAFS region of an XAS spectrum has an oscillatory fine structure, described by $\chi(E)$, due to photoscattering of ionised core electrons. When the incident photon energy reaches the ionisation threshold energy (E_0) of the core electrons for the absorbing atom (absorber), photoelectrons are ejected into the continuum of unbound states. Neighbouring atoms (scatterers) can backscatter the propagating waves, resulting in constructive and destructive interference,

which are seen in the spectra as areas of high and low intensity, respectively (Figure 1.6).¹⁷⁵

Figure 1.6 Scattering interference and transition metal XAS spectrum with EXAFS region expanded (inset)



With careful analysis, the following structural information is often available from EXAFS data: scattering atom identity ($Z \pm 1$); number of each type of atom

($N \pm 25\%$); and interatomic distance between the absorbing and scattering atoms ($R \pm 0.02 \text{ \AA}$).¹⁷⁵

The relevant structural properties and the EXAFS parameters affected by them are listed in Table 1.1.

Table 1.1 Structural properties and the EXAFS parameters that they affect

Structural Properties	Parameter Affected
Type and number of scatterers; distance between absorber and scatterer	Amplitude
Distance between absorber and scatterer	Frequency
Type of absorber and scatterer	Phase shift

In order to analyse EXAFS data, a number of variables must be considered. Some parameters are calculated or determined from model compounds whereas others are refined in the fitting process. Equation 1.1 is the single-scattering EXAFS equation, which can be separated into the amplitude function and the phase function. Overall, Equation 1.1 describes the sum of all absorber-scatterer interactions, each of which is represented by a damped sine wave.¹⁷⁵

Equation 1.1 EXAFS single-scattering equation

$$\chi(k) = S_0^2 \underbrace{\sum_i \frac{N_i A_i(k)}{k R_i^2} \exp(-2R_i / \lambda(k)) \exp(-2\sigma_i^2 k^2)}_{\text{amplitude function}} \underbrace{\sin[2kR_i + \phi_i(k)]}_{\text{phase function}}$$

Where:

N_i = number of atom i scatterers

R_i = absorber-backscatterer distance for atom i

σ_i^2 = mean-square deviation in R_i (part of the Debye-Waller factor)

S_0^2 = total amplitude reduction factor; accounts for electronic relaxation

$\lambda(k)$ = photoelectron mean free path function

$A_i(k)$ = backscattering amplitude function (including amplitude reduction function, $S_i(k)$ and EXAFS amplitude function, $f_i(k)$); $A_i(k) = S_i(k)f_i(k)$

$\phi_i(k)$ = total EXAFS phase shift function (including scatterer, $\psi_i(k)$, and absorber, $\delta_a(k)$, phase shift functions); $\phi_i(k) = \psi_i(k) + \delta_a(k)$

k = photoelectron wavenumber (see Equation 1.2)

The photoelectron wavenumber, k , is used to express the photon energy, which is convenient for mathematical manipulations and results in more evenly-spaced oscillations.¹⁷⁵

Equation 1.2 Photoelectron wavenumber, k

$$k = \sqrt{\frac{2m_e}{\hbar^2}(E - E_0)}$$

Where:

m_e = mass of the photoelectron

\hbar = Planck's constant, h , divided by 2π

E = incident photon energy

E_0 = ionisation energy of the core electron (IE)

From Equation 1.1, the term:

$$\exp(-2R_i / \lambda(k))$$

is related to the mean-free path, which accounts for the inelastic loss.¹⁷⁵

From Equation 1.1, the term:

$$\exp(-2\sigma_i^2 k^2)$$

is called the Debye-Waller factor and describes the static and thermal disorders that dampen the amplitude.¹⁷⁵ Lower experimental temperatures reduce the thermal vibration, resulting in larger amplitudes and improved signal-to-noise ratios.

Equation 1.1 is for the single-scattering model where each photoelectron is backscattered from one atom. Multiple-scattering can also occur in which the photoelectron is scattered by two or more atoms before returning to the absorber. This is especially important for rigid structures at longer distances from the absorbing atom ($>3 \text{ \AA}$) and at large scattering angles ($>150^\circ$);¹⁶³ the software programs used to analyse EXAFS data can include multiple-scattering paths.

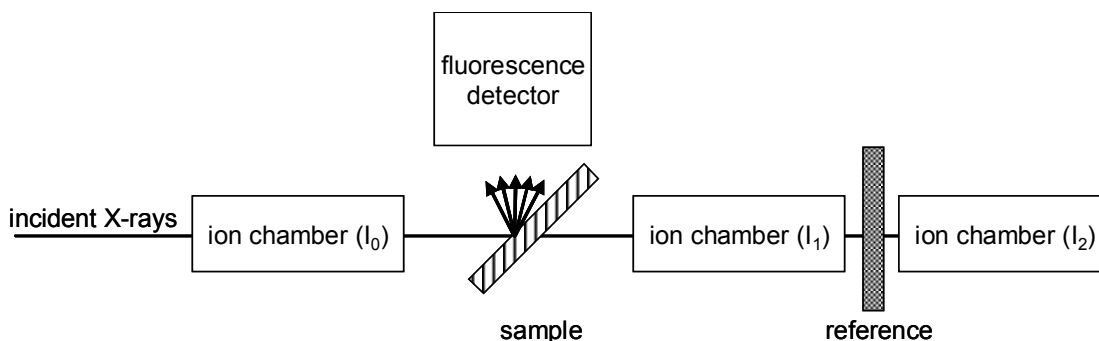
1.4.4. Experimental Set-up

The X-ray source for XAS experiments is a synchrotron facility that utilises a booster ring to accelerate electrons and inject them into a larger storage ring where bending magnets direct the electrons around the ring. Insertion devices, such as undulators and wigglers, containing a specialised set of magnets are used to produce radiation with particular properties.¹⁷⁶ Each change in the path of the electrons results in a tangential emission of photons and loss of energy; some of this loss is restored in radio frequency accelerating cavities around the ring.¹⁷⁶ The emitted photons contain electromagnetic radiation ranging from the far-IR to hard X-rays, and they can be tuned to a desired wavelength using various optical devices and filters.¹⁷⁶ For more detailed explanations about synchrotron technology and recent advancements, see, for example, references 177 and 178.

The basic set-up for a hard X-ray experiment ($h\nu = 5\text{-}30$ keV) is illustrated in Figure 1.7. The incident X-ray beam (I_0) goes through an ion chamber detector (filled with $\text{N}_2(\text{g})$ or $\text{Ar}(\text{g})$) and then hits the sample. The transmitted light (I_1) is detected in a second ion chamber, providing the transmission data as I_1/I_0 . Next, the beam hits a reference sample corresponding to the element under investigation and the transmitted light (I_2) is detected in a third ion chamber, providing the reference transmission as I_2/I_1 . Fluorescence detection for the sample is also possible and this is particularly useful for dilute solution samples. The Ge detector has an array of germanium crystals that simultaneously collect fluorescence data, which are averaged together to reduce noise. The sample is

located in a vacuum chamber with a helium cryostat that maintains a constant low temperature (usually < 20 K), which helps prevent or reduce photoreduction of sensitive samples as well as minimise the disorder.

Figure 1.7 Basic XAS experimental set-up



1.4.5. Data Reduction and Analysis

Numerous steps are required to properly process and analyse XAS data and a variety of computer programs are available; to complete this thesis work, the programs employed were PeakFit¹⁷⁹ and SIXPack¹⁸⁰ (a graphical user interface that runs the command line program IFEFFIT¹⁸¹ using the ab initio code FEFF¹⁸²). The data must be carefully checked to ensure that there are no artificial features or distortions and that the noise level is acceptable. For fluorescence data, each channel corresponding to a Ge crystal is examined individually and then the data are averaged for that energy sweep.^{***} Two or more sweeps are required for each run (each experiment or sample) to ensure that the data are reproducible, that no photoreduction or photodegradation has occurred, and to reduce noise in the averaged spectra. For both transmission and fluorescence data, the sweeps of a run are averaged together, and the

^{***} One sweep corresponds to the energy scan from low to high energy for the relevant region, producing an XAS spectrum.

energy position is calibrated using a reference to allow comparisons to other data. Energy calibration usually assigns the lowest-energy inflection point (the lowest-energy maximum of the first derivative) of the reference spectra to the accepted threshold energy (E_0) value; for example, the ruthenium K-edge is set to 22117 eV for the Ru (0) reference foil.¹⁶⁴ The sweeps can be averaged before energy calibration if there is no energy shift during the run, that is, if all the spectra are overlapping. In the case of an energy shift during the run, which is particularly common if a lot of sweeps have been taken or if there has been a beam injection between sweeps, each sweep must be energy calibrated individually and then all sweeps are averaged.

The averaged spectra are processed in different ways to obtain useable XANES and EXAFS data. For the XANES region, smooth pre-edge and post-edge backgrounds are subtracted and the spectra are normalised such that the edge-step is set to unity. The intensity of the edge jump is concentration dependent; thus, normalisation is required to enable comparisons between different samples. At this point, spectra from different samples can be qualitatively compared in terms of the position and intensity of the pre-edge features and as well as the energy position of the inflection point of the rising edge. For a more quantitative comparison, the features of the spectra are individually fit with a software package such as PeakFit.¹⁷⁹

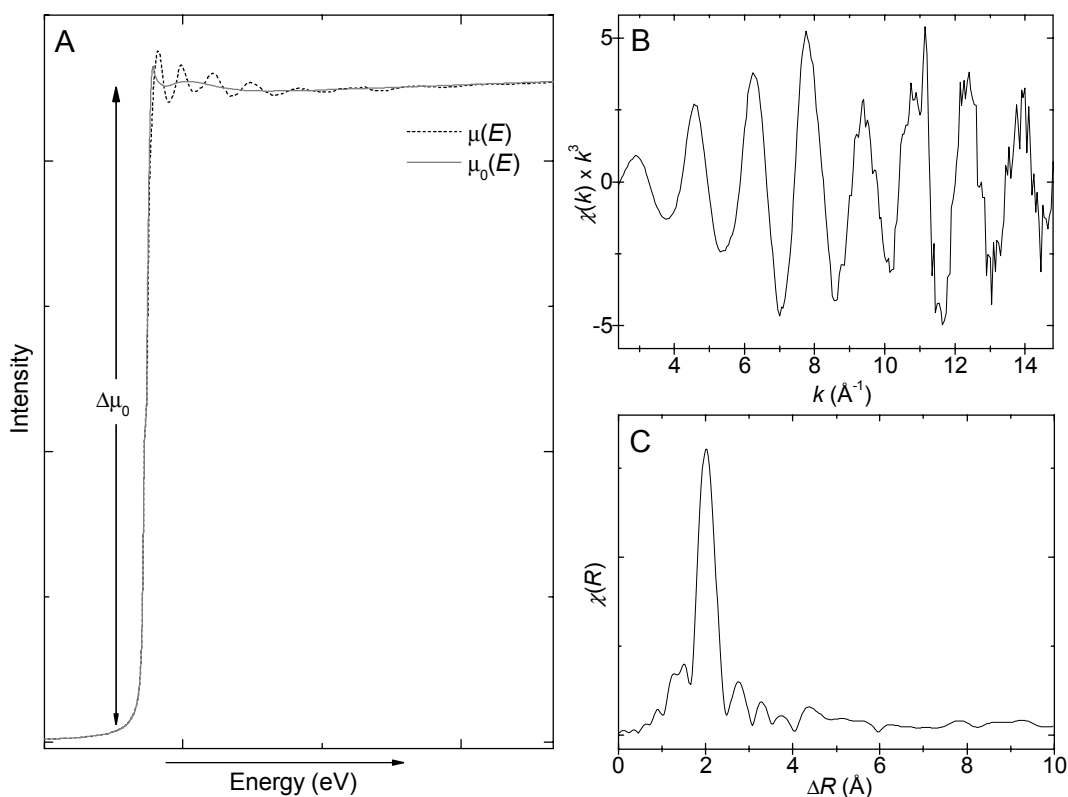
The EXAFS region has an oscillatory fine structure described by $\chi(E)$, which results from the photoelectron wave interfering with backscattering atoms. To process the data in this region, a smooth pre-edge function is first subtracted,

then $\chi(E)$ is extracted from the spectra by subtracting a smooth atomic background, $\mu_0(E)$ (spline function), from the total absorption coefficient, $\mu(E)$, and normalising to the edge jump of the smooth atomic-like background, $\Delta\mu_0$ (Equation 1.3; Figure 1.8: A).¹⁶⁵

Equation 1.3 Oscillatory fine structure, $\chi(E)$

$$\chi(E) = \frac{\mu(E) - \mu_0(E)}{\Delta\mu_0}$$

Figure 1.8 EXAFS data processing: spline function (A), k^3 -space (B) and R -space (B) plots



Once the $\chi(E)$ is isolated, the oscillations can be viewed and fit in k -space (\AA^{-1}), which is usually weighted as k^3 to enhance the dampened high k region (Figure 1.8: B).¹⁷⁵ The Fourier-Transform of the k -space plot results in a more conceptually-useful depiction in R -space (\AA) (Figure 1.8: C).¹⁶³ Although the R -

space plot is shifted and does not represent exact bond distances, examination ensures that the processing procedures have been successful and can indicate the relative number and distance of scattering atoms. To extract quantitative information from the EXAFS oscillations, some parameters are determined from model compounds or ab initio calculations. Those parameters are used for iterative data fitting.¹⁶³ Table 1.2 lists the variables that are commonly calculated and those that are refined during the fitting process. Because there is no unique fit for EXAFS data, refinements must be evaluated and compared statistically to find the best fit(s).

Table 1.2 Calculated and refined parameters in the EXAFS fitting routine

Calculated		Refined	
Backscattering amplitude function	$A_i(k)$	Interatomic distances	R_i
Total phase shift function	$\phi(k)$	Number of scatterers	N_i
Mean free path function	$\lambda(k)$	Disorder parameters	σ_i^2
		Amplitude reduction factor	S_0^2
		Threshold energy	E_0

1.5. Conclusion

Ruthenium-catalysed olefin metathesis is a very important reaction, yet the mechanistic details are not fully understood. In particular, the differences in reactivity between the first-generation complex (**1**; L = PCy₃) and second-generation complex (**2**; L = H₂IMes) have not been fully explained. The experimental and computational investigations of phosphines and N-heterocyclic carbenes have aimed to establish the electronic and steric parameters of these ligands, yet there remain uncertainties. Few spectroscopic studies have been applied to these systems and Ru K-edge XAS is a useful technique that has been employed in the work presented herein.

This introductory chapter has provided the background necessary to understand the work presented in the following chapters of this thesis. Chapters 2 to 4 each contain a description of one part of this work on ruthenium complexes of relevance to olefin metathesis. Chapter 5 is a general conclusion to the thesis and a discussion of related future work.

1.6. References

- (1) Fürstner, A. *Angew. Chem. Int. Ed.* **2000**, *39*, 3012-3043.
- (2) Trnka, T. M.; Grubbs, R. H. *Acc. Chem. Res.* **2001**, *34*, 18-29.
- (3) Grubbs, R. H. *Tetrahedron* **2004**, *60*, 7117-7140.
- (4) Katz, T. J. *Angew. Chem. Int. Ed.* **2005**, *44*, 3010-3019.
- (5) *Handbook of Metathesis*; Grubbs, R. H., Ed.; Wiley-VHC: Weinheim, 2003.
- (6) 2005 Nobel Prize in Chemistry.
http://nobelprize.org/nobel_prizes/chemistry/laureates/2005/index.html (accessed January 2008).
- (7) Kadota, I.; Takamura, H.; Sato, K.; Ohno, A.; Matsuda, K.; Yamamoto, Y. *J. Am. Chem. Soc.* **2003**, *125*, 46-47.
- (8) Yee, N. K.; Farina, V.; Houpis, I. N.; Haddad, N.; Frutos, R. P.; Gallou, F.; Wang, X. j.; Wei, X.; Simpson, R. D.; Feng, X.; Fuchs, V.; Xu, Y.; Tan, J.; Zhang, L.; Xu, J.; Smith-Keenan, L. L.; Vitous, J.; Ridges, M. D.; Spinelli, E. M.; Johnson, M.; Donsbach, K.; Nicola, T.; Brenner, M.; Winter, E.; Kreye, P.; Samstag, W. *J. Org. Chem.* **2006**, *71*, 7133-7145.
- (9) Nicola, T.; Brenner, M.; Donsbach, K.; Kreye, P. *Org. Process Res. Dev.* **2005**, *9*, 513-515.
- (10) White, S. R.; Sottos, N. R.; Geubelle, P. H.; Moore, J. S.; Kessler, M. R.; Sriram, S. R.; Brown, E. N.; Viswanathan, S. *Nature* **2001**, *409*, 794-797.
- (11) Rule, J. D.; Brown, E. N.; Sottos, N. R.; White, S. R.; Moore, J. S. *Adv. Mater.* **2005**, *17*, 205-208.
- (12) Mohr, B.; Sauvage, J.-P.; Grubbs, R. H.; Weck, M. *Angew. Chem. Int. Ed. Engl.* **1997**, *36*, 1308-1310.
- (13) Kilbinger, A. F. M.; Cantrill, S. J.; Waltman, A. W.; Day, M. W.; Grubbs, R. H. *Angew. Chem. Int. Ed.* **2003**, *42*, 3281-3285.
- (14) Guidry, E. N.; Cantrill, S. J.; Stoddart, J. F.; Grubbs, R. H. *Org. Lett.* **2005**, *7*, 2129-2132.
- (15) Harris, R. F.; Ricci, M. J.; Farrer, R. A.; Praino, J.; Miller, S. J.; Saleh, B. E. A.; Teich, M. C.; Fourkas, J. T. *Adv. Mater.* **2005**, *17*, 39-42.
- (16) Chen, W. Z.; Protasiewicz, J. D.; Davis, S. A.; Updegraff, J. B.; Ma, L. Q.; Fanwick, P. E.; Ren, T. *Inorg. Chem.* **2007**, *46*, 3775-3782.
- (17) Truett, W. L.; Johnson, D. R.; Robinson, I. M.; Montague, B. A. *J. Am. Chem. Soc.* **1960**, *82*, 2337-2340.
- (18) Natta, G.; Dall'Asta, G.; Mazzanti, G.; Motroni, G. *Makromol. Chem.* **1963**, *69*, 163-179.
- (19) Natta, G.; Dall'asta, G.; Motroni, G. *J. Polymer Sci., Polymer Lett.* **1964**, *B2*, 349-351.
- (20) Fischer, E. O.; Maasböl, A. *Angew. Chem. Int. Ed. Engl.* **1964**, *3*, 580-581.
- (21) Calderon, N.; Chen, H. Y.; Scott, K. W. *Tetrahedron Lett.* **1967**, *8*, 3327-3329.
- (22) Calderon, N.; Ofstead, E. A.; Ward, J. P.; Judy, W. A.; Scott, K. W. *J. Am. Chem. Soc.* **1968**, *90*, 4133-4140.
- (23) Bradshaw, C. P. C.; Howman, E. J.; Turner, L. *J. Catal.* **1967**, *7*, 269-276.
- (24) Banks, R. L.; Bailey, G. C. *J. Catal.* **1969**, *14*, 276-278.
- (25) Hérisson, J. L.; Chauvin, Y. *Makromol. Chem.* **1971**, *141*, 161-176.
- (26) Katz, T. J.; McGinnis, J. *J. Am. Chem. Soc.* **1975**, *97*, 1592-1594.
- (27) Katz, T. J.; Rothchild, R. *J. Am. Chem. Soc.* **1976**, *98*, 2519-2526.
- (28) Grubbs, R. H.; Carr, D. D.; Hoppin, C.; Burk, P. L. *J. Am. Chem. Soc.* **1976**, *98*, 3478-3483.
- (29) Grubbs, R. H.; Burk, P. L.; Carr, D. D. *J. Am. Chem. Soc.* **1975**, *97*, 3265-3267.
- (30) Casey, C. P.; Burkhardt, T. J. *J. Am. Chem. Soc.* **1973**, *95*, 5833-5834.
- (31) Lee, S. J.; McGinnis, J.; Katz, T. J. *J. Am. Chem. Soc.* **1976**, *98*, 7818-7819.
- (32) McGinnis, J.; Katz, T. J.; Hurwitz, S. *J. Am. Chem. Soc.* **1976**, *98*, 605-606.
- (33) Katz, T. J.; Acton, N. *Tetrahedron Lett.* **1976**, *17*, 4251-4254.
- (34) Tebbe, F. N.; Parshall, G. W.; Reddy, G. S. *J. Am. Chem. Soc.* **1978**, *100*, 3611-3613.
- (35) Howard, T. R.; Lee, J. B.; Grubbs, R. H. *J. Am. Chem. Soc.* **1980**, *102*, 6876-6878.

- (36) Schrock, R.; Rocklage, S.; Wengrovius, J.; Rupprecht, G.; Fellmann, J. *J. Mol. Catal.* **1980**, *8*, 73-83.
- (37) Schrock, R. R.; DePue, R. T.; Feldman, J.; Schaverien, C. J.; Dewan, J. C.; Liu, A. H. *J. Am. Chem. Soc.* **1988**, *110*, 1423-1435.
- (38) Schrock, R. R.; Murdzek, J. S.; Bazan, G. C.; Robbins, J.; DiMare, M.; O'Regan, M. J. *Am. Chem. Soc.* **1990**, *112*, 3875-3886.
- (39) Fu, G. C.; Grubbs, R. H. *J. Am. Chem. Soc.* **1992**, *114*, 7324-7325.
- (40) Fu, G. C.; Grubbs, R. H. *J. Am. Chem. Soc.* **1992**, *114*, 5426-5427.
- (41) Oskam, J. H.; Schrock, R. R. *J. Am. Chem. Soc.* **1992**, *114*, 7588-7590.
- (42) Michelotti, F. W.; Keaveney, W. P. *J. Polym. Sci. Part A* **1965**, *3*, 895-905.
- (43) Novak, B. M.; Grubbs, R. H. *J. Am. Chem. Soc.* **1988**, *110*, 960-961.
- (44) Novak, B. M.; Grubbs, R. H. *J. Am. Chem. Soc.* **1988**, *110*, 7542-7543.
- (45) Nguyen, S. T.; Johnson, L. K.; Grubbs, R. H.; Ziller, J. W. *J. Am. Chem. Soc.* **1992**, *114*, 3974-3975.
- (46) Nguyen, S. T.; Grubbs, R. H.; Ziller, J. W. *J. Am. Chem. Soc.* **1993**, *115*, 9858-9859.
- (47) Schwab, P.; Grubbs, R. H.; Ziller, J. W. *J. Am. Chem. Soc.* **1996**, *118*, 100-110.
- (48) Schwab, P.; France, M. B.; Ziller, J. W.; Grubbs, R. H. *Angew. Chem. Int. Ed. Engl.* **1995**, *34*, 2039-2041.
- (49) Dias, E. L.; Nguyen, S. T.; Grubbs, R. H. *J. Am. Chem. Soc.* **1997**, *119*, 3887-3897.
- (50) Sanford, M. S.; Love, J. A.; Grubbs, R. H. *J. Am. Chem. Soc.* **2001**, *123*, 6543-6554.
- (51) Sanford, M. S.; Ulman, M.; Grubbs, R. H. *J. Am. Chem. Soc.* **2001**, *123*, 749-750.
- (52) Chianese, A. R.; Li, X.; Janzen, M. C.; Faller, J. W.; Crabtree, R. H. *Organometallics* **2003**, *22*, 1663-1667.
- (53) Diggle, R. A.; Macgregor, S. A.; Whittlesey, M. K. *Organometallics* **2004**, *23*, 1857-1865.
- (54) Lee, M. T.; Hu, C. H. *Organometallics* **2004**, *23*, 976-983.
- (55) Magill, A. M.; Cavell, K. J.; Yates, B. F. *J. Am. Chem. Soc.* **2004**, *126*, 8717-8724.
- (56) Crabtree, R. H. *J. Organomet. Chem.* **2005**, *690*, 5451-5457.
- (57) Dorta, R.; Stevens, E. D.; Scott, N. M.; Costabile, C.; Cavallo, L.; Hoff, C. D.; Nolan, S. P. *J. Am. Chem. Soc.* **2005**, *127*, 2485-2495.
- (58) Ackermann, L.; Furstner, A.; Weskamp, T.; Kohl, F. J.; Herrmann, W. A. *Tetrahedron Lett.* **1999**, *40*, 4787-4790.
- (59) Chatterjee, A. K.; Grubbs, R. H. *Org. Lett.* **1999**, *1*, 1751-1753.
- (60) Huang, J.; Schanz, H. J.; Stevens, E. D.; Nolan, S. P. *Organometallics* **1999**, *18*, 5375-5380.
- (61) Huang, J. K.; Stevens, E. D.; Nolan, S. P.; Petersen, J. L. *J. Am. Chem. Soc.* **1999**, *121*, 2674-2678.
- (62) Scholl, M.; Ding, S.; Lee, C. W.; Grubbs, R. H. *Org. Lett.* **1999**, *1*, 953-956.
- (63) Scholl, M.; Trnka, T. M.; Morgan, J. P.; Grubbs, R. H. *Tetrahedron Lett.* **1999**, *40*, 2247-2250.
- (64) Weskamp, T.; Kohl, F. J.; Herrmann, W. A. *J. Organomet. Chem.* **1999**, *582*, 362-365.
- (65) Weskamp, T.; Kohl, F. J.; Hieringer, W.; Gleich, D.; Herrmann, W. A. *Angew. Chem. Int. Ed.* **1999**, *38*, 2416-2419.
- (66) Bielawski, C. W.; Robert H. Grubbs *Angew. Chem. Int. Ed.* **2000**, *39*, 2903-2906.
- (67) Chatterjee, A. K.; Morgan, J. P.; Scholl, M.; Grubbs, R. H. *J. Am. Chem. Soc.* **2000**, *122*, 3783-3784.
- (68) Love, J. A.; Sanford, M. S.; Day, M. W.; Grubbs, R. H. *J. Am. Chem. Soc.* **2003**, *125*, 10103-10109.
- (69) Adlhart, C.; Chen, P. *Helv. Chim. Acta* **2003**, *86*, 941-949.
- (70) Straub, B. F. *Angew. Chem. Int. Ed.* **2005**, *44*, 5974-5978.
- (71) Sanford, M. S.; Love, J. A.; Grubbs, R. H. *Organometallics* **2001**, *20*, 5314-5318.
- (72) Love, J. A.; Morgan, J. P.; Trnka, T. M.; Grubbs, R. H. *Angew. Chem. Int. Ed.* **2002**, *41*, 4035-4037.
- (73) Trnka, T. M.; Dias, E. L.; Day, M. W.; Grubbs, R. H. *Arkivoc* **2002**, *13*, 28-41.
- (74) Hong, S. H.; Wenzel, A. G.; Salguero, T. T.; Day, M. W.; Grubbs, R. H. *J. Am. Chem. Soc.* **2007**, *129*, 7961-7968.

- (75) Carlson, R. G.; Gile, M. A.; Heppert, J. A.; Mason, M. H.; Powell, D. R.; Velde, D. V.; Vilain, J. M. *J. Am. Chem. Soc.* **2002**, *124*, 1580-1581.
- (76) Macnaughtan, M. L.; Johnson, M. J. A.; Kampf, J. W. *J. Am. Chem. Soc.* **2007**, *129*, 7708-7709.
- (77) Macnaughtan, M. L.; Johnson, M. J. A.; Kampf, J. W. *Organometallics* **2007**, *26*, 780-782.
- (78) Romero, P. E.; Piers, W. E.; McDonald, R. *Angew. Chem. Int. Ed.* **2004**, *43*, 6161-6165.
- (79) Dubberley, S. R.; Romero, P. E.; Piers, W. E.; McDonald, R.; Parvez, M. *Inorg. Chim. Acta* **2006**, *359*, 2658-2664.
- (80) Sanford, M. S.; Henling, L. M.; Day, M. W.; Grubbs, R. H. *Angew. Chem. Int. Ed.* **2000**, *39*, 3451-3453.
- (81) Hinderling, C.; Adlhart, C.; Chen, P. *Angew. Chem. Int. Ed.* **1998**, *37*, 2685-2689.
- (82) Adlhart, C.; Hinderling, C.; Baumann, H.; Chen, P. *J. Am. Chem. Soc.* **2000**, *122*, 8204-8214.
- (83) Adlhart, C.; Chen, P. *Helv. Chim. Acta* **2000**, *83*, 2192-2196.
- (84) Kunkely, H.; Vogler, A. *Inorg. Chim. Acta* **2001**, *325*, 179-181.
- (85) Trnka, T. M.; Day, M. W.; Grubbs, R. H. *Organometallics* **2001**, *20*, 3845-3847.
- (86) Anderson, D. R.; Hickstein, D. D.; O'Leary, D. J.; Grubbs, R. H. *J. Am. Chem. Soc.* **2006**, *128*, 8386-8387.
- (87) Tallarico, J. A.; Bonitatebus, P. J.; Snapper, M. L. *J. Am. Chem. Soc.* **1997**, *119*, 7157-7158.
- (88) Romero, P. E.; Piers, W. E. *J. Am. Chem. Soc.* **2005**, *127*, 5032-5033.
- (89) Romero, P. E.; Piers, W. E. *J. Am. Chem. Soc.* **2007**, *129*, 1698-1704.
- (90) Wenzel, A. G.; Grubbs, R. H. *J. Am. Chem. Soc.* **2006**, *128*, 16048-16049.
- (91) Correa, A.; Cavallo, L. *J. Am. Chem. Soc.* **2006**, *128*, 13352-13353.
- (92) Adlhart, C.; Chen, P. *J. Am. Chem. Soc.* **2004**, *126*, 3496-3510.
- (93) Suresh, C. H.; Baik, M.-H. *Dalton Trans.* **2005**, 2982-2984.
- (94) Lord, R. L.; Wang, H.; Vieweger, M.; Baik, M.-H. *J. Organomet. Chem.* **2006**, *691*, 5505-5512.
- (95) Webster, C. E. *J. Am. Chem. Soc.* **2007**, *129*, 7490-7491.
- (96) Aagaard, O. M.; Meier, R. J.; Buda, F. *J. Am. Chem. Soc.* **1998**, *120*, 7174-7182.
- (97) Adlhart, C.; Chen, P. *Angew. Chem. Int. Ed.* **2002**, *41*, 4484-4487.
- (98) Cavallo, L. *J. Am. Chem. Soc.* **2002**, *124*, 8965-8973.
- (99) Vyboishchikov, S. F.; Bühl, M.; Thiel, W. *Chem. Eur. J.* **2002**, *8*, 3962-3975.
- (100) Fomine, S.; Vargas, S. M.; Tlenkopatchev, M. A. *Organometallics* **2003**, *22*, 93-99.
- (101) Suresh, C. H.; Koga, N. *Organometallics* **2004**, *23*, 76-80.
- (102) Benitez, D.; Goddard III, W. A. *J. Am. Chem. Soc.* **2005**, *127*, 12218-12219.
- (103) van Rensburg, W. J.; Steynberg, P. J.; Kirk, M. M.; Meyer, W. H.; Forman, G. S. *J. Organomet. Chem.* **2006**, *691*, 5312-5325.
- (104) Fomine, S.; Tlenkopatchev, M. A. *Organometallics* **2007**, *26*, 4491-4497.
- (105) Krapp, A.; Pandey, K. K.; Frenking, G. *J. Am. Chem. Soc.* **2007**, *129*, 7596-7610.
- (106) Wong, C.-Y.; Chan, M. C. W.; Zhu, N.; Che, C.-M. *Organometallics* **2004**, *23*, 2263-2272.
- (107) Delgado-Jaime, M. U.; Conrad, J. C.; Fogg, D. E.; Kennepohl, P. *Inorg. Chim. Acta* **2006**, *359*, 3042-3047.
- (108) Kunkely, H.; Vogler, A. *Inorg. Chem. Commun.* **2007**, *10*, 117-119.
- (109) Tolman, C. A. *J. Am. Chem. Soc.* **1970**, *92*, 2953-2956.
- (110) Tolman, C. A. *J. Am. Chem. Soc.* **1970**, *92*, 2956-2965.
- (111) Tolman, C. A. *Chem. Rev.* **1977**, *77*, 313-348.
- (112) *Inorganic Chemistry: Principles of Structure and Reactivity, Fourth Edition* Huheey, J. E.; Keiter, E. A.; Keiter, R. L., Eds.; HarperCollins: New York, 1993.
- (113) Frenking, G.; Wichmann, K.; Frohlich, N.; Grobe, J.; Golla, W.; Van, D. L.; Krebs, B.; Lage, M. *Organometallics* **2002**, *21*, 2921-2930.
- (114) Marynick, D. S. *J. Am. Chem. Soc.* **1984**, *106*, 4064-4065.
- (115) Pacchioni, G.; Bagus, P. S. *Inorg. Chem.* **1992**, *31*, 4391-4398.
- (116) Golovin, M. N.; Rahman, M. M.; Belmonte, J. E.; Giering, W. P. *Organometallics* **1985**, *4*, 1981-1991.

- (117) Rahman, M. M. L.; Hong Ye; Eriks, K.; Prock, A.; Giering, W. P. *Organometallics* **1989**, *8*, 1-7.
- (118) Hammett, L. P. *J. Am. Chem. Soc.* **1937**, *59*, 96-103.
- (119) Cobley, C. J.; Pringle, P. G. *Inorg. Chim. Acta* **1997**, *265*, 107-115.
- (120) Alyea, E. C.; Song, S. *Comments Inorg. Chem.* **1996**, *18*, 189-221.
- (121) Drago, R. S.; Joerg, S. *J. Am. Chem. Soc.* **1996**, *118*, 2654-2663.
- (122) Fernandez, A.; Reyes, C.; Wilson, M. R.; Woska, D. C.; Prock, A.; Giering, W. P. *Organometallics* **1997**, *16*, 342-348.
- (123) Fernandez, A. L.; Lee, T. Y.; Reyes, C.; Prock, A.; Giering, W. P. *Organometallics* **1998**, *17*, 3169-3175.
- (124) Joerg, S.; Drago, R. S.; Sales, J. *Organometallics* **1998**, *17*, 589-599.
- (125) Woska, D.; Prock, A.; Giering, W. P. *Organometallics* **2000**, *19*, 4629-4638.
- (126) Suresh, C. H.; Koga, N. *Inorg. Chem.* **2002**, *41*, 1573-1578.
- (127) Giering, W. P.; Prock, A.; Fernandez, A. L. *Inorg. Chem.* **2003**, *42*, 8033-8037.
- (128) Wanzlick, H.-W.; Schönherr, H. *J. Angew. Chem. Int. Ed. Engl.* **1968**, *7*, 141-142.
- (129) Öfele, K. *J. Organomet. Chem.* **1968**, *12*, P42-P43.
- (130) Arduengo III, A. J.; Harlow, R. L.; Kline, M. *J. Am. Chem. Soc.* **1991**, *113*, 361-363.
- (131) *N-Heterocyclic Carbenes in Transition Metal Catalysis*; Glorius, F., Ed.; Springer: Berlin, 2007.
- (132) Herrmann, W. A. *Angew. Chem. Int. Ed.* **2002**, *41*, 1291-1309.
- (133) Cavallo, L.; Correa, A.; Costabile, C.; Jacobsen, H. *J. Organomet. Chem.* **2005**, *690*, 5407-5413.
- (134) Arduengo III, A. J.; Dias, H. V. R.; Harlow, R. L.; Kline, M. *J. Am. Chem. Soc.* **1992**, *114*, 5530-5534.
- (135) Herrmann, W. A.; Runte, O.; Artus, G. *J. Organomet. Chem.* **1995**, *501*, C1-C4.
- (136) Green, J. C.; Scurr, R. G.; Arnold, P. L.; Geoffrey, F.; Cloke, N. *Chem. Commun.* **1997**, 1963-1964.
- (137) Bourissou, D.; Guerret, O.; Gabbai, F. P.; Bertrand, G. *Chem. Rev.* **2000**, *100*, 39-92.
- (138) Green, J. C.; Herbert, B. *J. Dalton Trans.* **2005**, 1214-1220.
- (139) Heinemann, C.; Müller, T.; Apeloig, Y.; Schwarz, H. *J. Am. Chem. Soc.* **1996**, *118*, 2023-2038.
- (140) Herrmann, W. A.; Köcher, C. *Angew. Chem. Int. Ed.* **1997**, *36*, 2162-2187.
- (141) Boehme, C.; Frenking, G. *Organometallics* **1998**, *17*, 5801-5809.
- (142) Boehme, C.; Frenking, G. *J. Am. Chem. Soc.* **1996**, *118*, 2039-2046.
- (143) Niehues, M.; Erker, G.; Kehr, G.; Schwab, P.; Frohlich, R.; Blacque, O.; Berke, H. *Organometallics* **2002**, *21*, 2905-2911.
- (144) Termaten, A. T.; Schakel, M.; Ehlers, A. W.; Lutz, M.; Spek, A. L.; Lammertsma, K. *Chem. Eur. J.* **2003**, *9*, 3577-3582.
- (145) Frohlich, N.; Pidun, U.; Stahl, M.; Frenking, G. *Organometallics* **1997**, *16*, 442-448.
- (146) Fantasia, S.; Petersen, J. L.; Jacobsen, H.; Cavallo, L.; Nolan, S. P. *Organometallics* **2007**, *26*, 5880-5889.
- (147) Diez-Gonzalez, S.; Nolan, S. P. *Coord. Chem. Rev.* **2007**, *251*, 874-883.
- (148) Kelly III, R. A.; Clavier, H.; Giudice, S.; Scott, N. M.; Stevens, E. D.; Bordner, J.; Samardjiev, I.; Hoff, C. D.; Cavallo, L.; Nolan, S. P. *Organometallics* **2008**, *27*, 202-210.
- (149) Herrmann, W. A.; Schutz, J.; Frey, G. D.; Herdtweck, E. *Organometallics* **2006**, *25*, 2437-2448.
- (150) Garrison, J. C.; Simons, R. S.; Kofron, W. G.; Tessier, C. A.; Youngs, W. J. *Chem. Commun.* **2001**, 1780-1781.
- (151) Scott, N. M.; Dorta, R.; Stevens, E. D.; Correa, A.; Cavallo, L.; Nolan, S. P. *J. Am. Chem. Soc.* **2005**, *127*, 3516-3526.
- (152) Süßner, M.; Plenio, H. *Chem. Commun.* **2005**, 5417-5419.
- (153) Tulloch, A. A. D.; Danopoulos, A. A.; Kleinhenz, S.; Light, M. E.; Hursthouse, M. B.; Eastham, G. *Organometallics* **2001**, *20*, 2027-2031.
- (154) Tafipolsky, M.; Scherer, W.; Öfele, K.; Artus, G.; Pedersen, B.; Herrmann, W. A.; McGrady, G. S. *J. Am. Chem. Soc.* **2002**, *124*, 5865-5880.
- (155) Hu, X.; Tang, Y.; Gantzel, P.; Meyer, K. *Organometallics* **2003**, *22*, 612-614.

- (156) Hu, X.; Castro-Rodriguez, I.; Olsen, K.; Meyer, K. *Organometallics* **2004**, *23*, 755-764.
- (157) Nemcsok, D.; Wichmann, K.; Frenking, G. *Organometallics* **2004**, *23*, 3640-3646.
- (158) Jacobsen, H.; Correa, A.; Costabile, C.; Cavallo, L. *J. Organomet. Chem.* **2006**, *691*, 4350-4358.
- (159) Sanderson, M. D.; Kamplain, J. W.; Bielawski, C. W. *J. Am. Chem. Soc.* **2006**, *128*, 16514-16515.
- (160) Khramov, D. M.; Lynch, V. M.; Bielawski, C. W. *Organometallics* **2007**, *26*, 6042-6049.
- (161) Frenking, G.; Wichmann, K.; Frohlich, N.; Loschen, C.; Lein, M.; Frunzke, J.; Rayon, V. M. *Coord. Chem. Rev.* **2003**, *238-239*, 55-82.
- (162) *International Union of Pure and Applied Chemistry: Quantities, Units and Symbols in Physical Chemistry, 2nd edition*; Mills, I.; Cvitas, T.; Homann, K.; Kallay, N.; Kuchitsu, K., Eds.; Blackwell Science: Oxford, 1993.
- (163) Penner-Hahn, J. E. *Coord. Chem. Rev.* **2005**, *249*, 161-177.
- (164) *X-ray Data Booklet*; Thompson, A.; Vaughan, D., Eds.; Lawrence Berkeley National Laboratory: Berkeley, 2001.
- (165) Wende, H. *Rep. Prog. Phys.* **2004**, *67*, 2105-2181.
- (166) Westre, T. E.; Kennepohl, P.; DeWitt, J. G.; Hedman, B.; Hodgson, K. O.; Solomon, E. I. *J. Am. Chem. Soc.* **1997**, *119*, 6297-6314.
- (167) Hahn, J. E.; Scott, R. A.; Hodgson, K. O.; Doniach, S.; Desjardins, S. R.; Solomon, E. I. *Chem. Phys. Lett.* **1982**, *88*, 595-598.
- (168) Bair, R. A.; Goddard III, W. A. *Phys. Rev. B* **1980**, *22*, 2767-2776.
- (169) Brouder, C. *J. Phys.: Condens. Matter* **1990**, *2*, 701-738.
- (170) Shulman, R. G.; Yafet, Y.; Eisenberger, P.; Blumberg, W. E. *Proc. Natl. Acad. Sci. U.S.A.* **1976**, *73*, 1384-1388.
- (171) Roe, A. L.; Schneider, D. J.; Mayer, R. J.; Pyrz, J. W.; Widom, J.; Que, L. *J. Am. Chem. Soc.* **1984**, *106*, 1676-1681.
- (172) Randall, C. R.; Shu, L.; Chiou, Y.-M.; Hagen, K. S.; Ito, M.; Kitajima, N.; Lachicotte, R. J.; Zang, Y.; Que, L. *Inorg. Chem.* **1995**, *34*, 1036-1039.
- (173) DuBois, J. L.; Mukherjee, P.; Stack, T. D. P.; Hedman, B.; Solomon, E. I.; Hodgson, K. O. *J. Am. Chem. Soc.* **2000**, *122*, 5775-5787.
- (174) de Groot, F. *Chem. Rev.* **2001**, *101*, 1779-1808.
- (175) Zhang, H. H.; Hedman, B.; Hodgson, K. O. In *Inorganic Electronic Structure and Spectroscopy, Volume I: Methodology*; Solomon, E. I., Lever, A. B. P., Eds.; John Wiley & Sons: New York, 1999, p 513-554.
- (176) Solomon, E. I. *Coord. Chem. Rev.* **2005**, *249*, 1-2.
- (177) Duke, P. J. *Synchrotron Radiation: Production and Properties*; Oxford University Press: Oxford, 2000.
- (178) Clarke, J. A. *The Science and Technology of Undulators and Wigglers*; Oxford University Press: Oxford, 2004.
- (179) PeakFit4.12; SeaSolve Software Inc, 2003.
- (180) Webb, S. M. *Phys. Scr.* **2005**, *T115*, 1011-1014.
- (181) Newville, M. *J. Synchrotron Rad.* **2001**, *8*, 322-324.
- (182) Rehr, J. J.; Ankudinov, A. L. *J. Synchrotron Rad.* **2003**, *10*, 43-45.

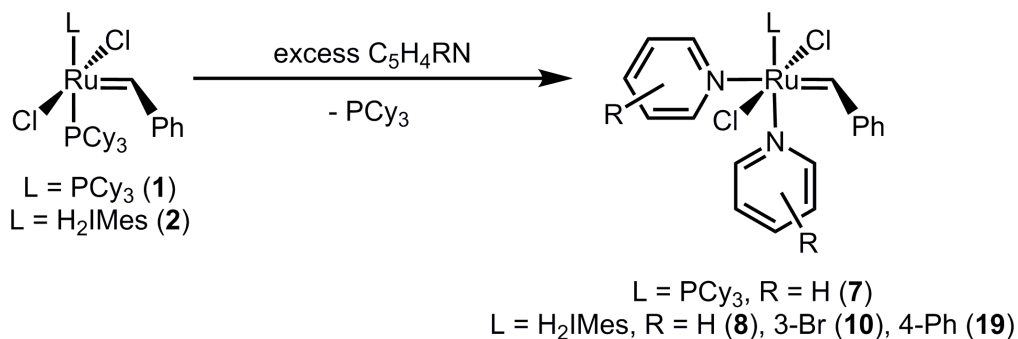
CHAPTER 2: BISPYRIDINE RUTHENIUM BENZYLIDENE

SYNTHESIS*

2.1. Introduction

Ruthenium-catalysed olefin metathesis is a broadly successful carbon-carbon bond-forming method.¹⁻⁵ The ruthenium complexes that catalyse metathesis are typically four-, five-, or six-coordinate ruthenium-alkylidene complexes. The commercially-available five-coordinate Grubbs complexes **1** and **2** react with excess unsubstituted or monosubstituted pyridine to form six-coordinate bispyridine analogues that contain two pyridine ligands in place of one phosphine ligand. Four of these complexes have been synthesised by Grubbs and coworkers (Scheme 2.1).⁶⁻⁸ Interestingly, kinetic data indicate that this ligand-exchange reaction is associative in contrast to the initiation step of the olefin metathesis mechanism, which is dissociative.⁶

Scheme 2.1 Synthesis of bispyridine ruthenium-benzylidene complexes by Grubbs and coworkers



* A version of this chapter has been published. Getty, K.; Delgado-Jaime, M. U.; Kennepohl, P., Assignment of Pre-edge Features in the Ru K-edge X-ray Absorption Spectra of Organometallic Ruthenium Complexes. *Inorg. Chim. Acta* **2008**, *361*, 1059-1065.

Compound **8** is a convenient precursor for complexes analogous to **2** with a variety of PR_3 ligands.⁶ These transformations are possible through direct exchange; however, faster reactions and higher yields can be obtained via the bispyridine complex (**8**).⁶ Additionally, the chloride ligands of **8** are more substitutionally labile than those of **2**, permitting the formation of an array of new complexes,^{6,9} such as the four-coordinate compound: $\text{H}_2\text{IMes}(\text{O}^t\text{Bu})_2\text{Ru}=\text{CHPh}$ (**23**; see Section 1.2.9).⁶

The bispyridine ruthenium benzylidenes avoid some of the problems with the precursor complexes; specifically, the propensity for re-association of phosphine by the first-generation complex **1** and slow initiation of the second-generation complex **2**.⁷ Indeed, the bispyridine complexes (sometimes referred to as third-generation Grubbs catalysts) exhibit rapid initiation⁷ and no possibility for re-associated phosphine as well as apparently low rates of pyridine re-association. Despite these benefits, the complexes tend to be unstable in solution and often degrade after only a few catalytic turnovers as they cannot sustain the propagating methyldiene species in the metathesis mechanism.^{8,10}

The monopyridine analogue of compound **7** was found to have poor RCM activity in which initiation was rapid, but the propagating species decomposed quickly, even with the addition of excess pyridine.⁸ Grubbs and coworkers also investigated the ROMP and CM catalytic activities of three second-generation bispyridines ($\text{R} = \text{H}$ (**8**), 3-Br (**10**), 4-Ph (**19**)).⁷ Complex **10** has the highest catalytic activity presumably because it favours turnover conditions by rapid dissociation, slows re-association of the 3-bromopyridine ligands, or both.⁷

Complex **10** catalyses the controlled living polymerisation of norbornene and oxo-norbornene derivatives with higher activity and better control than complex **2**.¹¹ Recently, complex **8** has been successfully employed in the tandem ROMP–hydrogenation synthesis of functionalised polynorbornenes.¹²

Because the metathesis activity of these complexes varies substantially for differently-substituted pyridines, we anticipated that corresponding changes may be observable in the spectroscopic data of such compounds (See Chapters 3 & 4); thus, we proceeded to synthesise a series of bispyridine ruthenium benzylidenes as described herein.

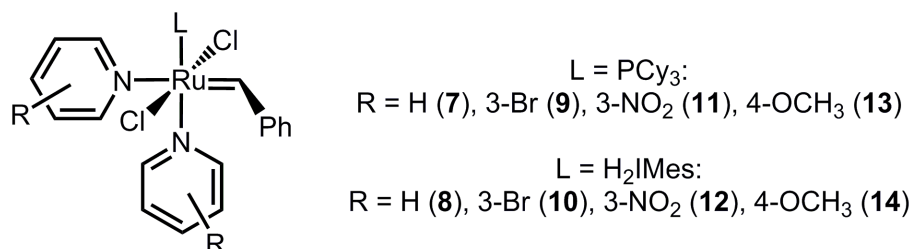
2.2. Results and Discussion

Eight bispyridine ruthenium-benzylidene complexes (**7** to **14**; Chart 2.1) were synthesised and characterised in an analogous manner to published procedures⁶⁻⁸ for **7**, **8**, **10** and **19**. The colour changes are immediate and the reactions are complete within 10 minutes at room temperature by adding a large excess[†] of the appropriate pyridine to complexes **1** or **2**. With pyridine and 3-bromopyridine, the reactions can be carried out neat or in toluene. 4-Methoxypyridine is not sufficiently miscible with pentane to allow precipitation of the product; therefore, toluene was used as the primary solvent in those reactions. Toluene was also used as the solvent for reactions with 3-nitropyridine, which is a solid at room temperature. Pentane was used for precipitation and washing of all products; ether was also used to wash

[†] 40 to 100 molar equiv of the various pyridines were used. 10 equiv are sufficient for the second-generation complexes, but did not provide complete conversion for the first-generation complexes.

complexes **11** & **12** because the solid 3-nitropyridine is not very soluble in pentane. Washing with ether allows isolation of the pure product, but tended to reduce the yield relative to other complexes.

Chart 2.1 Bispyridine ruthenium-benzylidene complexes synthesised in this work



The benzylidene proton (Ru=CHPh) of ruthenium-benzylidene complexes is very deshielded; thus the ¹H NMR signal for this proton is far downfield (between 18 and 21 ppm). This feature is useful for determining the purity of the complexes because it is completely separated from all other signals. Additionally, the NMR shifts may correlate with the electron-donating or electron-withdrawing properties of the particular pyridine ligand (Table 2.1). According to Hammett substituent constants,¹³ the order from electron-donating to electron-withdrawing pyridine substituents is: R = 4-OCH₃ (**13** & **14**), H (**7** & **8**), 3-Br (**9** & **10**), 3-NO₂ (**11** & **12**). For the first-generation bispyridines, the ¹H NMR signals for the benzylidene protons exhibit an upfield shift with increasing electron-withdrawing character of the pyridine substituent. The changes are smaller in the second-generation bispyridines and this trend is in a slightly different order with R = H and R = 4-OCH₃ reversed. The apparent trend is opposite what might be expected because a more electron-withdrawing ligand should provide less electron density to the metal centre, which may then accept more electron

density from the benzylidene, resulting in a downfield shift. Similarly, the benzylidene signals for the monopyridine analogues of **8**, **10** and **12** appear upfield to the bispyridine, which is contrary to expectations for a complex that has lost an electron-donating ligand. At this point, it is unclear how the electronic structure of the complex changes in response to these ligand modifications and whether the benzylidene signal is a useful measure of differences. The ^{31}P NMR signal corresponding to tricyclohexylphosphine in the first-generation complexes follows the expected trend: a downfield shift with increasing electron-withdrawing character of the pyridine substituent. Because the phosphorus atoms are directly bound to the ruthenium centres, they may be more sensitive than the benzylidene protons to the electronic properties of the other ligands.

Table 2.1 Hammett substituent constants, benzylidene ^1H NMR signals, and PCy_3 ^{31}P NMR signals for complexes **7-14**

Complex Number	R	Hammett Substituent Constant (σ) ^a	^1H NMR Benzylidene Signal	^{31}P NMR Signal
13	4-OCH ₃	-0.27	19.97	35.96
7	H	0.00	19.90	36.90
9	3-Br	0.39	19.70	38.78
11	3-NO ₂	0.71	19.67	39.55
14	4-OCH ₃	-0.27	19.11	-
8	H	0.00	19.14	-
10	3-Br	0.39	19.07	-
12	3-NO ₂	0.71	19.05	-

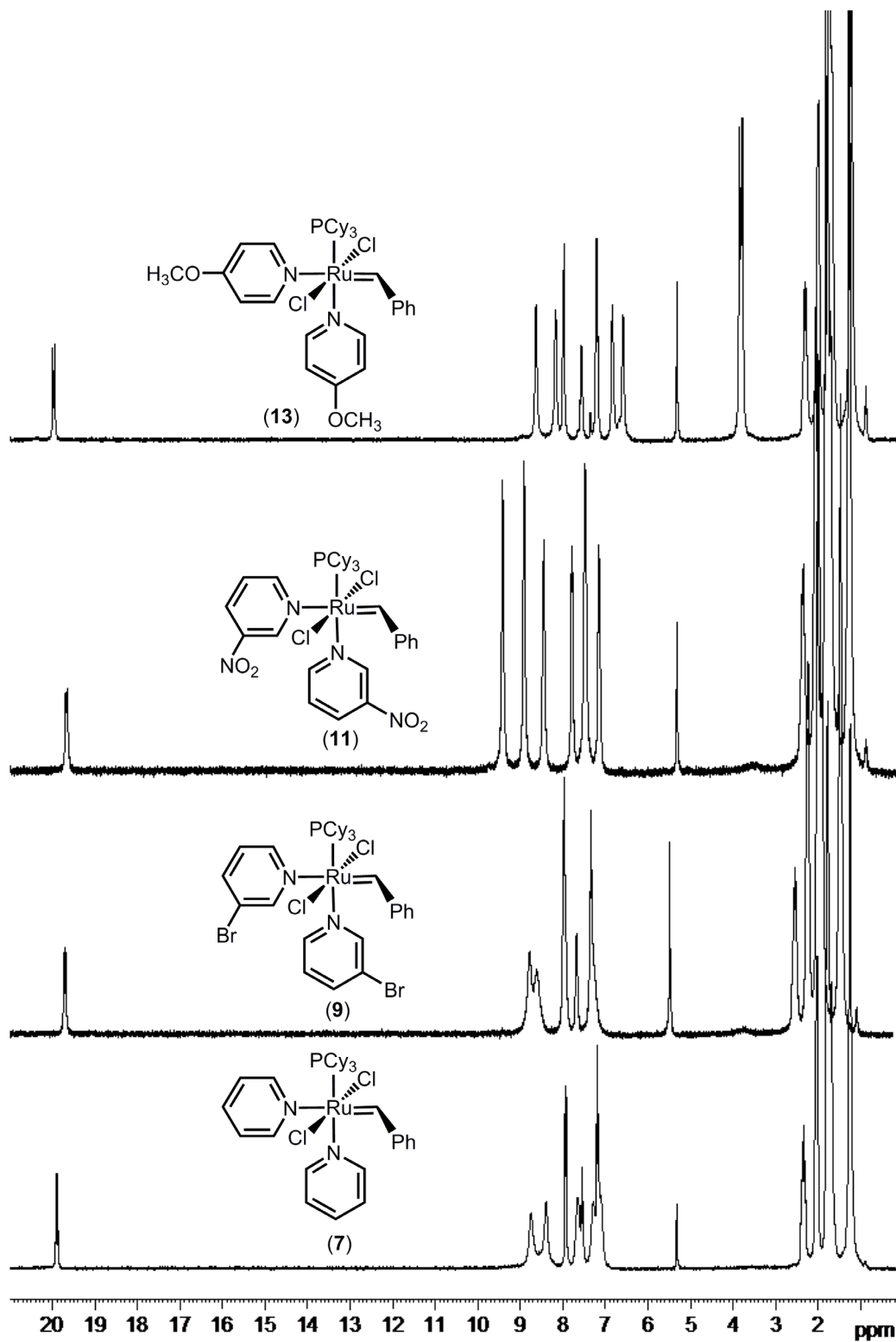
^a The Hammett substituent constants correspond to *meta*- (3) or *para*- (4) substitution as appropriate; values obtained from reference 13.

Figure 2.1 (first-generation) and Figure 2.2 (second-generation) show the ^1H NMR spectra of the bispyridine ruthenium-benzylidene complexes. The H–P coupling of the benzylidene proton in the first-generation bispyridine complexes was verified by phosphorus-decoupled proton ($^1\text{H}\{^{31}\text{P}\}$) NMR spectra in which

the benzylidene proton is observed as a singlet. The ^1H NMR spectra of complexes **8**, **10** and **12** contain a second small singlet[‡] in the benzylidene region (δ 18.53), which is likely due to the monopyridine analogue. The CHN elemental analyses for the solid samples are consistent with the bispyridine adducts and the signal is not present when pyridine- d_5 is used as the NMR solvent. These observations suggest that one pyridine ligand is somewhat more labile than the other, a finding that is consistent with previous reports.^{6,7}

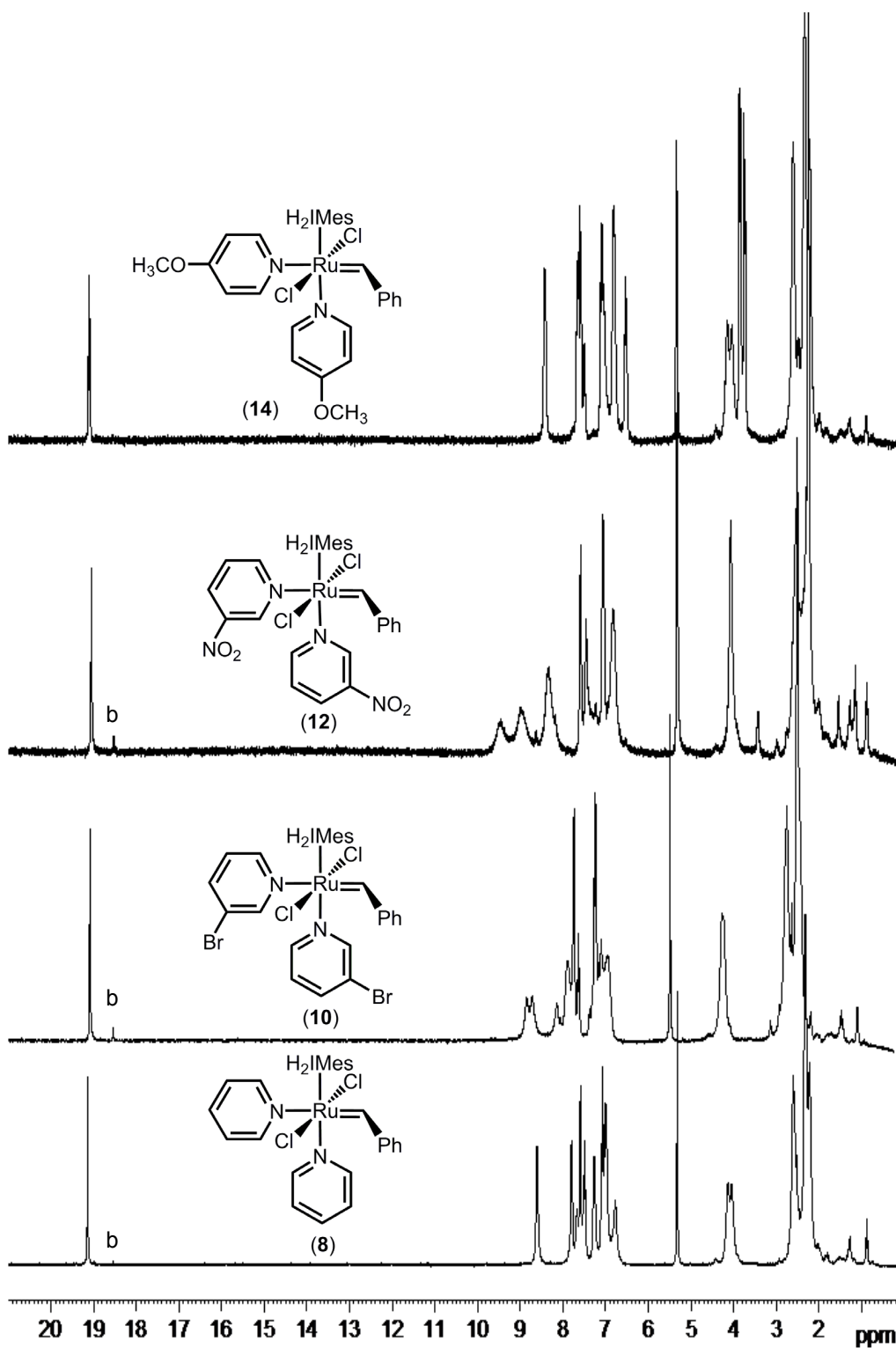
[‡] The additional singlet usually corresponds to $\leq 5\%$ of total benzylidene signal

Figure 2.1 ^1H NMR spectra of first-generation bispyridine ruthenium-benzylidene complexes^a



^a NMR spectra were collected at ambient temperature in dichloromethane- d_2 at 300 MHz.

Figure 2.2 ^1H NMR spectra of second-generation bispyridine ruthenium-benzylidene complexes^a

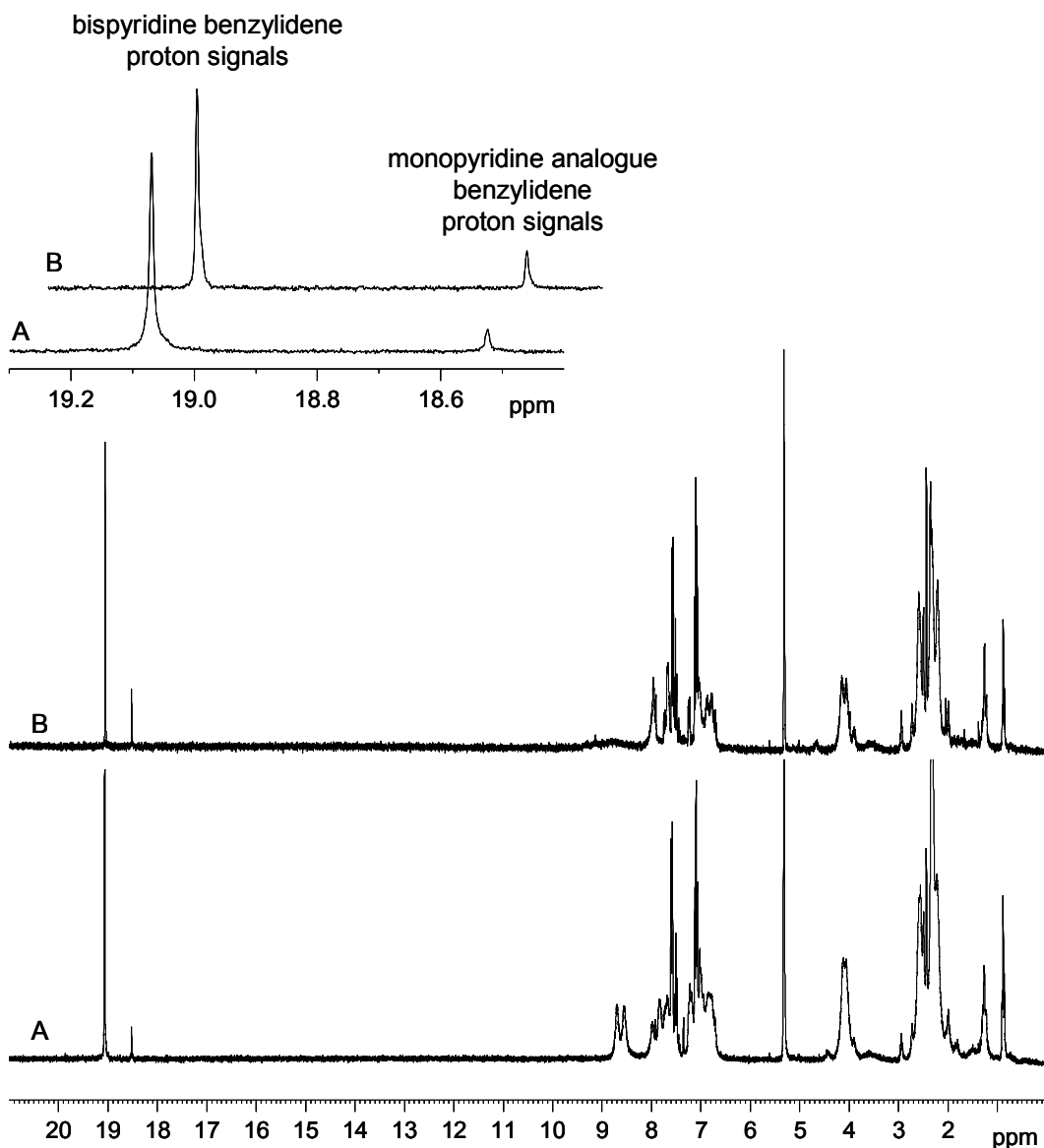


^a NMR spectra were collected at ambient temperature in dichloromethane- d_2 at 300 MHz.

^b These signals likely correspond to the monopyridine adduct.

The monopyridine analogue of complex **7** was previously synthesised in the Grubbs group⁸ by heating a toluene solution of **7** at 35 °C under vacuum and removing the solvent together with the dissociated pyridine as an azeotrope. Grubbs and coworkers also reported that the elemental analysis of complex **8** corresponded to the monopyridine adduct, which was presumed to have formed under high vacuum.⁶ I attempted to generate the monopyridine analogue of **10** by putting the isolated solid under dynamic vacuum. The pure monopyridine analogue has not yet been isolated although the amount of the five-coordinate species has been observed to increase from approximately 8% to 19% after a number of hours under vacuum (Figure 2.3). Low heat should increase the amount of monopyridine adduct; however, to isolate the pure product, it may be more effective to follow the procedure for the isolation of **7** by Grubbs (as above).

Figure 2.3 ^1H NMR spectra of mixtures of bispyridine complex **10** and its monopyridine analogue before (A) and after (B) treatment under vacuum with an expanded view of the benzylidene region (inset)^a



^a NMR spectra were collected at ambient temperature in dichloromethane- d_2 at 300 MHz.

For all of the bispyridine ruthenium-benzylidene complexes (**7-14**), an additional benzylidene proton feature in the NMR spectrum tends to form or, if already present, to increase over time relative to the predominant feature. This suggests that the ratio of bispyridine:monopyridine adduct decreases, that is,

some of the bispyridine species converts to the monopyridine species while in solution. Additionally, the total benzylidene signal decreases relative to the solvent signal, indicating decomposition of both the bispyridine and monopyridine ruthenium benzylidenes over time in solution. This loss of benzylidene proton signal is quite rapid for NMR samples prepared in air, but is much slower for samples handled in an inert atmosphere (nitrogen-filled glove box), especially if they are capped with a septum or J. Young valve. Relative to dichloromethane- d_2 , toluene- d_8 appears to slow the decomposition somewhat; however, the residual solvent peaks from toluene- d_8 have significant overlap with those of the complexes, so dichloromethane- d_2 was primarily used.

Synthesis of bispyridine complexes with 4-cyanopyridine and 3-aminopyridine was unsuccessful. 3-Aminopyridine is not very soluble in toluene, dichloromethane, or benzene, so the reaction was carried out in tetrahydrofuran in which 3-aminopyridine is quite soluble. 4-Cyanopyridine is soluble in toluene, so all corresponding reactions were performed in that solvent. Reactions of complexes **1** or **2** with either 4-cyanopyridine or 3-aminopyridine resulted in a mixture of products that included only a small amount of ruthenium-benzylidene (according to ^1H NMR data). For the 4-cyanopyridine reactions, using a smaller excess (10x) or larger excess (50x), and allowing the reaction to proceed longer (up to 30 minutes) failed to result in a single product. These reactions were not investigated further because the purpose of this synthetic work was to produce a series of pure bispyridine ruthenium benzylidenes with a range of electronic properties and this was successfully achieved with eight products.

Other synthetic goals in our group include the study of ruthenacyclobutane species and ruthenium benzylidenes that contain small, photodissociable ligands. Our work on the ruthenacyclobutane complex **15**, including synthesis and initial XAS investigation, is described in Appendix 1. Preliminary low-temperature studies with CO and bipyridine ruthenium benzylidenes resulted in fast decomposition of the benzylidene fragment. Reactions with complex **1** are more promising and some initial results are presented in Appendix 2.

2.3. Conclusions

A series of four first-generation and four second-generation bipyridine ruthenium-benzylidene complexes have been synthesised; five of the complexes are new. The pyridine ligands in the complexes span a broad range of electronic properties with the order from electron-donating to electron-withdrawing groups as follows: R = 4-OCH₃ (**13** & **14**), H (**7** & **8**), 3-Br (**9** & **10**), 3-NO₂ (**11** & **12**). Although most of these complexes are not expected to be highly-active olefin metathesis catalysts, activity has been shown by others to vary with different pyridine substituents. One of our goals is to explore systematic variations in electronic structure and their effects on spectroscopic data and reactivity.

2.4. Experimental

2.4.1. General Considerations

All storage and manipulations of compounds were carried out under an inert atmosphere of nitrogen using standard Schlenk line or glove box

techniques. ^1H and ^{31}P NMR spectra were collected on a Bruker Avance 300 MHz spectrometer at ambient temperature. The following abbreviations are used below: s = singlet, d = doublet, t = triplet, m = multiplet, and br. = broad signal. Elemental analyses were performed with a Carlo Erba EA 1108 elemental analyser.

2.4.2. Materials

Toluene, ether, and pentane were degassed and dried by passage through an mBraun solvent purification system containing 3 Å molecular sieves. Complexes **1** and **2**, pyridine- d_5 , and anhydrous pyridine were purchased from Sigma-Aldrich and used as received. Ampoules of dichloromethane- d_2 and toluene- d_8 were purchased from Cambridge Isotope Laboratories and used as received. 3-Bromopyridine was purchased from AlfaAesar and 4-methoxypyridine was purchased from Sigma-Aldrich; both were dried over 4 Å molecular sieves. 3-Nitropyridine was purchased from AlfaAesar and dried under vacuum.

2.4.3. $[(\text{PCy}_3)(\text{py})_2(\text{Cl})_2\text{Ru}=\text{CHPh}]$ (**7**)

Pyridine (2.0 mL, 25 mmol) was added to **1** (0.2015 g, 0.2448 mmol) in a 20 mL vial (no other solvent used). The mixture was stirred at ambient temperature for 10 minutes and a colour change from purple to green was observed. Room-temperature pentane (15 mL) was added and a precipitate began to form. The vial was capped and stored in a freezer (-25°C) overnight. The precipitate was vacuum-filtered, washed four times with 5 mL room-

temperature pentane, and dried under vacuum. The green solid **7** was collected in 72% yield (0.1229 g, 0.1754 mmol). $^{31}\text{P}\{^1\text{H}\}$ NMR (CD_2Cl_2): δ 36.90 (s). ^1H NMR (CD_2Cl_2): δ 19.90 (d, 1H, *CHPh*, $J_{\text{HP}} = 11.7$ Hz), 8.74 (br. s, 2H, pyridine), 8.38 (br. s, 2H, pyridine) 7.93 (d, 2H, *ortho CH*, $J_{\text{HH}} = 7.3$ Hz), 7.64 (br. s, 2H, pyridine), 7.54 (t, 1H, *para CH*, $J_{\text{HH}} = 7.3$ Hz), 7.29 (br. s, 2H, pyridine), 7.18 (t, 2H, *meta CH*, $J_{\text{HH}} = 7.7$ Hz), 7.11 (br. s, 2H, pyridine), 2.42-1.01 (br. multiple peaks, 33H, $\text{P}(\text{C}_6\text{H}_{11})_3$). Anal. Calcd for $\text{C}_{35}\text{H}_{49}\text{Cl}_2\text{N}_2\text{PRu}$ (700.73): C, 59.99; H, 7.05; N, 4.00. Found: C, 60.37; H, 7.12; N, 4.05.

2.4.4. $[(\text{PCy}_3)(3\text{-Br-py})_2(\text{Cl})_2\text{Ru}=\text{CHPh}]$ (**9**)

3-Bromopyridine (1.0 mL, 10 mmol) was added to **1** (0.0978 g, 0.1188 mmol) in a 20 mL vial (no other solvent used). The mixture was stirred at ambient temperature for 10 minutes and a colour change from purple to green was observed. Room-temperature pentane (15 mL) was added and a precipitate began to form. The vial was capped and stored in a freezer (-25°C) overnight. The precipitate was vacuum-filtered, washed four times with 5 mL room-temperature pentane, and dried under vacuum. The green solid **9** was collected in 71% yield (0.0723 g, 0.0842 mmol). $^{31}\text{P}\{^1\text{H}\}$ NMR (CD_2Cl_2): δ 38.78 (s). ^1H NMR (CD_2Cl_2): δ 19.70 (d, 1H, *CHPh*, $J_{\text{HP}} = 11.3$ Hz), 8.65 (br. s, 2H, pyridine), 8.48 (br. s, 2H, pyridine) 7.85 (d, 4H, *ortho CH*, $J_{\text{HH}} = 7.7$ Hz, pyridine), 7.54 (t, 1H, *para CH*, $J_{\text{HH}} = 7.1$ Hz), 7.20 (t, 4H, *meta CH*, $J_{\text{HH}} = 7.3$ Hz, pyridine), 2.44-1.07 (br. multiple peaks, 33H, $\text{P}(\text{C}_6\text{H}_{11})_3$). Anal. Calcd for $\text{C}_{35}\text{H}_{47}\text{Cl}_2\text{N}_2\text{Br}_2\text{PRu}$ (858.52): C, 48.97; H, 5.52; N, 3.26. Found: C, 49.32; H, 5.50; N, 3.26.

2.4.5. [(PCy₃)(3-NO₂-py)₂(Cl)₂Ru=CHPh] (11)

3-Nitropyridine (0.7456 g, 6.008 mmol) was added to a solution of **1** (0.1009 g, 0.1226 mmol) dissolved in 2 mL toluene in a 20 mL vial. The mixture was stirred at ambient temperature for 10 minutes and a colour change from purple to brown was observed. Room-temperature pentane (15 mL) was added and a precipitate began to form. The vial was capped and stored in a freezer (-25°C) overnight. The precipitate was vacuum-filtered, washed four times with 5 mL room-temperature pentane, washed two times with 5 mL room-temperature ether to remove excess solid 3-nitropyridine, and dried under vacuum. The brown solid **11** was collected in 35% yield (0.0341 g, 0.0431 mmol). ³¹P{¹H} NMR (CD₂Cl₂): δ 39.55 (s). ¹H NMR (CD₂Cl₂): δ 19.67 (d, 1H, CHPh, J_{HP} = 11.3 Hz), 9.42 (br. s, 2H, pyridine), 8.91 (br. s, 2H, pyridine), 8.45 (d, 2H, *ortho* CH, J_{HH} = 6.7 Hz), 7.79 (d, 2H, *para* CH, J_{HH} = 6.9 Hz, pyridine), 7.48 (br. s, 3H, pyridine), 7.15 (t, 2H, *meta* CH, J_{HH} = 7.1 Hz), 2.44-1.10 (br. multiple peaks, 33H, P(C₆H₁₁)₃). Anal. Calcd for C₃₅H₄₇Cl₂N₄O₄PRu (790.72): C, 53.16; H, 5.99; N, 7.09. Found: C, 53.15; H, 5.99; N, 7.12.

2.4.6. [(PCy₃)(4-OMe-py)₂(Cl)₂Ru=CHPh] (13)

4-Methoxypyridine (0.5 mL, 4.9 mmol) was added to a solution of **1** (0.1027 g, 0.1248 mmol) dissolved in 1 mL toluene in a 20 mL vial. The mixture was stirred at ambient temperature for 10 minutes and a colour change from purple to green was observed. Room-temperature pentane (15 mL) was added and a precipitate began to form. The vial was capped and stored in a freezer (-25°C) overnight. The precipitate was vacuum-filtered, washed four times with 5

mL room-temperature pentane, and dried under vacuum. The green solid **13** was collected in 47% yield (0.0450 g, 0.0591 mmol). $^{31}\text{P}\{^1\text{H}\}$ NMR (CD_2Cl_2): δ 35.96 (s). ^1H NMR (CD_2Cl_2): δ 19.97 (d, 1H, *CHPh*, $J_{\text{HP}} = 11.7$ Hz), 8.63 (br. s, 2H, pyridine), 8.17 (br. s, 2H, pyridine), 7.99 (d, 2H, *ortho CH*, $J_{\text{HH}} = 7.7$ Hz), 7.56 (t, 1H, *para CH*, $J_{\text{HH}} = 7.1$ Hz), 7.20 (t, 2H, *meta CH*, $J_{\text{HH}} = 7.7$ Hz), 6.83 (br. s, 2H, pyridine), 6.58 (br. s, 2H, pyridine), 3.85 (s, 3H, OCH_3), 3.78 (s, 3H, OCH_3), 2.39-1.00 (br. multiple peaks, 33H, $\text{P}(\text{C}_6\text{H}_{11})_3$). Anal. Calcd for $\text{C}_{37}\text{H}_{53}\text{Cl}_2\text{N}_2\text{O}_2\text{PRu}$ (760.78): C, 58.41; H, 7.02; N, 3.68. Found: C, 58.76; H, 7.04; N, 3.75.

2.4.7. $[(\text{H}_2\text{IMes})(\text{py})_2(\text{Cl})_2\text{Ru}=\text{CHPh}]$ (**8**)

Pyridine (1.0 mL, 12 mmol) was added to a solution of **2** (0.0998 g, 0.1176 mmol) dissolved in 1 mL toluene in a 20 mL vial. The mixture was stirred at ambient temperature for 10 minutes and a colour change from red to green was observed. Room-temperature pentane (15 mL) was added and a precipitate began to form. The vial was capped and stored in a freezer (-25°C) overnight. The precipitate was vacuum-filtered, washed four times with 5 mL room-temperature pentane, and dried under vacuum. The green solid **8** was collected in 53% yield (0.0455 g, 0.0626 mmol). ^1H NMR (CD_2Cl_2): δ 19.14 (s, 1H, *CHPh*), 8.61 (br. s, 2H, pyridine), 7.79 (d, 2H, pyridine), 7.67 (br. s, 1H, pyridine) 7.59 (d, 2H, *ortho CH*, $J_{\text{HH}} = 7.7$ Hz), 7.49 (t, 2H, *para CH*, $J_{\text{HH}} = 7.3$ Hz, pyridine), 7.26 (br. s, 2H, pyridine), 7.08 (t, 2H, *meta CH*, $J_{\text{HH}} = 7.7$ Hz), 7.03-6.70 (br. multiple peaks, 6H, Mes *CH*, pyridine), 4.09 (br. d, 4H, $\text{NCH}_2\text{CH}_2\text{N}$), 2.69-2.14 (br. multiple peaks, 18H, Mes CH_3). Anal. Calcd for $\text{C}_{38}\text{H}_{42}\text{Cl}_2\text{N}_4\text{Ru}$ (726.74): C, 62.80; H, 5.83; N, 7.71. Found: C, 62.77; H, 6.10; N, 7.88.

2.4.8. [(H₂IMes)(3-Br-py)₂(Cl)₂Ru=CHPh] (10)

3-Bromopyridine (1.0 mL, 10 mmol) was added to a solution of **2** (0.0993 g, 0.1170 mmol) dissolved in 1 mL toluene in a 20 mL vial. The mixture was stirred at ambient temperature for 10 minutes and a colour change from red to green was observed. Room-temperature pentane (15 mL) was added and a precipitate began to form. The vial was capped and stored in a freezer (-25°C) overnight. The precipitate was vacuum-filtered, washed four times with 5 mL room-temperature pentane, and dried under vacuum. The green solid **10** was collected in 55% yield (0.0564 g, 0.0638 mmol). ¹H NMR (CD₂Cl₂): δ 19.07 (s, 1H, CHPh), 8.65 (br. d, 2H, pyridine), 8.00 (br. s, 1H, pyridine), 7.74 (br. s, 2H, pyridine), 7.60 (d, 2H, *ortho* CH, J_{HH} = 7.3 Hz), 7.49 (t, 1H, *para* CH, J_{HH} = 7.1 Hz), 7.09 (t, 3H, *meta* CH, J_{HH} = 7.5 Hz, pyridine), 7.00-6.76 (br. multiple peaks, 6H, Mes CH, pyridine), 4.07 (br. d, 4H, NCH₂CH₂N), 2.69-2.14 (br. multiple peaks, 18H, Mes CH₃). Anal. Calcd for C₃₈H₄₂Cl₂N₄Ru (884.53): C, 62.80; H, 5.83; N, 7.71. Found: C, 62.77; H, 6.10; N, 7.88.

2.4.9. [(H₂IMes)(3-NO₂-py)₂(Cl)₂Ru=CHPh] (12)

3-Nitropyridine (0.7223 g, 5.820 mmol) was added to a solution of **2** (0.1056 g, 0.1244 mmol) dissolved in 2 mL toluene in a 20 mL vial. The mixture was stirred at ambient temperature for 10 minutes and a colour change from red to brown was observed. Room-temperature pentane (15 mL) was added and a precipitate began to form. The vial was capped and stored in a freezer (-25°C) overnight. The precipitate was vacuum-filtered, washed four times with 5 mL room-temperature ether to remove excess solid 3-nitropyridine, washed once

with 5 mL room-temperature pentane, and dried under vacuum. The brown solid **12** was collected in 50% yield (0.0513 g, 0.0628 mmol). ^1H NMR (CD_2Cl_2): δ 19.05 (s, 1H, *CHPh*), 9.21 (br. d, 3H, pyridine), 8.34 (br. t, 3H, pyridine), 7.59 (d, 2H, *ortho CH*, $J_{\text{HH}} = 8.1$ Hz), 7.46 (t, 2H, *para CH*, $J_{\text{HH}} = 7.1$ Hz, pyridine), 7.06 (t, 3H, *meta CH*, $J_{\text{HH}} = 7.7$ Hz, pyridine), 6.81 (d, 4H, Mes *CH*), 4.07 (br. s, 4H, $\text{NCH}_2\text{CH}_2\text{N}$), 2.66-2.18 (br. multiple peaks, 18H, Mes CH_3). Anal. Calcd for $\text{C}_{38}\text{H}_{40}\text{Cl}_2\text{N}_6\text{O}_4\text{Ru}$ (816.74): C, 55.88; H, 4.94; N, 10.29. Found: C, 55.70; H, 5.15; N, 10.17.

2.4.10. $[(\text{H}_2\text{IMes})(4\text{-OMe-py})_2(\text{Cl})_2\text{Ru}=\text{CHPh}]$ (**14**)

4-Methoxypyridine (0.5 mL, 4.9 mmol) was added to a solution of **2** (0.0990 g, 0.1166 mmol) dissolved in 1 mL toluene in a 20 mL vial. The mixture was stirred at ambient temperature for 10 minutes and a colour change from red to green was observed. Room-temperature pentane (15 mL) was added and a precipitate began to form. The vial was capped and stored in a freezer (-25°C) overnight. The precipitate was vacuum-filtered, washed four times with 5 mL room-temperature pentane, and dried under vacuum. The green solid **14** was collected in 69% yield (0.0633 g, 0.0805 mmol). ^1H NMR (CD_2Cl_2): δ 19.11 (d, 1H, *CHPh*, $J_{\text{HH}} = 7.7$ Hz), 8.43 (br. s, 2H, pyridine), 7.73-6.48 (br. multiple peaks, 15H, *ortho*, *meta*, *para CH*, Mes *CH*, pyridine), 4.09 (br. d, 4H, $\text{NCH}_2\text{CH}_2\text{N}$), 3.85 (d, 3H, OCH_3 , $J_{\text{HH}} = 8.1$ Hz), 3.74 (d, 3H, OCH_3 , $J_{\text{HH}} = 7.7$ Hz), 2.75-2.13 (br. multiple peaks, 18H, Mes CH_3). Anal. Calcd for $\text{C}_{40}\text{H}_{46}\text{Cl}_2\text{N}_4\text{O}_2\text{Ru}$ (786.79): C, 61.06; H, 5.89; N, 7.12. Found: C, 61.35; H, 6.16; N, 6.99.

2.4.11. Monopyridine Analogue

Approximately 10 mg of complex **10** was weighed into a vial in a glove box and then attached via cannula to a Schlenk line and kept under dynamic vacuum overnight (≥ 12 hours). The ^1H NMR spectrum exhibited a bispyridine:monopyridine benzylidene signal ratio of 1:0.23 (19%). This is an increase in monopyridine signal compared to a spectrum for that sample before prolonged exposure to vacuum where a 1:0.09 (8%) ratio was found. Concomitant decreases in pyridine signals are also observed in the ^1H NMR spectrum.

2.5. References

- (1) Fürstner, A. *Angew. Chem. Int. Ed.* **2000**, *39*, 3012-3043.
- (2) Trnka, T. M.; Grubbs, R. H. *Acc. Chem. Res.* **2001**, *34*, 18-29.
- (3) *Handbook of Metathesis*; Grubbs, R. H., Ed.; Wiley-VHC: Weinheim, 2003.
- (4) Grubbs, R. H. *Tetrahedron* **2004**, *60*, 7117-7140.
- (5) Katz, T. J. *Angew. Chem. Int. Ed.* **2005**, *44*, 3010-3019.
- (6) Sanford, M. S.; Love, J. A.; Grubbs, R. H. *Organometallics* **2001**, *20*, 5314-5318.
- (7) Love, J. A.; Morgan, J. P.; Trnka, T. M.; Grubbs, R. H. *Angew. Chem. Int. Ed.* **2002**, *41*, 4035-4037.
- (8) Trnka, T. M.; Dias, E. L.; Day, M. W.; Grubbs, R. H. *Arkivoc* **2002**, *13*, 28-41.
- (9) Conrad, J. C.; Parnas, H. H.; Snelgrove, J. L.; Fogg, D. E. *J. Am. Chem. Soc.* **2005**, *127*, 11882-11883.
- (10) Hong, S. H.; Wenzel, A. G.; Salguero, T. T.; Day, M. W.; Grubbs, R. H. *J. Am. Chem. Soc.* **2007**, *129*, 7961-7968.
- (11) Choi, T.-L.; Grubbs, R. H. *Angew. Chem. Int. Ed.* **2003**, *42*, 1743-1746.
- (12) Camm, K. D.; Martinez Castro, N.; Liu, Y.; Czechura, P.; Snelgrove, J. L.; Fogg, D. E. *J. Am. Chem. Soc.* **2007**, *129*, 4168-4169.
- (13) Hansch, C.; Leo, A.; Taft, R. W. *Chem. Rev.* **1991**, *91*, 165-195.

CHAPTER 3: PRE-EDGE FEATURES*

3.1. Introduction

In transition metal K-edge X-ray absorption spectroscopy (XAS), the X-ray absorption near-edge structure (XANES) can provide electronic structure information as well as details about the coordination number and geometry around the metal centre (see also Section 1.4.2).¹ The principal spectral feature is an edge jump resulting from ionisation of 1s electrons ($\infty \leftarrow 1s$ transitions). Peaks called pre-edge features are sometimes observed at energies below that of the ionisation edge. These features typically result from bound-state transitions to empty or partially-empty valence orbitals. Solomon and coworkers have developed a systematic and effective methodology for electronic structure analysis of first-row transition metals using metal K-edge XAS. For example, ligand field and electronic structure effects on the pre-edge features of a large number of Fe complexes have been systematically explored and assigned.² In general, the low energy pre-edge features are attributable to metal $3d \leftarrow 1s$ transitions and are well-separated from the edge feature.

For centrosymmetric complexes, metal $3d \leftarrow 1s$ transitions are electric dipole forbidden due to parity conservation. Regardless of symmetry, minor contributions from $3d \leftarrow 1s$ transitions are expected through electric-quadrupole mechanisms;³ thus, pre-edge features corresponding to these transitions are

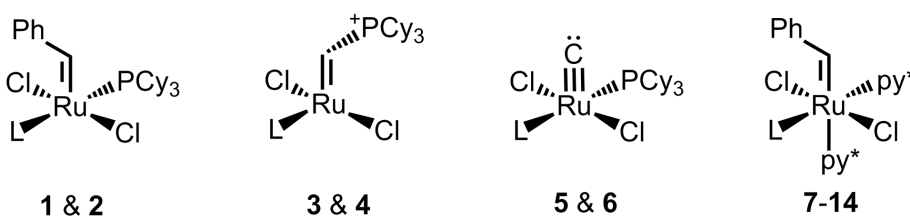
* A version of this chapter has been published. Getty, K.; Delgado-Jaime, M. U.; Kennepohl, P., Assignment of Pre-edge Features in the Ru K-edge X-ray Absorption Spectra of Organometallic Ruthenium Complexes. *Inorg. Chim. Acta* **2008**, *361*, 1059-1065.

very weak for centrosymmetric complexes. Electric-quadrupole contributions are known to be approximately two orders of magnitude less intense than dipole mechanisms;^{4,5} therefore, even minimal electric-dipole-allowed character in the metal $3d \leftarrow 1s$ transitions can bring about considerable increases in intensity. Mixing of metal 4p and 3d orbitals occurs for complexes that are non-centrosymmetric, which imparts electric-dipole-allowed character to the metal $3d \leftarrow 1s$ transitions. Generally, a larger distortion from centrosymmetry results in a greater increase in intensity of the pre-edge features. For first-row transition metals, pre-edge features have been used extensively to obtain information regarding the electronic structure of the metal centre and its local symmetry.

Substantially shorter core-hole lifetimes for second-row transition metals lead to intrinsically broader features in their resultant K-edge XAS spectra compared to first-row metals.⁶ Consequently, this lower resolution and decreased energy separation of the pre-edge and edge features render the analysis of the XANES region more difficult. Nevertheless, the information potentially available from these studies could be invaluable to understanding the roles of heavier transition metals in biological and homogeneous catalysis. By analogy to first-row metals, it has commonly been assumed that the pre-edge features for second-row transition metals correspond to $4d \leftarrow 1s$ transitions although the possibility of $5p \leftarrow 1s$ transitions has often not been excluded.⁷⁻¹⁰ Some detailed studies of Mo¹¹ and Pd¹² K-edges have assigned the pre-edge features for these metals as due to metal $4d \leftarrow 1s$ transitions.

Ruthenium is a second-row transition metal that is widely utilised in homogeneous catalysis.¹³⁻¹⁵ Olefin metathesis catalysed by ruthenium-carbene species has been remarkably successful, largely owing to the work of Grubbs and coworkers.¹⁶ Despite the achievements in this field, there remain unanswered questions about the mechanistic intermediates as well as the precatalysts themselves. The nature of relevant ruthenium carbenes has been investigated theoretically,¹⁷⁻³² but little attention has been given to spectroscopic approaches,³³⁻³⁶ which can provide detailed electronic structure insight into these important catalytic centres. We anticipated that Ru K-edge XAS may be a useful spectroscopic tool for studying ruthenium-carbene complexes. The unambiguous assignment of Ru K-edge pre-edge features is a crucial first step in such investigations; thus, we have obtained the necessary data for a series of compounds (Chart 3.1).

Chart 3.1 Complexes investigated in this study



Abbreviations: L = PCy₃ (odd numbers, tricyclohexylphosphine) or H₂IMes (even numbers, 1,3-bis(2,4,6-trimethylphenyl)-4,5-dihydroimidazol-2-ylidene); Ph = phenyl; py* = pyridine (7 & 8), 3-bromopyridine (9 & 10), 3-nitropyridine (11 & 12), 4-methoxypyridine (13 & 14).

We have examined organometallic ruthenium complexes related to the first- (L = PCy₃; odd numbers) and second- (L = H₂IMes; even numbers) generation Grubbs-type complexes of relevance to olefin metathesis (Chart 3.1). Relative to the original Grubbs complexes^{37,38} (1 & 2), the phosphonium alkylidenes³⁹ (3 & 4) have a phosphine transferred onto the alkylidene carbon

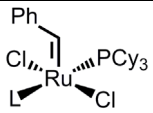
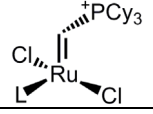
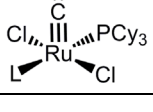
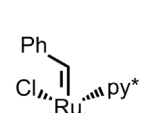
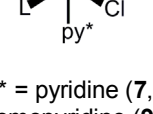
whereas the carbides⁴⁰ (**5** & **6**) contain a triply-bonded carbide in place of the benzylidene ligand. Two pyridine ligands replace one phosphine of the Grubbs complexes, resulting in the six-coordinate bispyridine compounds^{41,42} (**7-14**). The pyridines are mono-substituted as follows: py* = pyridine (**7** & **8**); 3-bromopyridine (**9** & **10**); 3-nitropyridine (**11** & **12**); or 4-methoxypyridine (**13** & **14**). The 3-bromopyridine complex with L = H₂IMes (**10**) is a fast-initiating precatalyst that has been particularly successful for metathesis polymerisation reactions and is sometimes called a third-generation Grubbs catalyst. Analysis of the Ru K-edge XAS data for these complexes has allowed us to assign the spectral pre-edge features and establish that this technique can indeed provide information regarding the geometry around the metal centre; this information could be particularly valuable for reactive intermediates in the olefin metathesis cycle.

3.2. Results and Discussion

A noticeable pre-edge feature is present in the XANES region of Ru K-edge XAS spectra for all complexes in a series of ruthenium compounds related to the first- and second-generation Grubbs precatalysts. This feature is observed as a shoulder on the rising edge; the energy splitting between the features is only about 6 eV. By contrast, there is a greater energy separation of the pre-edge and ionisation edge for first-row transition metals (~10 eV for Fe); the larger splitting combined with sharper features leads to better resolution for first-row transition metals than for heavier metals. The intensity of the pre-edge peak is

dependent on the geometry of the complex and varies for each class of compounds investigated (Table 3.1).

Table 3.1 Complexes **1-14** with coordination number, approximate symmetry, pre-edge feature area and pre-edge energy position

Complex	L	Coordination Number	Approximate Symmetry	Pre-edge Area	Pre-edge Energy (eV)	
	1	PCy ₃	5	C _{4v}	1.9	22116.4
	2	H ₂ IMes	5	C _{4v}	1.8	22116.9
	3^a	PCy ₃	4	C _s	1.7	22117.1
	4^a	H ₂ IMes	4	C _s	2.3	22117.5
	5	PCy ₃	5	C _{4v}	2.7	22118.4
	6	H ₂ IMes	5	C _{4v}	3.0	22118.8
	7	PCy ₃	6	O _h	1.0	22117.7
	8	H ₂ IMes	6	O _h	1.0	22117.5
	9	PCy ₃	6	O _h	1.0	22117.6
	10	H ₂ IMes	6	O _h	1.3	22117.5
<p>py* = pyridine (7,8); 3-bromopyridine (9,10); 3-nitropyridine (11,12); 4-methoxypyridine (13,14)</p>	11	PCy ₃	6	O _h	1.1	22117.6
	12	H ₂ IMes	6	O _h	1.1	22117.4
	13	PCy ₃	6	O _h	1.0	22117.5
	14	H ₂ IMes	6	O _h	1.1	22117.4

^a The edge features for complexes **3** and **4** were broader than for other complexes; thus, constraints on the edge widths were used. See Section 3.4.5 for additional details.

The normalised spectra for the first-generation (L = PCy₃; Figure 3.1) and second-generation (L = H₂IMes; Figure 3.2) complexes exhibit the same trend of pre-edge feature intensity as follows: **7-14** << **1 & 2** < **3 & 4** << **5 & 6** (Scheme 3.1). The pre-edge features for the bispyridine complexes are all very low intensity as illustrated in Figure 3.3 (L = PCy₃) and Figure 3.4 (L = H₂IMes). Insets in each figure show an expanded view of the pre-edge region.

Figure 3.1 Ru K-edge XAS spectra for first-generation complexes **1**, **3**, **5**, and **7** with pre-edge feature expanded (inset)

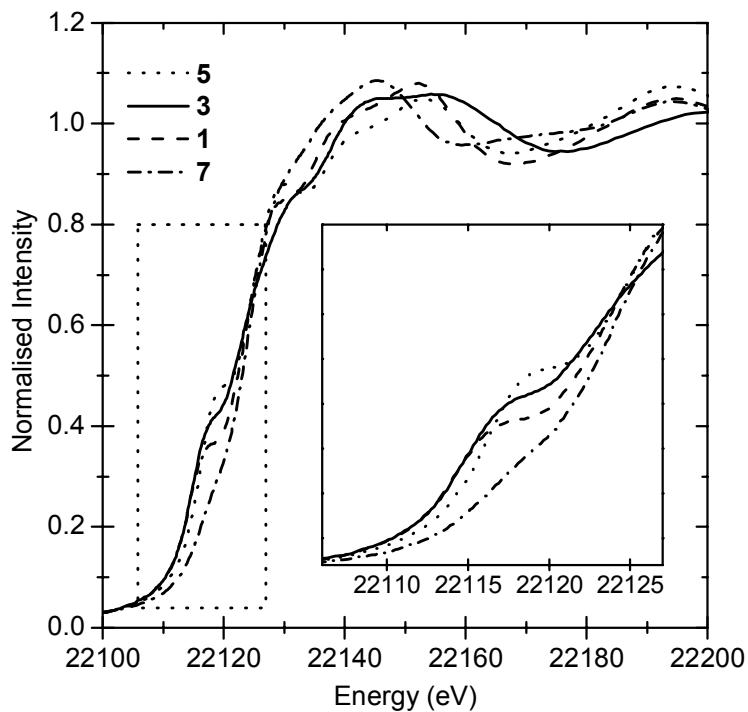


Figure 3.2 Ru K-edge XAS spectra for second-generation complexes **2**, **4**, **6**, and **8** with pre-edge feature expanded (inset)

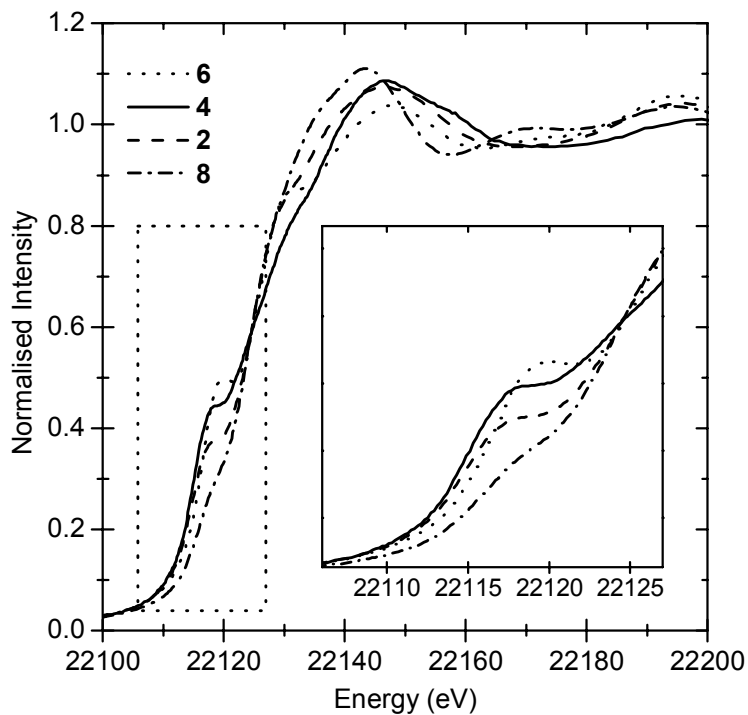


Figure 3.3 Ru K-edge XAS spectra for first-generation bispyridine complexes **7**, **9**, **11**, and **13** with pre-edge feature expanded (inset)

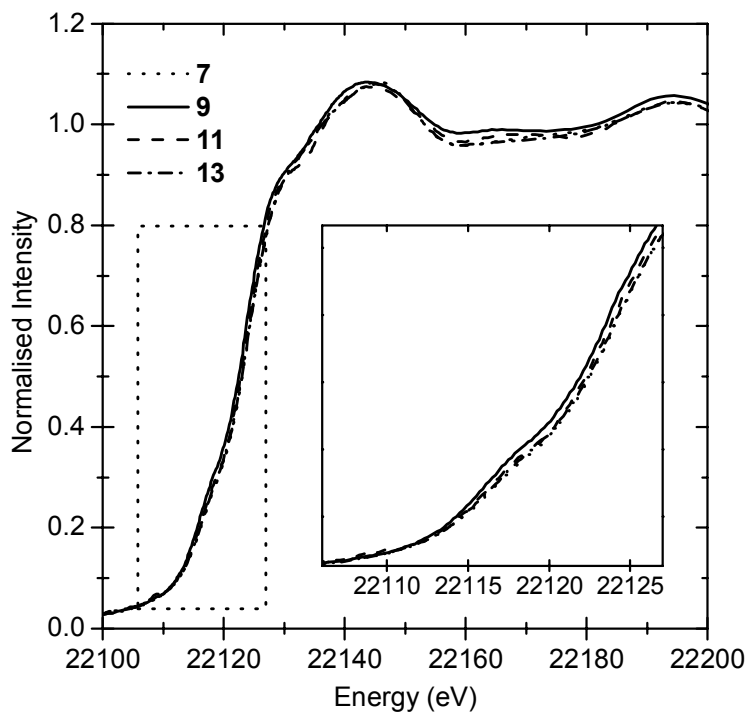
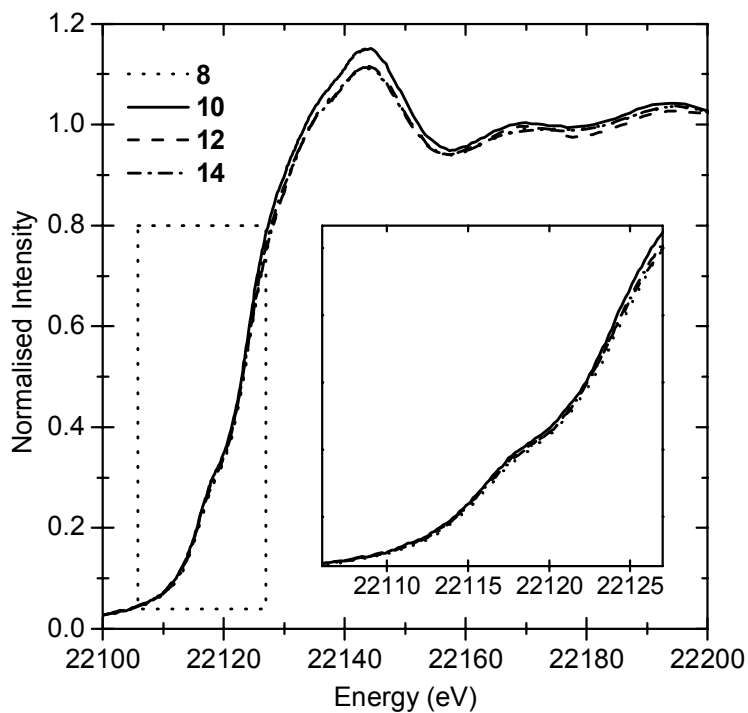
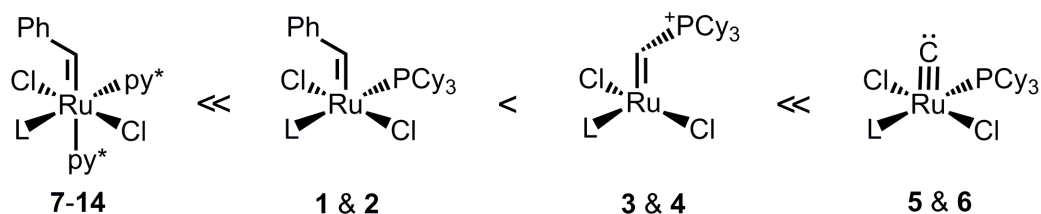


Figure 3.4 Ru K-edge XAS spectra for second-generation bispyridine complexes **8**, **10**, **12**, and **14** with pre-edge feature expanded (inset)



Scheme 3.1 Ruthenium complexes listed in order of increasing pre-edge intensity



The pre-edge features arise from transitions to empty or partially-empty valence orbitals. Probable bound-state transitions include electric-dipole-forbidden Ru $4d \leftarrow 1s$ transitions and electric-dipole-allowed Ru $5p \leftarrow 1s$ transitions. Second-row transition metal $4d$ and $5p$ orbitals should be close in energy; therefore, it may be expected that the observed pre-edges result from $5p \leftarrow 1s$ transitions because these are electric dipole allowed and would overwhelm the intensity of $4d \leftarrow 1s$ features, if present. Differentiation between these two potential transitions is possible by examining the behaviour of the pre-edge features upon changes in compound geometry. Specifically, the intensity of pre-edge features due to dipole-allowed metal $5p \leftarrow 1s$ transitions should be relatively independent of geometry whereas metal $4d \leftarrow 1s$ transitions are expected to be extremely sensitive to symmetry because small contributions from $5p$ mixing into the $4d$ orbitals would have a significant impact on the intensity of the feature.

In an octahedral low-spin d^6 Ru(II) complex, the symmetry of the empty $4d_{\sigma^*}$ orbitals (e_g) prevents mixing with the $5p$ orbitals (t_{1u}) and enforces the electric-dipole-forbidden nature of the Ru $4d \leftarrow 1s$ transitions while permitting only the weak electric-quadrupole mechanism. Accordingly, the six-coordinate

pseudo-octahedral bispyridine complexes (**7-14**) exhibit only very low-intensity pre-edge features. Also, as expected, a single pre-edge feature is observed for these complexes because there is no splitting of the empty $4d_{\sigma^*}$ orbitals and, therefore, the system has only one available 2E_g ligand field excited state.^{†2}

Lower-symmetry complexes exhibit very different pre-edge behaviour. For instance, the five-coordinate Grubbs complexes (**1 & 2**) have considerably more intense pre-edge features consistent with the loss of centrosymmetry due to the absence of a ligand along the Ru=C axis (relative to the bispyridine structures). Loss of an additional ligand, as in the case of the phosphonium alkylidenes (**3 & 4**), generates a different type of distortion with similar intensity of the pre-edge features. Alternatively, in complexes **5 & 6**, the apical benzylidene ligand in **1 & 2** has been replaced with a terminal carbide, resulting in a substantial increase in the pre-edge intensity. This effect corresponds with the much shorter M-C bond in the triply-bonded carbides (**6**: 1.650 Å⁴⁰) as compared to the benzylidenes (**1**: 1.838 Å⁴¹, **2**: 1.835 Å⁴³, **8**: 1.873 Å⁴¹) and phosphonium alkylidenes (**4**: 1.817 Å³⁹).

Density functional calculations for complexes **1-4** were performed and analysed by my coworkers (see Appendix 2 for details). In agreement with the pre-edge features corresponding to Ru $4d \leftarrow 1s$ transitions, the calculations indicate significant contributions of Ru $5p$ character into Ru $4d$ orbital manifold. The nature of the mixing depends on the type of structural distortion involved. In the five-coordinate complexes (**1 & 2**), the principal distortion occurs along the

[†] This nomenclature describes the valence final state and neglects the core-hole effect. Including the core-hole effect does not change the symmetry, but results in either a singlet or triplet rather than doublet final state.

Ru=C bond and produces a pseudo-square-pyramidal structure. As a result, mixing of 5p orbitals is primarily along this axis in the form of $4d_{z^2}$ - $5p_z$ mixing; the equatorial $5p_{x,y}$ orbitals do not contribute significantly because the orbitals that have the correct symmetry for mixing with them ($4d_{xz,yz}$) are full. The four-coordinate complexes (**3** & **4**), on the other hand, show considerable mixing along the axes of both vacant sites (relative to the octahedral complex); specifically, along the Ru=C and the Ru-L bonds. For these complexes, only the 5p orbital along the axis of the trans Ru-Cl bonds is not significantly involved in 5p-4d mixing. These findings are consistent with previous analyses of iron complexes in which the nature of 4p-3d mixing is anisotropic and correlates with specific structural distortions.²

Our assignment of the pre-edge features in the Ru K-edge XAS spectrum is supported by DFT computations and provides the foundation for further study of ruthenium complexes. In particular, the XAS technique accommodates non-crystalline samples of solids or solutions at a range of temperatures; therefore, it can be employed for reactive intermediates. Electronic and geometric information should be obtainable for species involved in the olefin metathesis mechanism, such as the ruthenacyclobutane structure.⁴⁴ Ru K-edge XAS pre-edge analysis is expected to offer important contributions to the study of ruthenium-catalysed reactions.

3.3. Conclusions

Through examination of four classes of organometallic ruthenium compounds, we have unambiguously assigned the Ru K-edge XAS pre-edge

features as due to electric-dipole-forbidden Ru 4d←1s transitions. Because this feature is extremely sensitive to geometry, it should be useful in the determination of coordination number and geometry for difficult-to-characterise complexes, such as the reactive intermediates in the olefin metathesis mechanism.

3.4. Experimental

3.4.1. General Considerations

All storage and manipulations of compounds were carried out under an inert atmosphere of nitrogen using standard Schlenk line or glove box techniques.

3.4.2. Materials

Complexes **1** & **2** were purchased from Sigma-Aldrich and used as received. Compounds **3-6** were synthesised as described elsewhere^{39,40} and obtained from the group of Warren E. Piers. I synthesised compounds **7-14** as explained in Chapter 2.

3.4.3. XAS Sample Preparation

All sample preparation was performed in a nitrogen-filled glove box and samples were kept in an inert atmosphere or frozen in liquid nitrogen prior to and during data acquisition. Each solid was diluted approximately seven-fold with boron nitride and the mixture was gently ground for >5 minutes using a mortar and pestle to generate homogenous, finely dispersed powders. Each mixture

was then pressed into a 0.5 mm thick aluminum spacer that was sealed on both sides with Kapton tape.

3.4.4. XAS Data Acquisition

Ru K-edge X-ray absorption spectroscopic data were collected at the Stanford Synchrotron Radiation Laboratory (SSRL) on beamline 7-3 under ring conditions 80-100 mA at 3.0 GeV. This beamline has a 20-pole, 2 Tesla wiggler, 0.8 mrad beam and a Si (220) double-crystal monochromator that was detuned by 50% intensity to minimise higher harmonic contamination. The incident X-ray intensity (I_0), sample absorption (I_1), and Ru reference absorption (I_2) were measured as transmittance in three consecutive argon-filled ionisation chambers and fluorescence data were collected using a 30-element Ge detector array. Two to four sweeps were taken for each sample and all data were measured to $k = 18 \text{ \AA}^{-1}$ at $13 \pm 3 \text{ K}$ within an Oxford Instruments CF1208 continuous-flow liquid helium cryostat. The initial beamline motor configurations are listed in Table 3.2.

Table 3.2 Initial motor configuration on SSRL beamline 7-3

Motor	Position
M0TOPSLT	1.499
M0BOTSLT	1.499
M0VERT	5.311
M0PITCH	0.012
M0BEND	200.000
GIRDER	0.000
MONOBOTSLT	2.000
MONTOPSLT	2.000
MONOBOTSLT	22500.023
TABLEVERT	88.733 ^a
TABLEHORX	-9.279
TABLEPITCH	0.000
S1VGAP	1.000 ^a
S1VTRAN	0.000
S1HGAP	5.000 ^a
S1HTRAN	0.000
CRYOHOR	3.100 ^a
CRYOVERT	5.631 ^a

^a These motors were optimised for each run.

3.4.5. XAS Data Processing and Analysis

X-ray absorption data were processed using the SIXPack software package.⁴⁵ Transmission and fluorescence data consistently yielded similar edge and pre-edge features; transmission data are reported for Chapters 3 and 4. All identical transmission sweeps for a complex were averaged and energy calibrated using the internal reference spectra of Ru foil; the lowest-energy inflection point was assigned as 22117 eV. Background subtraction and normalisation were performed simultaneously using a linear pre-edge function and a quadratic post-edge function.

The commercially-available PeakFit software package⁴⁶ was used to fit the pre-edge feature with a single Voigt amplitude function (Equation 3.1) and the ionisation edge feature with a cumulative Gaussian/Lorentzian function⁴⁷

(Equation 3.2). The spectra were fit over the energy region from 22090 eV to 22128 eV. A representative example of a fitted spectrum is illustrated in Figure 3.5 and detailed results of the fit are shown in Table 3.3.

Equation 3.1 Pre-edge: Voigt Amplitude Function

$$y = \frac{a_0 \int_{-\infty}^{\infty} \frac{\exp(-t^2)}{a_3^2 + \left(\frac{x-a_1-t}{a_2}\right)^2} dt}{\int_{-\infty}^{\infty} \frac{\exp(-t^2)}{a_3^2 + t^2} dt}$$

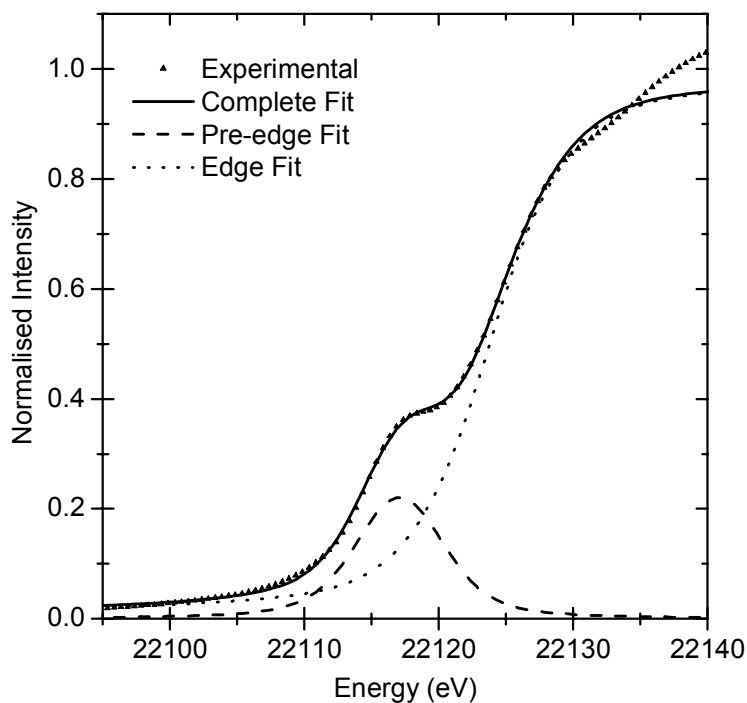
a_0 = amplitude
 a_1 = centre
 a_2 = width (>0)
 a_3 = shape (≥ 0)

Equation 3.2 Ionisation edge: Cumulative Gaussian/Lorentzian Function

$$y = a_4 \times \frac{a_0}{2} \left[1 + \operatorname{erf} \left(\frac{x-a_1}{\sqrt{a_2}} \right) \right] + (1-a_4) \times \frac{a_0}{\pi} \left[\tan^{-1} \left(\frac{x-a_1}{a_3} \right) + \frac{\pi}{2} \right]$$

a_0 = amplitude
 a_1 = inflection point
 a_2 = Gaussian width
 a_3 = Lorentzian width
 a_4 = shape

Figure 3.5 Ru K-edge XAS experimental data and fit for complex 2



The pre-edge features were well-modelled with a fixed 1:1 ratio of Gaussian:Lorentzian shapes ($a_3 = 0.5$). A pre-edge width (a_2) of 3.1 eV was fixed for all complexes as it successfully reproduced acceptable fits for the series of complexes and prevented distortions due to variations in the background. The amplitude (a_0) and energy position of the centre of the peak (a_1) were varied.

The edge features were generally well-modelled with a fixed 1:1 ratio of cumulative Gaussian:Lorentzian shapes ($a_4 = 0.5$). The amplitude (a_0), energy position of the inflection point (a_1) and width of Gaussian (a_2) and Lorentzian (a_3) shapes were varied. The edge widths for complexes **3** & **4** were fixed at the maximum value found for all other complexes to ensure reasonable values. The Gaussian and Lorentzian edge widths for the fourteen complexes averaged 4.4 eV ($1\sigma = 0.8$ eV) and 4.6 eV ($1\sigma = 0.8$ eV), respectively.

Table 3.3 Results from least-squares fitting of pre-edge and edge features

Complex	Number of Sweeps Averaged	Pre-edge			Edge			r^2
		Amp, a_0	Energy (eV), a_1	Area	Amp, a_0	Gaussian Width, a_2	Lorentzian Width, a_3	
1	4	0.21	22116.4	1.9	1.00	3.9	5.1	1.0000
2	3	0.21	22116.9	1.8	0.99	5.3	4.3	0.9999
3	2	0.20	22117.1	1.7	0.99	5.5 ^a	5.1	0.9998
4	2	0.26	22117.5	2.3	1.00	5.5 ^a	5.5 ^a	0.9997
5	2	0.30	22118.4	2.7	0.99	3.3	4.5	0.9999
6	2	0.33	22118.8	3.0	0.99	3.5	5.5	0.9999
7	2	0.11	22117.7	1.0	0.99	3.8	4.6	1.0000
8	2	0.12	22117.5	1.0	0.99	4.8	4.2	0.9999
9	2	0.11	22117.6	1.0	0.99	5.5	2.6	0.9999
10	2	0.14	22117.5	1.3	0.99	3.9	4.2	0.9999
11	2	0.12	22117.6	1.1	1.00	3.6	4.5	0.9999
12	2	0.13	22117.4	1.1	1.00	4.0	5.4	0.9999
13	3	0.11	22117.5	1.0	0.99	4.1	4.3	0.9999
14	3	0.12	22117.4	1.1	0.99	4.5	4.3	1.0000

^a These values were fixed in the fitting routine.

3.5. References

- (1) Penner-Hahn, J. E. *Coord. Chem. Rev.* **2005**, *249*, 161-177.
- (2) Westre, T. E.; Kennepohl, P.; DeWitt, J. G.; Hedman, B.; Hodgson, K. O.; Solomon, E. I. *J. Am. Chem. Soc.* **1997**, *119*, 6297-6314.
- (3) Hahn, J. E.; Scott, R. A.; Hodgson, K. O.; Doniach, S.; Desjardins, S. R.; Solomon, E. I. *Chem. Phys. Lett.* **1982**, *88*, 595-598.
- (4) Bair, R. A.; Goddard III, W. A. *Phys. Rev. B* **1980**, *22*, 2767-2776.
- (5) Brouder, C. *J. Phys.: Condens. Matter* **1990**, *2*, 701-738.
- (6) Fister, T. T.; Seidler, G. T.; Rehr, J. J.; Kas, J. J.; Elam, W. T.; Cross, J. O.; Nagle, K. P. *Phys. Rev. B* **2007**, *75*, 174106.
- (7) Kostroun, V. O.; Fairchild, R. W.; Kukkonen, C. A.; Wilkins, J. W. *Phys. Rev. B* **1976**, *13*, 3268-3271.
- (8) Wang, C. M.; Cargill III, G. S.; Chan, H. M.; Harmer, M. P. *J. Am. Ceram. Soc.* **2002**, *85*, 2492-2498.
- (9) Ressler, T.; Timpe, O.; Neisius, T.; Find, J.; Mestl, G.; Dieterle, M.; Schlogl, R. *J. Catal.* **2000**, *191*, 75-85.
- (10) Okamoto, K.; Miyawaki, J.; Nagai, K.; Matsumura, D.; Nojima, A.; Yokoyama, T.; Kondoh, H.; Ohta, T. *Inorg. Chem.* **2003**, *42*, 8682-8689.
- (11) Laplaza, C. E.; Johnson, M. J. A.; Peters, J. C.; Odom, A. L.; Kim, E.; Cummins, C. C.; George, G. N.; Pickering, I. J. *J. Am. Chem. Soc.* **1996**, *118*, 8623-8638.
- (12) Tromp, M.; van Bokhoven, J. A.; van Strijdonck, G. P. F.; van Leeuwen, P. W. N. M.; Koningsberger, D. C.; Ramaker, D. E. *J. Am. Chem. Soc.* **2005**, *127*, 777-789.
- (13) Pagliaro, M.; Campestrini, S.; Ciriminna, R. *Chem. Soc. Rev.* **2005**, *34*, 837-845.
- (14) Severin, K. *Curr. Org. Chem.* **2006**, *10*, 217-224.
- (15) Dragutan, V.; Dragutan, I.; Delaude, L.; Demonceau, A. *Coord. Chem. Rev.* **2007**, *251*, 765-794.
- (16) *Handbook of Metathesis*; Grubbs, R. H., Ed.; Wiley-VHC: Weinheim, 2003.
- (17) Aagaard, O. M.; Meier, R. J.; Buda, F. *J. Am. Chem. Soc.* **1998**, *120*, 7174-7182.
- (18) Adlhart, C.; Chen, P. *Angew. Chem. Int. Ed.* **2002**, *41*, 4484-4487.
- (19) Cavallo, L. *J. Am. Chem. Soc.* **2002**, *124*, 8965-8973.
- (20) Vyboishchikov, S. F.; Bühl, M.; Thiel, W. *Chem. Eur. J.* **2002**, *8*, 3962-3975.
- (21) Fomine, S.; Vargas, S. M.; Tlenkopatchev, M. A. *Organometallics* **2003**, *22*, 93-99.
- (22) Adlhart, C.; Chen, P. *J. Am. Chem. Soc.* **2004**, *126*, 3496-3510.
- (23) Suresh, C. H.; Koga, N. *Organometallics* **2004**, *23*, 76-80.
- (24) Benitez, D.; Goddard III, W. A. *J. Am. Chem. Soc.* **2005**, *127*, 12218-12219.
- (25) Straub, B. F. *Angew. Chem. Int. Ed.* **2005**, *44*, 5974-5978.
- (26) Suresh, C. H.; Baik, M.-H. *Dalton Trans.* **2005**, 2982-2984.
- (27) Correa, A.; Cavallo, L. *J. Am. Chem. Soc.* **2006**, *128*, 13352-13353.
- (28) Lord, R. L.; Wang, H.; Vieweger, M.; Baik, M.-H. *J. Organomet. Chem.* **2006**, *691*, 5505-5512.
- (29) van Rensburg, W. J.; Steynberg, P. J.; Kirk, M. M.; Meyer, W. H.; Forman, G. S. *J. Organomet. Chem.* **2006**, *691*, 5312-5325.
- (30) Fomine, S.; Tlenkopatchev, M. A. *Organometallics* **2007**, *26*, 4491-4497.
- (31) Krapp, A.; Pandey, K. K.; Frenking, G. *J. Am. Chem. Soc.* **2007**, *129*, 7596-7610.
- (32) Webster, C. E. *J. Am. Chem. Soc.* **2007**, *129*, 7490-7491.
- (33) Kunkely, H.; Vogler, A. *Inorg. Chim. Acta* **2001**, *325*, 179-181.
- (34) Wong, C. Y.; Chan, M. C. W.; Zhu, N.; Che, C. M. *Organometallics* **2004**, *23*, 2263-2272.
- (35) Delgado-Jaime, M. U.; Conrad, J. C.; Fogg, D. E.; Kennepohl, P. *Inorg. Chim. Acta* **2006**, *359*, 3042-3047.
- (36) Kunkely, H.; Vogler, A. *Inorg. Chem. Commun.* **2007**, *10*, 117-119.
- (37) Schwab, P.; Grubbs, R. H.; Ziller, J. W. *J. Am. Chem. Soc.* **1996**, *118*, 100-110.
- (38) Scholl, M.; Ding, S.; Lee, C. W.; Grubbs, R. H. *Org. Lett.* **1999**, *1*, 953-956.
- (39) Romero, P. E.; Piers, W. E.; McDonald, R. *Angew. Chem. Int. Ed.* **2004**, *43*, 6161-6165.

- (40) Carlson, R. G.; Gile, M. A.; Heppert, J. A.; Mason, M. H.; Powell, D. R.; Velde, D. V.; Vilain, J. M. *J. Am. Chem. Soc.* **2002**, *124*, 1580-1581.
- (41) Sanford, M. S.; Love, J. A.; Grubbs, R. H. *Organometallics* **2001**, *20*, 5314-5318.
- (42) Trnka, T. M.; Dias, E. L.; Day, M. W.; Grubbs, R. H. *Arkivoc* **2002**, *13*, 28-41.
- (43) Love, J. A.; Sanford, M. S.; Day, M. W.; Grubbs, R. H. *J. Am. Chem. Soc.* **2003**, *125*, 10103-10109.
- (44) Romero, P. E.; Piers, W. E. *J. Am. Chem. Soc.* **2005**, *127*, 5032-5033.
- (45) Webb, S. M. *Phys. Scr.* **2005**, *T115*, 1011-1014.
- (46) PeakFit4.12; SeaSolve Software Inc, 2003.
- (47) George, G. N.; EXAFSPAK; <http://ssrl.slac.stanford.edu/EXAFSPAK.html>, 2001.

CHAPTER 4: EDGE FEATURES*

4.1. Introduction

Phosphine ligands have played an important role in organometallic chemistry for decades (see also Section 1.3.1). Much of their success results from the predictability of their effect on the properties of a molecule.¹ Early work, largely by Tolman,²⁻⁴ aimed to quantify steric and electronic properties of phosphine ligands so that they could be ranked according to size and electron-donor ability. Despite their imperfections, these ordered series have been used quite successfully to design complexes with an optimised amount of electron donation or steric hindrance.

Although N-heterocyclic carbenes (NHCs) have been known since the 1960s,^{5,6} their widespread use only came about after the discovery of a stable NHC in 1991⁷ (see also Section 1.3.2). Since that discovery, employment of NHC ligands has progressively increased, particularly in the field of homogeneous catalysis.⁸ Because both phosphines and NHCs are neutral two-electron donors, NHCs have often replaced phosphine ligands in organometallic catalysts, usually resulting in favourable effects on activity.^{9,10} The desire to establish electronic and steric trends for a range of NHCs has been the impetus behind numerous studies of these properties. Two noteworthy conclusions came from the initial experimental and computational investigations: 1) NHCs are pure

* A version of this chapter has been published. Getty, K.; Delgado-Jaime, M. U.; Kennepohl, P., An Electronic Rationale for Observed Initiation Rates in Ruthenium-Mediated Olefin Metathesis: Charge Donation in Phosphine and N-Heterocyclic Carbene Ligands. *J. Am. Chem. Soc.* **2007**, *129*, 15774-15776.

σ -donors with negligible π -acceptor character¹¹⁻²¹ and 2) NHCs are stronger σ -donors than even the most basic phosphine ligands.^{22,23}

Several experimental measures are commonly used to evaluate the electronic properties of ligands; however, each of these is measuring a unique molecular property and careful analysis is required to determine the relevance and meaning of these quantities. The pK_a values of the conjugate acids of phosphine and NHC ligands suggest that NHCs are significantly more basic; for example, the experimentally-measured pK_a for IMe (1,3-dimethylimidazol-2-ylidene) is 23.0²⁴ whereas for PCy₃ (tricyclohexylphosphine) the pK_a is 9.7.²⁵ An uncertainty that arises when using pK_a values is that the interaction with the hard acid proton may be quite different from that with a soft acid transition metal, such as Ru(II). Table 4.1 lists some of the other experimental data that indirectly support the concept that NHCs donate more electron density to the metal centre than phosphine ligands. The values are for complexes where L = PCy₃ or H₂IMes (1,3-bis(2,4,6-trimethylphenyl)-4,5-dihydroimidazol-2-ylidene). Notably, the steric parameter (% V_{Bur}) is nearly the same for PCy₃ (26%) and H₂IMes (27%),²² therefore, observed differences are expected to be electronic in nature.

Table 4.1 Experimental data for complexes containing L = PCy₃ or L = H₂IMes

Measurement	L = PCy ₃	L = H ₂ IMes	Difference (PCy ₃ - H ₂ IMes)	Complex
Ru(II)/Ru(III) $E_{1/2}$ (V) ^a	0.585 ²⁶	0.447 ²⁶	0.138	Cl ₂ (L)(PCy ₃)Ru=CHPh
Ir(I)/Ir(III) $E_{1/2}$ (V) ^a	0.948 ²⁷	0.735 ²⁷	0.213	Ir(L)Cl(cod)
Relative BDE	10.5 ²⁸	16.8 ²⁸	-6.3	Cp*Ru(L)Cl
ν_{CO} (cm ⁻¹)	2056.4 ²	2051.5 ²²	4.9	Ni(L)(CO) ₃
ν_{CO}^{av} (cm ⁻¹)	2028.0 ²⁹	2024.6 ²³	3.4	Ir(L)Cl(CO) ₂

^a Reduction potentials referenced to FcMe₈ ($E_{1/2}$ = -0.010 V vs. Ag/AgCl); measured in dichloromethane.^{26,27}

The reduction potentials ($E_{1/2}$) for ruthenium²⁶ and iridium²⁷ complexes exhibit a cathodic shift upon changing L from PCy₃ to H₂IMes (Table 4.1). This is evidence that the NHC-bound metal centres are more electron-rich; however, this analysis assumes there are no differences in bonding interactions with oxidation state changes. The relative bond dissociation energy (BDE) is greater for NHC-bound complexes (Table 4.1),²⁸ which implies that the M-NHC bond is stronger than the M-PR₃ bond. Accordingly, it has been proposed that the stronger bond is due to more σ -donation from H₂IMes than PCy₃; this interpretation neglects other bonding components that may contribute to the bond strength. When L is changed from PCy₃ to H₂IMes in nickel^{2,22} and iridium^{23,29} carbonyl complexes, the CO stretching frequencies (ν_{CO}) decrease (Table 4.1), indicating that the C-O bond is weaker. This result is taken as evidence that the NHC donates more electron density to the metal centre, which subsequently increases the metal-to-carbon back-bonding; a rationale that may be correct, but cannot be confirmed until all the contributions to bonding are determined.

Establishing trends for a series of NHCs has been limited by the small measurable differences for many common methods, such as ν_{CO} values.²³ Importantly, even the expected differences between trialkylphosphines and N-heterocyclic carbenes do not always correlate with reactivity; this is likely related to the limitations of measurements used to estimate electronic properties. Phosphine dissociation rates in mixed NHC-PR₃ complexes compared to bisphosphine complexes are notable examples of unexplained reactivity. If NHCs

are stronger σ -donors than PR_3 ligands, phosphine dissociation is expected to be faster when one phosphine in a bisphosphine complex is replaced with an NHC ligand. The opposite dissociation kinetics have been observed in Ru(II) ^{30,31} and more recently in Rh(I) ^{32,33} complexes.

The Ru(II) case is that of the Grubbs olefin metathesis catalysts with the formula: $\text{Cl}_2\text{L}(\text{PR}_3)\text{Ru}=\text{CHR}$ (Chart 4.1). The first-generation complex is a bisphosphine precatalyst³⁴ (**1**, $\text{L} = \text{PCy}_3$) whereas the second-generation precatalyst is a mixed NHC- PR_3 complex³⁵ (**2**, $\text{L} = \text{H}_2\text{IMes}$). The basis for the replacement of one phosphine with an NHC was that, being the stronger σ -donor, the NHC would increase the rate of initiation (phosphine dissociation) and further stabilise the coordinatively-unsaturated intermediates.^{15,36-39} The significant improvement in overall activity of **2** compared to **1** (Table 4.2)^{35,40} suggested that this rationale was reasonable; however, kinetic data indicate that complex **2** initiates two orders of magnitude slower than complex **1** (Table 4.2)^{30,31} for reasons that have remained elusive. It is the preference of complex **2** to bind olefin over phosphine that is responsible for its high activity (Table 4.2). In this study, we report the first experimentally-verifiable rationale for the initiation rate differences between **1** and **2**. Our proposed explanation is based on unexpected electronic differences between PR_3 and NHC ligation in these and related complexes (**1-14**; Chart 4.1).

Chart 4.1 List of complexes included in this study

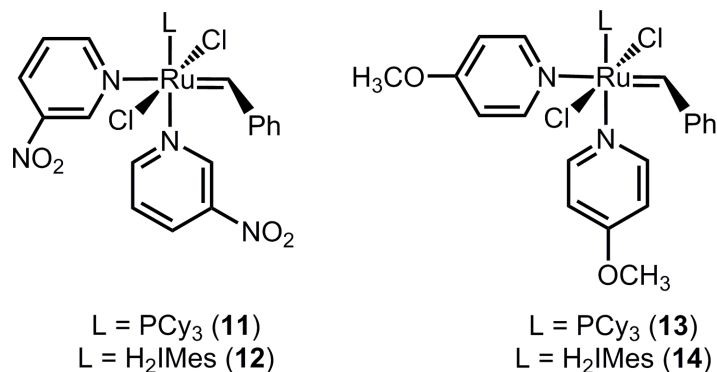
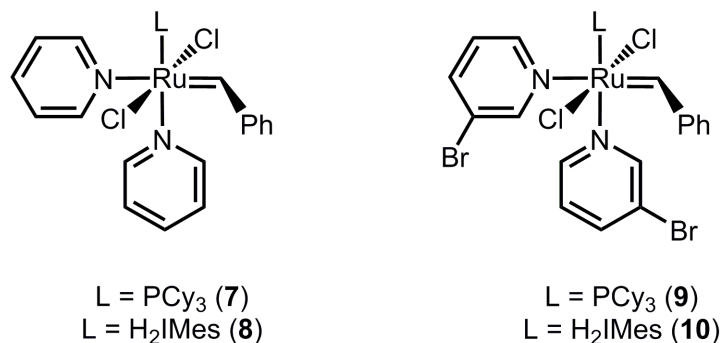
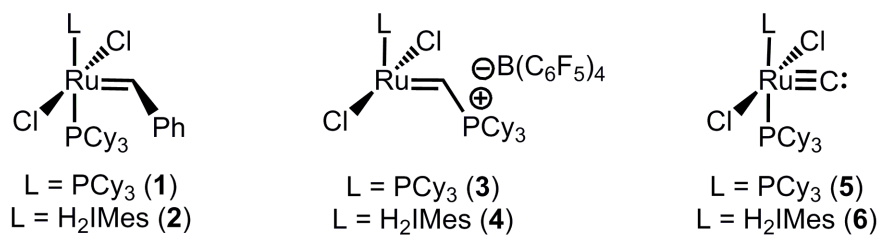


Table 4.2 Experimental olefin metathesis activity data for complexes **1** and **2**

Description	Measurement	1	2	Difference	Details
PCy ₃ dissociation rate	k_1 (s ⁻¹) ³¹	9.6	0.13	~ 2 orders of magnitude	per phosphine at 80°C
Relative rate constants	k_{rel} for RCM ⁴⁰	1	138	>2 orders of magnitude	RCM of 4,4-dicarboethoxy-2-methyl-1,6-heptadiene in C ₆ D ₆ at 40°C
	k_{rel} for ROMP ⁴⁰	1	27	>1 order of magnitude	ROMP of 1,5-cyclooctadiene in CD ₂ Cl ₂ at 25°C
Preference to bind PCy ₃ over olefin	k_{-1}/k_2 ³⁰	13000	1.25	>4 orders of magnitude	reaction with ethyl vinyl ether in toluene- <i>d</i> ₈ at 50°C

One approach to investigating the paradox of the observed kinetic differences between **1** and **2** is to study the metal centre. Metal K-edge X-ray absorption spectroscopy (XAS) is a useful probe of the electronic structure of a metal centre; therefore Ru K-edge XAS should provide information about the nature of the bonding in these complexes. In the near-edge region of the Ru K-edge XAS spectrum, two important features of relevance to ligand effects on the metal centre are expected (see also Section 1.4.2). First, pre-edge features corresponding to bound-state transitions are observed; these have been assigned as Ru $4d \leftarrow 1s$ transitions (see Chapter 3).⁴¹ Second, the predominant feature is an intense edge jump attributable to ionisation of Ru 1s electrons (Ru $\infty \leftarrow 1s$).^{42,43} Importantly, the energy of this metal 1s ionisation (IE_{1s}) is sensitive to the overall isotropic charge distribution at the metal centre; therefore, it is a good measure of the charge at the ruthenium centre (q_{Ru})⁴²⁻⁴⁶ and, consequently, of the net donor properties of the ligands surrounding the metal centre.⁴⁵⁻⁴⁸ Our initial studies indicated unexpected differences in the Ru K-edge XAS spectra for complexes **1** and **2**, and, as detailed below, we have explored this apparent inconsistency further.

4.2. Results and Discussion

Figure 4.1 shows the Ru K-edge XAS near-edge spectra for complexes **1** and **2**. The data were fit with a cumulative Gaussian/Lorentzian edge feature and a single Voigt pre-edge feature; these fits are also shown in dashed and dotted lines, respectively. The overall features of the spectra are quite similar, as expected, due to the structural similarities of the complexes near the metal

centre; however, a clear difference can be seen in the energies of the edge feature. As confirmed by fitting the edge jump and analysing the second derivatives of the data (inset; Figure 4.1), $I E_{1s}$ is lower for **1** than for **2** by 0.8 eV (Table 4.3).[†] The observed energy difference is smaller than that observed for oxidation state changes (~ 2 eV),⁴⁹ but greater than the experimental error.[‡] This shift to higher energy suggests that the charge on the ruthenium centre is larger (more positive) for the NHC-bound complex than for the bisphosphine complex. This result appears to contradict the generally-accepted properties of these ligands because it implies, at least to a first approximation, that H₂IMes is donating less electron density than PCy₃ to the ruthenium centre.

[†] $I E_{1s}$ values are taken from the inflection point of the function that was fit to the rising edge in each spectrum.

[‡] The experimental error is ~ 0.2 eV based on run-to-run deviations. Energy calibrations to Ru foil were accurate within 0.1 eV.

Figure 4.1 Near-edge Ru K-edge XAS spectra, fits to the data, and second-derivatives of the data (inset) for complexes **1** (L = PCy₃) and **2** (L = H₂IMes)

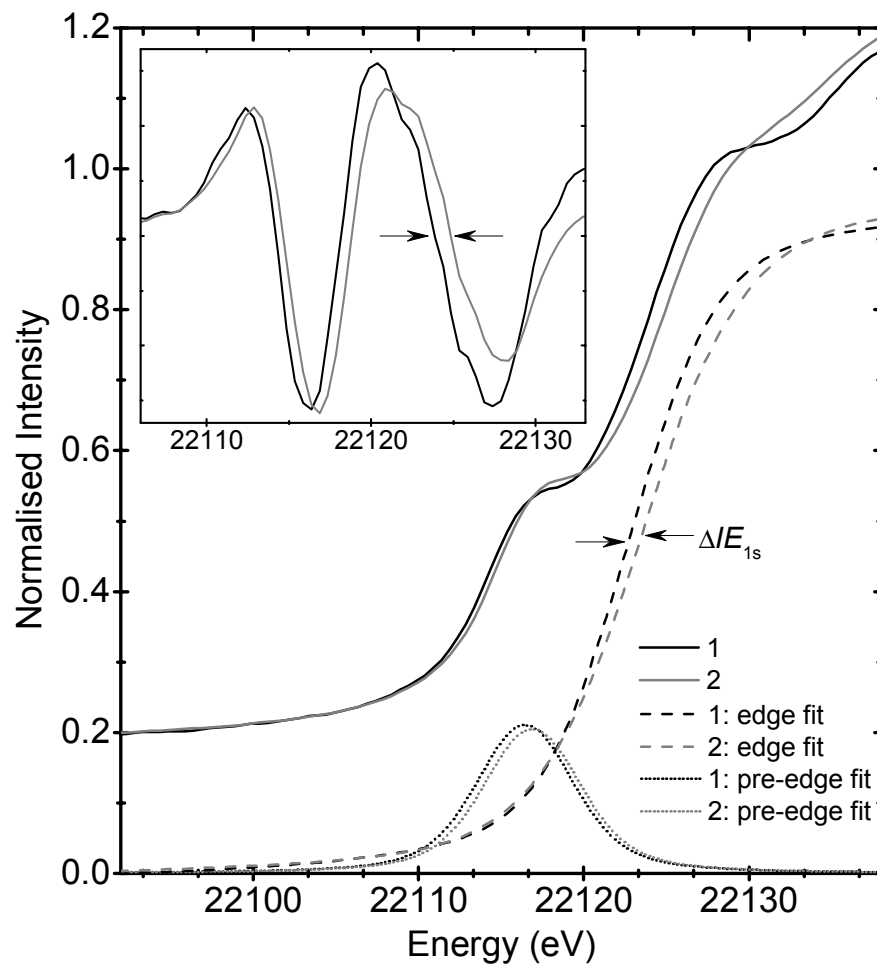


Table 4.3 Experimental pre-edge energies, ionisation energies, and DFT-calculated ruthenium charges for complexes **1-14**

Complex	Coordination Number	Pre-edge		Edge		MIK ^c		MDC ^d	
		Energy (eV)	Δ Energy ^b (eV)	IE_{1s} (eV)	ΔIE_{1s} ^b (eV)	q_{Ru}	Δq_{Ru} ^b	q_{Ru}	Δq_{Ru} ^b
1	5	22116.4	+0.5	22122.7	+0.8	0.36	+0.27	1.35	+0.26
2	5	22116.9		22123.5		0.63		1.61	
3^a	4	22117.1	+0.5	22122.7	+1.0	0.54	+0.31	1.79	+0.35
4^a	4	22117.5		22123.7		0.85		2.14	
5	5	22118.4	+0.4	22123.4	+0.8				
6	5	22118.8		22124.2					
7	6	22117.7	-0.2	22123.3	+0.2				
8	6	22117.5		22123.5					
9	6	22117.6	-0.1	22122.9	+0.4	0.83	+0.24	1.62	+0.21
10	6	22117.5		22123.3		1.07		1.83	
11	6	22117.6	-0.2	22123.1	+0.2				
12	6	22117.4		22123.3					
13	6	22117.5	-0.1	22123.2	+0.1				
14	6	22117.4		22123.3					

^a The edge features for complexes **3** and **4** were broader than for other complexes; thus, constraints on the edge widths were used. See Section 3.4.5 for additional details.

^b Differences defined as $\Delta X = X^{L = H2IMes} - X^{L = PCy3}$

^c MIK = Mulliken charge decomposition from DFT calculations (see Appendix 2)

^d MDC = Multipole Derived Charges including quadrupole contributions from DFT calculations (see Appendix 2)

To further investigate this effect, we compared IE_{1s} for three related classes of ruthenium complexes (Chart 4.1): the four-coordinate Piers phosphonium alkylidenes⁵⁰ (**3,4**; Figure 4.2), the five-coordinate Heppert carbides (**5,6**; Figure 4.3) and the six-coordinate bipyridine compounds^{51,52} (**7-14**; Figures 4.4 to 4.7). In each case, ΔIE_{1s} is positive with an average value of +0.5 eV over this series of fourteen complexes. The magnitude of ΔIE_{1s} decreases with increasing coordination number (Table 4.3), which implies that the other ligands mediate the effect through charge redistribution. Nevertheless, in every case, the result is the same: the metal centre is more positively charged with NHC ligation.

Figure 4.2 Near-edge Ru K-edge XAS spectra for complexes **3** (L = PCy₃) and **4** (L = H₂IMes)

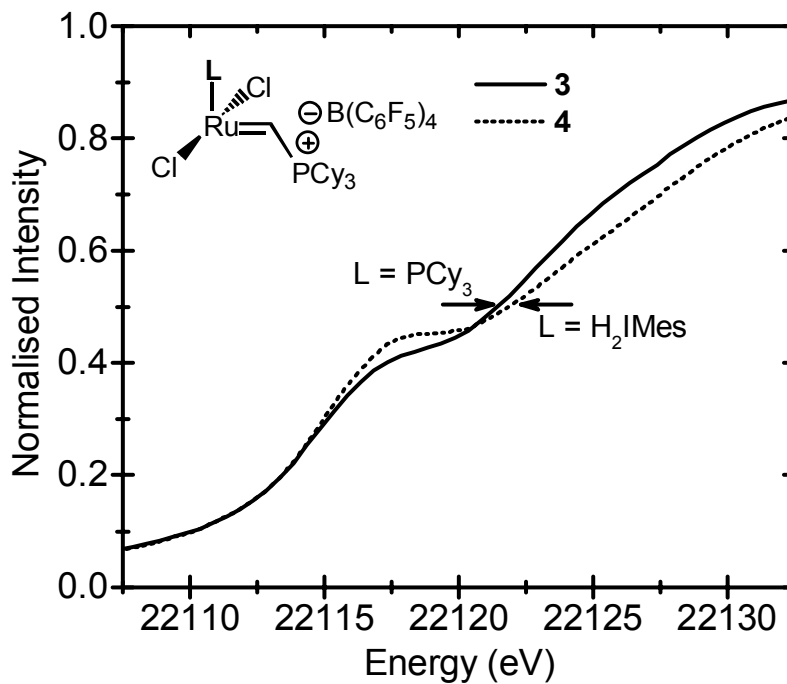


Figure 4.3 Near-edge Ru K-edge XAS spectra for complexes **5** (L = PCy₃) and **6** (L = H₂IMes)

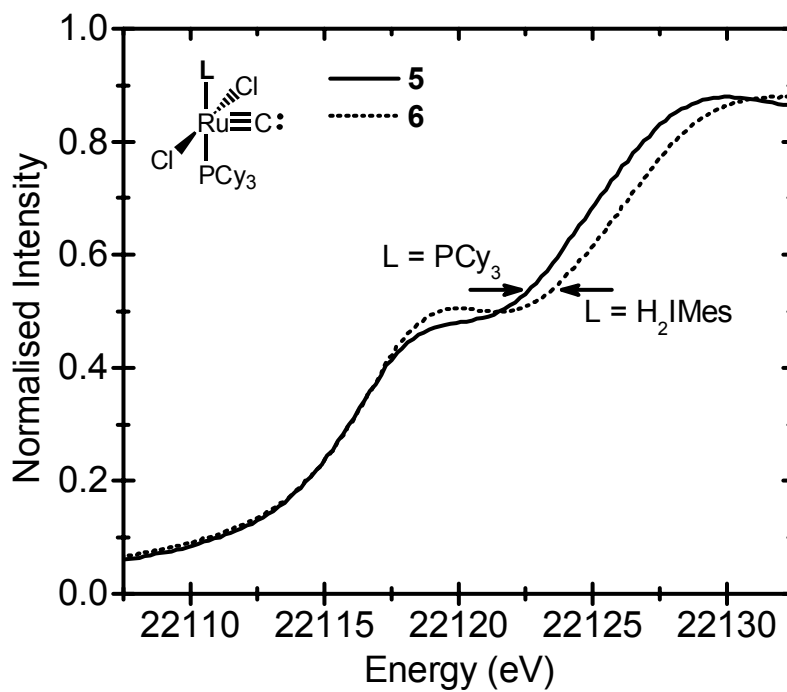


Figure 4.4 Near-edge Ru K-edge XAS spectra for complexes **7** (L = PCy₃) and **8** (L = H₂IMes)

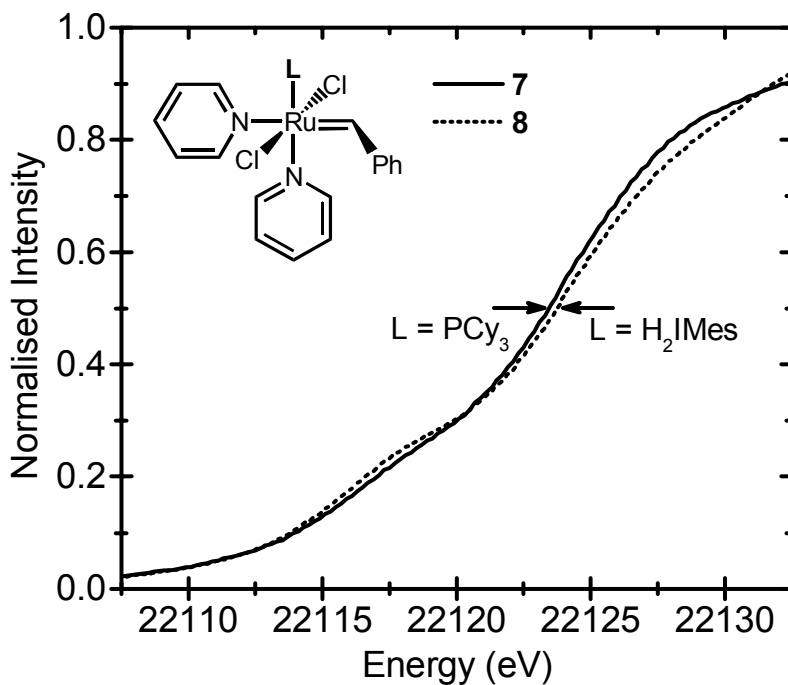


Figure 4.5 Near-edge Ru K-edge XAS spectra for complexes **9** (L = PCy₃) and **10** (L = H₂IMes)

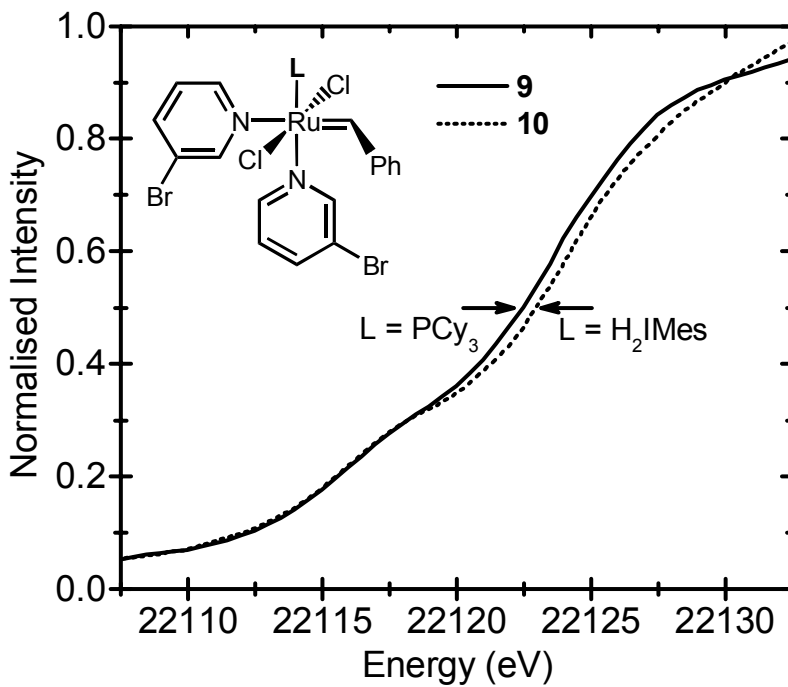


Figure 4.6 Near-edge Ru K-edge XAS spectra for complexes **11** (L = PCy₃) and **12** (L = H₂IMes)

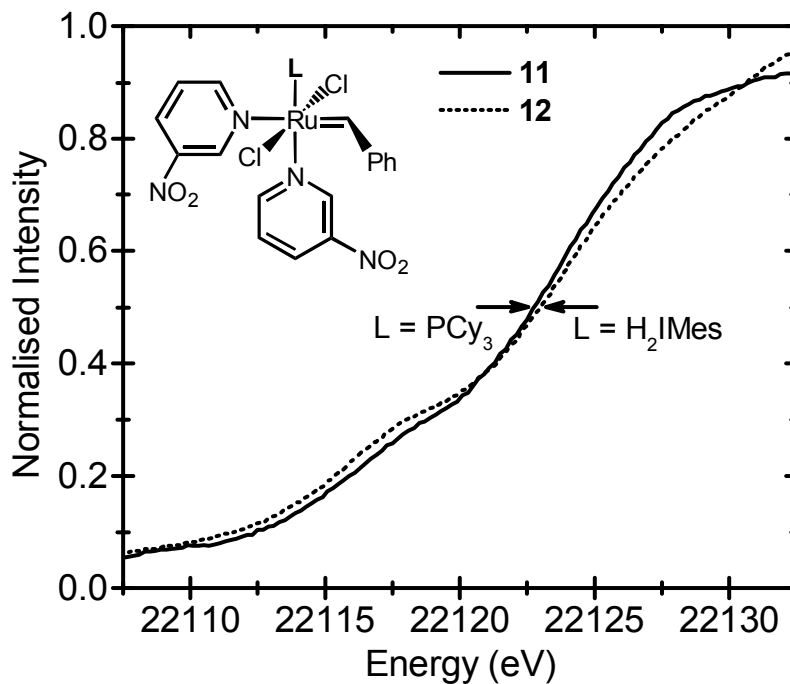
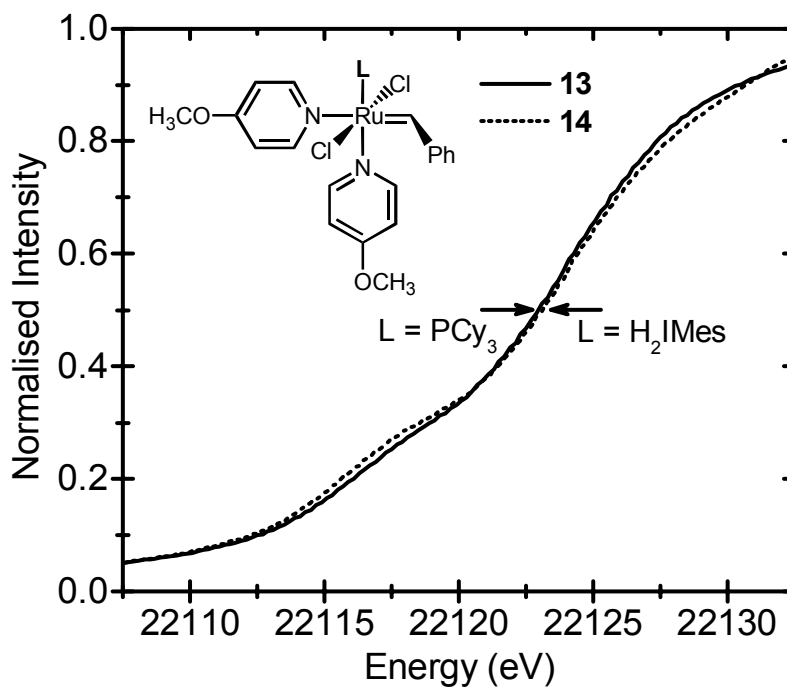


Figure 4.7 Near-edge Ru K-edge XAS spectra for complexes **13** (L = PCy₃) and **14** (L = H₂IMes)

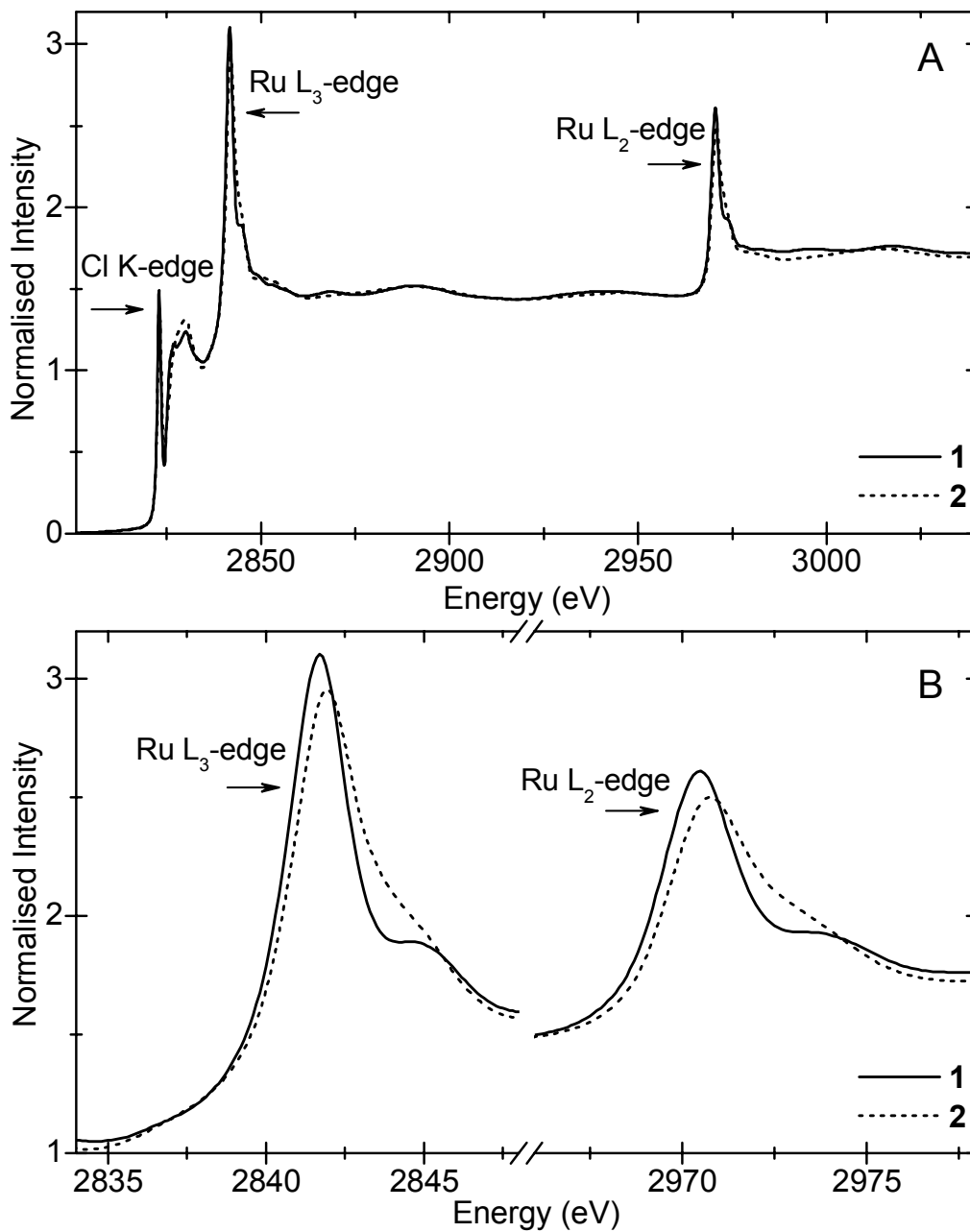


The Ru 4d←1s pre-edge features are also expected to shift to higher energy in response to increases in q_{Ru} .⁴⁴ This is clearly observed in **1,2** (+0.4 eV), **3,4** (+0.5 eV) and **5,6** (+0.4 eV) (Table 4.3).^{§41} Similarly, the energies of the electric-dipole-allowed Ru 4d←2p transitions in the Ru L_{2,3}-edge XAS spectra exhibit an analogous positive energy shift for **1,2** (Figure 4.8).^{**53} Both of these results are consistent with the assertion that the metal centre has less electron density in the NHC-bound complexes, which should be significant for understanding the relative reactivities of **1** and **2**.

[§] The energy positions of the pre-edges for complexes **7-14** are less reliable because they are extremely weak. In these cases, shifts are within experimental error.

^{**} The energy of Ru 4d←1s and Ru 4d←2p transitions are also affected by ligand field and multiplet effects. However, our DFT calculations indicate that the ligand field splitting changes by ~0.1 eV upon changing L. From this, we infer that the observed shifts in the energy of these transitions are dominated by differences in the energy of the core orbital(s).

Figure 4.8 Cl K-edge and Ru L_{2,3}-edge XAS spectra (A) and a rescaled view of the Ru L_{2,3}-edge XAS spectra (B) for complexes **1** and **2**^a



^a The spectra were normalised using a published procedure⁵³

In order to establish whether the unexpected experimental results are also observed theoretically and to explore the nature of the differences in charge donation, density functional calculations were performed and analysed by my

coworkers (see Appendix 2 for details). The findings are summarised here and greater detail can be found in reference 54.

In agreement with the experimental results, the calculated charge at the ruthenium centre is more positive for the complexes where $L = H_2IMes$ than where $L = PCy_3$ ($\Delta q_{Ru} > 0$; Table 4.3). This trend is consistent for the three pairs of complexes that were studied by DFT and also follows the experimental observation that the charge difference decreases with increasing coordination number (Δq_{Ru} : **3,4** > **1,2** > **9,10**).

Only slight differences in the entire near-edge region of the Ru K-edge spectra are observed for each pair of complexes where $L = PCy_3$ or H_2IMes (Figure 4.9). Additionally, there are only small changes in the Ru-Cl covalency for complexes **1** and **2**, as determined using Cl K-edge XAS.⁵³ The computational results are consistent with these experimental findings and reveal only minor alterations in the overall bonding of the complexes.⁵⁴ The largest differences in charge distribution between **1** and **2** occur in the electron occupancies of the Ru 4d and 5p orbitals (Table 4.4), which confirms that the differences are mainly due to changes in covalent interactions with the valence Ru 4d orbitals.^{††} These discrepancies arise from differences in the electron distribution at the metal centre, which are attributable to two distinct mechanisms: σ -donation and π -back-bonding.

^{††} Differences in the Ru 5s occupancy (+0.04) account for the remainder of the overall charge differential on the metal centre.

Figure 4.9 Extended energy region of Ru K-edge XAS spectra for complexes 1 to 14

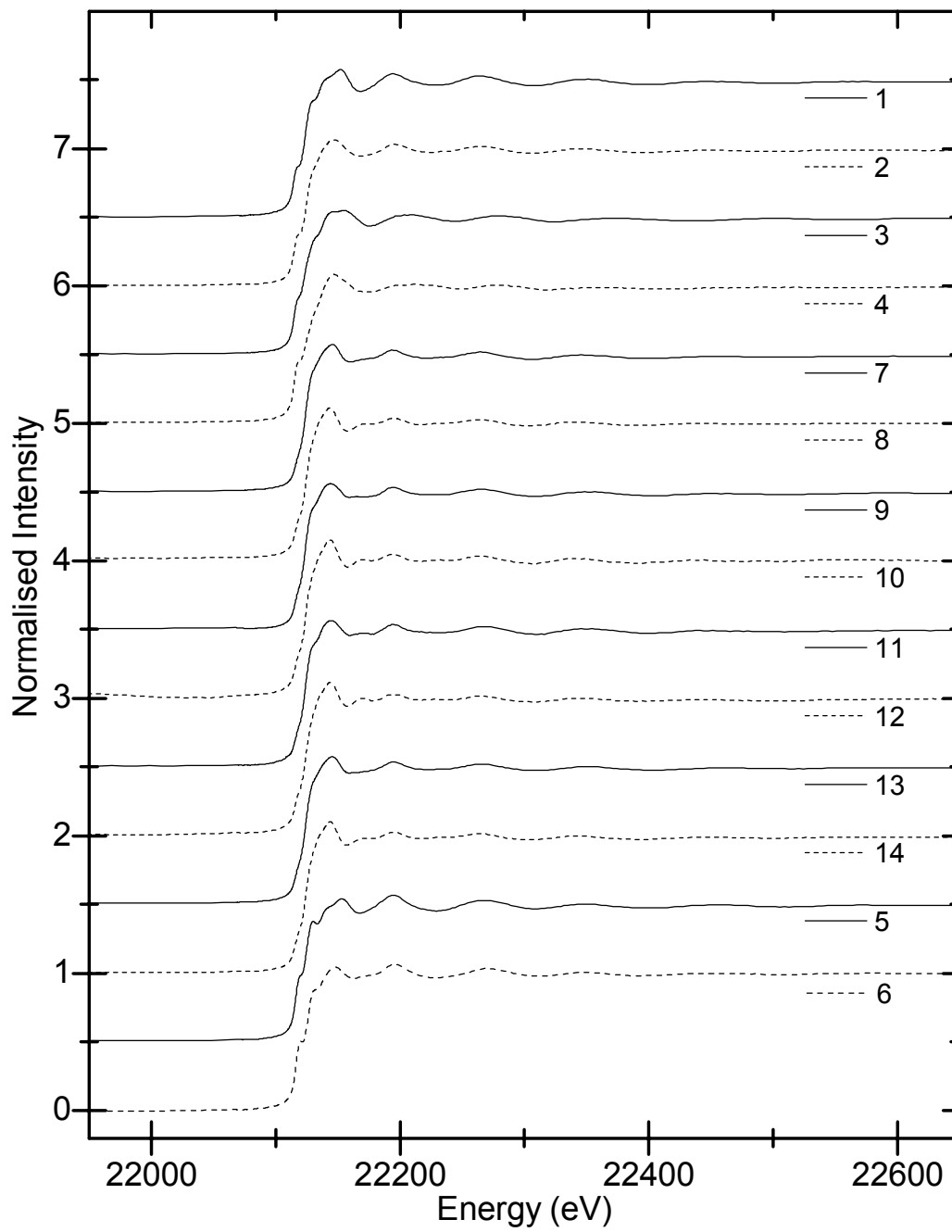


Table 4.4 Density functional computational results for complexes **1** and **2**^a

Complex	Ru 4d occupation	Ru 5p occupation	Charge donation from L to 4d _{σ*}	ΔCharge donation from L to 4d _{σ*}	π-acceptance from L	Δq _{Ru}
1	7.06e ⁻	0.47e ⁻	0.36e ⁻	0.16e ⁻	-	0.26e ⁻
2	6.94e ⁻	0.34e ⁻	0.20e ⁻		0.10e ⁻	

^a Results determined by a Mulliken-based decomposition of the relevant valence molecular orbitals

Electron delocalisation through σ -donor interactions from the ligands functions to increase electron density at the metal centre and this can be estimated from the charge donation into the two empty 4d_{σ*} orbitals. The calculated charge donation from L is substantially greater for PCy₃ in **1** (0.36e⁻) than for the NHC ring in **2** (0.20e⁻). In contrast to σ -donation, π -acceptance removes electron density from the metal centre. The orbital analysis indicates negligible π -contributions to Ru-PCy₃ bonding in both **1** and **2**;^{‡‡} however, a clear π -interaction is observed between the metal centre and the H₂IMes ligand in **2**. The interaction of the Ru-NHC π^* -orbital accounts for a 0.1e⁻ shift in electron density from the ruthenium centre to the ligand. The removal of electron density from the ruthenium centre and the reduced σ -donation from the NHC in complex **2** account for essentially all of the calculated Δq_{Ru} : 0.16e⁻ through a decrease in σ -donation and 0.10e⁻ due to π -back-bonding (Table 4.3 and Table 4.4)

Recent studies indicate that the bonding in NHCs is more variable than originally thought (see also Section 1.3.2) with NHC ligands able to donate^{26,55-58} as well as accept^{56,58-67} π -electron density under certain conditions. The nature of

^{‡‡} The weak π -acceptor character reflects the energy of the empty P-C(σ^*) and P 3d orbitals, which are >1.5 eV higher than the NHC(π^*) orbital involved in π -back-bonding.

the π -interactions is expected to be highly dependent on the particular metal centre⁶⁴, which means NHC properties may not be translatable between different complex fragments. Theoretical studies have estimated that non-negligible π -acceptance contributes up to 30% of the M-NHC bond energy.^{62,64} Notably, computational investigations of bonding in M-NHC⁶³ and M-PR₃⁶⁸ complexes have shown that electrostatic rather than covalent interactions are the major contributors to M-L bond strength for both phosphines and NHCs. These conclusions indicate that bond strength is not necessarily an indication of electron donor character. Taken together, these results and our experimental and computational findings, suggest that NHC ligands may bind more strongly to the ruthenium centre,^{4,22} but donate less charge to the metal than phosphine ligands.

The fact that there is greater charge delocalisation in the first-generation precatalyst, and that NHC ligation results in a more electron-deficient metal centre, should have implications regarding the relative reactivity of **1** and **2**. We propose that our results provide a compelling rationale for the experimentally-observed initiation rates in these precatalysts: the rate of phosphine dissociation is slower in **2** due to the reduced electron density of the ruthenium centre relative to **1**. We are currently exploring the possibility that this conclusion is applicable to other systems of importance in organometallic catalysis, such as the series of Rh(I) complexes that exhibit analogous phosphine dissociation kinetics.^{32,33}

4.3. Conclusions

Examination of the Ru K-edge XAS spectra of ruthenium complexes relevant to olefin metathesis has yielded an unexpected result: upon changing L from PR_3 to NHC, the metal centre becomes more electron-deficient. This is an apparent contradiction to the common understanding of these ligands, specifically, that NHCs donate more electron density to the metal centre than phosphines. Our findings may provide an explanation for another inconsistent observation: the phosphine dissociation rate of **2** is slower than **1** because the metal centre is more electron-deficient in **2**. Recent experimental and computational studies have shown that NHCs have flexible bonding character; indeed, the adaptable nature of NHCs may be responsible for their success in catalysis. We believe that our results are reconcilable with the existing data because different properties of the molecule are being measured in each case. The interpretation of various measures of ligand properties can be misleading when all of the components to bonding are not considered.

Our continuing efforts aim to further define the nature of charge delocalisation in these and related systems. Element-specific X-ray spectroscopies in conjunction with electronic structure calculations should provide a more complete understanding of the covalent contributions to bonding in complexes containing phosphine and N-heterocyclic carbene ligands.

4.4. Experimental

For complete experimental details, see Section 3.4.

4.5. References

- (1) Crabtree, R. H. *J. Organomet. Chem.* **2005**, *690*, 5451-5457.
- (2) Tolman, C. A. *J. Am. Chem. Soc.* **1970**, *92*, 2953-2956.
- (3) Tolman, C. A. *J. Am. Chem. Soc.* **1970**, *92*, 2956-2965.
- (4) Tolman, C. A. *Chem. Rev.* **1977**, *77*, 313-348.
- (5) Öfele, K. *J. Organomet. Chem.* **1968**, *12*, P42-P43.
- (6) Wanzlick, H.-W.; Schönherr, H. J. *Angew. Chem. Int. Ed. Engl.* **1968**, *7*, 141-142.
- (7) Arduengo III, A. J.; Harlow, R. L.; Kline, M. J. *J. Am. Chem. Soc.* **1991**, *113*, 361-363.
- (8) *N-Heterocyclic Carbenes in Transition Metal Catalysis*; Glorius, F., Ed.; Springer: Berlin, 2007.
- (9) Herrmann, W. A. *Angew. Chem. Int. Ed.* **2002**, *41*, 1291-1309.
- (10) Herrmann, W. A.; Schutz, J.; Frey, G. D.; Herdtweck, E. *Organometallics* **2006**, *25*, 2437-2448.
- (11) Green, J. C.; Scurr, R. G.; Arnold, P. L.; Geoffrey, F.; Cloke, N. *Chem. Commun.* **1997**, 1963-1964.
- (12) Bourissou, D.; Guerret, O.; Gabbai, F. P.; Bertrand, G. *Chem. Rev.* **2000**, *100*, 39-92.
- (13) Green, J. C.; Herbert, B. J. *Dalton Trans.* **2005**, 1214-1220.
- (14) Heinemann, C.; Müller, T.; Apeloig, Y.; Schwarz, H. *J. Am. Chem. Soc.* **1996**, *118*, 2023-2038.
- (15) Herrmann, W. A.; Köcher, C. *Angew. Chem. Int. Ed.* **1997**, *36*, 2162-2187.
- (16) Lee, M. T.; Hu, C. H. *Organometallics* **2004**, *23*, 976-983.
- (17) Boehme, C.; Frenking, G. *Organometallics* **1998**, *17*, 5801-5809.
- (18) Boehme, C.; Frenking, G. *J. Am. Chem. Soc.* **1996**, *118*, 2039-2046.
- (19) Niehues, M.; Erker, G.; Kehr, G.; Schwab, P.; Frohlich, R.; Blacque, O.; Berke, H. *Organometallics* **2002**, *21*, 2905-2911.
- (20) Termaten, A. T.; Schakel, M.; Ehlers, A. W.; Lutz, M.; Spek, A. L.; Lammertsma, K. *Chem. Eur. J.* **2003**, *9*, 3577-3582.
- (21) Frohlich, N.; Pidun, U.; Stahl, M.; Frenking, G. *Organometallics* **1997**, *16*, 442-448.
- (22) Dorta, R.; Stevens, E. D.; Scott, N. M.; Costabile, C.; Cavallo, L.; Hoff, C. D.; Nolan, S. P. *J. Am. Chem. Soc.* **2005**, *127*, 2485-2495.
- (23) Kelly III, R. A.; Clavier, H.; Giudice, S.; Scott, N. M.; Stevens, E. D.; Bordner, J.; Samardjiev, I.; Hoff, C. D.; Cavallo, L.; Nolan, S. P. *Organometallics* **2008**, *27*, 202-210.
- (24) Amyes, T. L.; Diver, S. T.; Richard, J. P.; Rivas, F. M.; Toth, K. *J. Am. Chem. Soc.* **2004**, *126*, 4366-4374.
- (25) Henderson, W. A.; Streuli, C. A. *J. Am. Chem. Soc.* **1960**, *82*, 5791-5794.
- (26) Süßner, M.; Plenio, H. *Chem. Commun.* **2005**, 5417-5419.
- (27) Leuthäuser, S.; Schwarz, D.; Plenio, H. *Chem. Eur. J.* **2007**, *13*, 7195-7203.
- (28) Hillier, A. C.; Sommer, W. J.; Yong, B. S.; Petersen, J. L.; Cavallo, L.; Nolan, S. P. *Organometallics* **2003**, *22*, 4322-4326.
- (29) Chen, W.; Esteruelas, M. A.; Martín, M.; Oliván, M.; Oro, L. A. *J. Organomet. Chem.* **1997**, *534*, 95-103.
- (30) Sanford, M. S.; Love, J. A.; Grubbs, R. H. *J. Am. Chem. Soc.* **2001**, *123*, 6543-6554.
- (31) Sanford, M. S.; Ullman, M.; Grubbs, R. H. *J. Am. Chem. Soc.* **2001**, *123*, 749-750.
- (32) Allen, D. P.; Crudden, C. M.; Calhoun, L. A.; Wang, R. *J. Organomet. Chem.* **2004**, *689*, 3203-3209.
- (33) Allen, D. P.; Crudden, C. M.; Calhoun, L. A.; Wang, R. Y.; Decken, A. *J. Organomet. Chem.* **2005**, *690*, 5736-5746.
- (34) Schwab, P.; Grubbs, R. H.; Ziller, J. W. *J. Am. Chem. Soc.* **1996**, *118*, 100-110.
- (35) Scholl, M.; Ding, S.; Lee, C. W.; Grubbs, R. H. *Org. Lett.* **1999**, *1*, 953-956.
- (36) Huang, J.; Schanz, H. J.; Stevens, E. D.; Nolan, S. P. *Organometallics* **1999**, *18*, 5375-5380.
- (37) Huang, J. K.; Schanz, H. J.; Stevens, E. D.; Nolan, S. P. *Organometallics* **1999**, *18*, 2370-2375.

- (38) Huang, J. K.; Stevens, E. D.; Nolan, S. P.; Petersen, J. L. *J. Am. Chem. Soc.* **1999**, *121*, 2674-2678.
- (39) Scholl, M.; Trnka, T. M.; Morgan, J. P.; Grubbs, R. H. *Tetrahedron Lett.* **1999**, *40*, 2247-2250.
- (40) Trnka, T. M.; Morgan, J. P.; Sanford, M. S.; Wilhelm, T. E.; Scholl, M.; Choi, T.-L.; Ding, S.; Day, M. W.; Grubbs, R. H. *J. Am. Chem. Soc.* **2003**, *125*, 2546-2558.
- (41) Getty, K.; Delgado-Jaime, M. U.; Kennepohl, P. *Inorg. Chim. Acta* **2008**, *361*, 1059-1065.
- (42) de Groot, F. *Chem. Rev.* **2001**, *101*, 1779-1808.
- (43) Tromp, M.; van Bokhoven, J. A.; van Strijdonck, G. P. F.; van Leeuwen, P. W. N. M.; Koningsberger, D. C.; Ramaker, D. E. *J. Am. Chem. Soc.* **2005**, *127*, 777-789.
- (44) Westre, T. E.; Kennepohl, P.; DeWitt, J. G.; Hedman, B.; Hodgson, K. O.; Solomon, E. I. *J. Am. Chem. Soc.* **1997**, *119*, 6297-6314.
- (45) Cramer, S. P.; Eccles, T. K.; Kutzler, F. W.; Hodgson, K. O.; Mortenson, L. E. *J. Am. Chem. Soc.* **1976**, *98*, 1287-1288.
- (46) Wang, C. M.; Cargill III, G. S.; Chan, H. M.; Harmer, M. P. *J. Am. Ceram. Soc.* **2002**, *85*, 2492-2498.
- (47) Hu, Y.; Corbett, M. C.; Fay, A. W.; Webber, J. A.; Hodgson, K. O.; Hedman, B.; Ribbe, M. W. *Proc. Natl. Acad. Sci. U.S.A.* **2006**, *103*, 17119-17124.
- (48) Hyung, K. W.; Kwon, T. K.; Jeon, Y. *Solid State Commun.* **2003**, *125*, 259-264.
- (49) Hwang, B. J.; Chen, C. H.; Sarma, L. S.; Chen, J. M.; Wang, G. R.; Tang, M. T.; Liu, D. G.; Lee, J. F. *J. Phys. Chem. B* **2006**, *110*, 6475-6482.
- (50) Romero, P. E.; Piers, W. E.; McDonald, R. *Angew. Chem. Int. Ed.* **2004**, *43*, 6161-6165.
- (51) Love, J. A.; Morgan, J. P.; Trnka, T. M.; Grubbs, R. H. *Angew. Chem. Int. Ed.* **2002**, *41*, 4035-4037.
- (52) Trnka, T. M.; Dias, E. L.; Day, M. W.; Grubbs, R. H. *Arkivoc* **2002**, *13*, 28-41.
- (53) Delgado-Jaime, M. U.; Conrad, J. C.; Fogg, D. E.; Kennepohl, P. *Inorg. Chim. Acta* **2006**, *359*, 3042-3047.
- (54) Getty, K.; Delgado-Jaime, M. U.; Kennepohl, P. *J. Am. Chem. Soc.* **2007**, *129*, 15774-15776.
- (55) Garrison, J. C.; Simons, R. S.; Kofron, W. G.; Tessier, C. A.; Youngs, W. J. *Chem. Commun.* **2001**, 1780-1781.
- (56) Cavallo, L.; Correa, A.; Costabile, C.; Jacobsen, H. *J. Organomet. Chem.* **2005**, *690*, 5407-5413.
- (57) Scott, N. M.; Dorta, R.; Stevens, E. D.; Correa, A.; Cavallo, L.; Nolan, S. P. *J. Am. Chem. Soc.* **2005**, *127*, 3516-3526.
- (58) Diez-Gonzalez, S.; Nolan, S. P. *Coord. Chem. Rev.* **2007**, *251*, 874-883.
- (59) Tulloch, A. A. D.; Danopoulos, A. A.; Kleinhenz, S.; Light, M. E.; Hursthouse, M. B.; Eastham, G. *Organometallics* **2001**, *20*, 2027-2031.
- (60) Tafipolsky, M.; Scherer, W.; Ofele, K.; Artus, G.; Pedersen, B.; Herrmann, W. A.; McGrady, G. S. *J. Am. Chem. Soc.* **2002**, *124*, 5865-5880.
- (61) Hu, X.; Tang, Y.; Gantzel, P.; Meyer, K. *Organometallics* **2003**, *22*, 612-614.
- (62) Hu, X.; Castro-Rodriguez, I.; Olsen, K.; Meyer, K. *Organometallics* **2004**, *23*, 755-764.
- (63) Nemcsok, D.; Wichmann, K.; Frenking, G. *Organometallics* **2004**, *23*, 3640-3646.
- (64) Jacobsen, H.; Correa, A.; Costabile, C.; Cavallo, L. *J. Organomet. Chem.* **2006**, *691*, 4350-4358.
- (65) Sanderson, M. D.; Kamplain, J. W.; Bielawski, C. W. *J. Am. Chem. Soc.* **2006**, *128*, 16514-16515.
- (66) Fantasia, S.; Petersen, J. L.; Jacobsen, H.; Cavallo, L.; Nolan, S. P. *Organometallics* **2007**, *26*, 5880-5889.
- (67) Khramov, D. M.; Lynch, V. M.; Bielawski, C. W. *Organometallics* **2007**, *26*, 6042-6049.
- (68) Frenking, G.; Wichmann, K.; Frohlich, N.; Grobe, J.; Golla, W.; Van, D. L.; Krebs, B.; Lage, M. *Organometallics* **2002**, *21*, 2921-2930.

CHAPTER 5: CONCLUSIONS AND RECOMMENDATIONS

Ruthenium K-edge X-ray absorption spectroscopy has been used to investigate fifteen organometallic ruthenium complexes of relevance to olefin metathesis. As part of the study, eight bispyridine ruthenium-benzylidene complexes have been synthesised. The unsubstituted and monosubstituted pyridine ligands in these complexes cover a wide range of electronic properties. Major differences corresponding to these electronic variations were not observed in the Ru K-edge XAS spectra, thereby suggesting that the ruthenium centre is relatively insensitive to these electronic differences. It would be very interesting to further examine this issue with ligand K-edge XAS spectra (namely, Cl K-edge, C K-edge, and P K-edge) of these complexes in order to determine whether any other ligands are affected by the electron-donating or withdrawing properties of the differently-substituted pyridine ligands. Additionally, synthesis of the analogous monopyridine ruthenium benzylidenes is possible for at least some of the complexes and would provide another interesting structural variation for further study.

The ruthenium centre was found to be sensitive to changes in the neutral donor ligand (L): the charge on the ruthenium centre becomes considerably more positive when $L = \text{PCy}_3$ (first generation) is replaced with $L = \text{H}_2\text{IMes}$ (second generation). This charge increase is observed in the Ru K-edge XAS spectrum as an increase in the ionisation energy of 1s electrons and indicates that the ruthenium centre has less electron density in the second-generation complexes. The implications of this unexpected result are significant for

understanding olefin metathesis catalysts as well as gaining insight into the nature of bonding in NHC and PR_3 complexes in the broader field of organometallic chemistry.

NHC ligands were initially considered pure σ -donors¹⁻¹¹; however, that concept has been increasingly challenged and is no longer the current view. Nevertheless, NHCs are still thought to generally be stronger electron donors than trialkylphosphines based on a variety of indirect experimental evidence.^{12,13} On the contrary, our Ru K-edge data in conjunction with density-functional calculations suggest that, for these ruthenium complexes, the NHC ligand is donating less σ -electron density than the PR_3 ligand and that the NHC is accepting significant π -back-donation. Our measurement of the charge on the metal centre is also an indirect measure of ligand donation, and we believe our results can be reconciled with other available data by including additional components to bonding in the interpretation, specifically, π -acceptance and electrostatic interactions.

Our findings appear to offer the first experimentally-verifiable rationale for the apparently inconsistent behaviour of the initiation rates of first- and second-generation Grubbs catalysts: the phosphine dissociation rate of **2** is slower than **1** because the metal centre is more electron-deficient in **2**. To further define the nature of charge delocalisation in these and related systems, ligand K-edge XAS analysis should be very informative. Additionally, experiments that can significantly improve the resolution of Ru K-edge XAS are currently being planned; these would allow verification of our results and may be sensitive

enough to observe electronic differences between more closely related ruthenium complexes, such as $L = H_2IMes$ and $L = IMes$. Furthermore, analogous XAS studies would be informative for systems with other metal centres; of initial interest are a series of rhodium(I) complexes from the group of Cathleen Crudden (Queen's University) that exhibit the same phosphine dissociation behaviour as ruthenium compounds **1** and **2**.^{14,15}

In order to extract all available information from Ru K-edge XAS spectra, the observable features in the XANES region must be assigned. Two main features are present: a pre-edge and a rising edge. The rising edge is known to correspond to ionisation of 1s electrons. The pre-edge was previously unassigned in the ruthenium spectrum and this work has led to the unambiguous assignment of the features as due to Ru $4d \leftarrow 1s$ transitions. The assignment is based on the sensitivity of the pre-edge features to geometry, which implicates these electric-dipole-forbidden transitions. Ru K-edge XAS should provide valuable information about reactive species in the ruthenium-catalysed olefin metathesis mechanism.

One such reactive species is the ruthenacyclobutane structure (see Appendix 1). The ruthenacycle (**15**) discovered by Piers and coworkers is an excellent candidate for study by XAS because, at low temperatures, it is formed in high purity and is stable for several hours. In collaboration with the Piers group, we are working toward sample preparation and XAS data acquisition for this complex. Various challenges have thus far prevented the achievement of

these tasks; nevertheless, we are confident that the methodology under development will be successful.

Another important species in the olefin metathesis mechanism is the four-coordinate active catalyst. Other members of our group have performed preliminary studies on trapping this species. In a related project, I have carried out some initial investigations into synthesis of precatalysts with small, photodissociable ligands (see Appendix 2). This exploration is only in the preliminary stages; however, if successful, these types of complexes may allow us to trap the four-coordinate intermediate.

Overall, the work in this thesis has shown that Ru K-edge XAS is a valuable tool for studying ruthenium complexes of relevance to olefin metathesis. We have gained insight into the previously unexplained behaviour of ruthenium olefin metathesis precatalysts and also contributed to the current understanding of NHC and PR_3 ligands. There are numerous promising directions for further study using Ru K-edge XAS and related techniques.

5.1. References

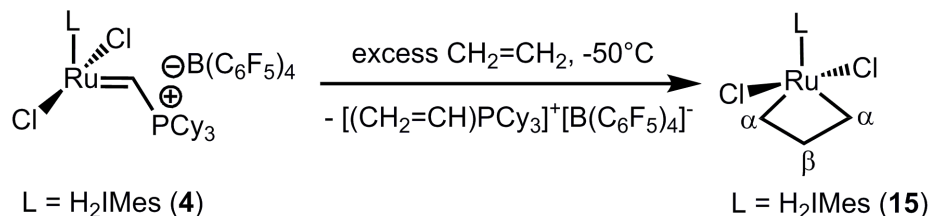
- (1) Green, J. C.; Scurr, R. G.; Arnold, P. L.; Geoffrey, F.; Cloke, N. *Chem. Commun.* **1997**, 1963-1964.
- (2) Bourissou, D.; Guerret, O.; Gabbai, F. P.; Bertrand, G. *Chem. Rev.* **2000**, *100*, 39-92.
- (3) Green, J. C.; Herbert, B. J. *Dalton Trans.* **2005**, 1214-1220.
- (4) Heinemann, C.; Muller, T.; Apeloig, Y.; Schwarz, H. *J. Am. Chem. Soc.* **1996**, *118*, 2023-2038.
- (5) Herrmann, W. A.; Köcher, C. *Angew. Chem. Int. Ed.* **1997**, *36*, 2162-2187.
- (6) Lee, M. T.; Hu, C. H. *Organometallics* **2004**, *23*, 976-983.
- (7) Boehme, C.; Frenking, G. *Organometallics* **1998**, *17*, 5801-5809.
- (8) Boehme, C.; Frenking, G. *J. Am. Chem. Soc.* **1996**, *118*, 2039-2046.
- (9) Niehues, M.; Erker, G.; Kehr, G.; Schwab, P.; Frohlich, R.; Blacque, O.; Berke, H. *Organometallics* **2002**, *21*, 2905-2911.
- (10) Termaten, A. T.; Schakel, M.; Ehlers, A. W.; Lutz, M.; Spek, A. L.; Lammertsma, K. *Chem. Eur. J.* **2003**, *9*, 3577-3582.
- (11) Frohlich, N.; Pidun, U.; Stahl, M.; Frenking, G. *Organometallics* **1997**, *16*, 442-448.
- (12) Dorta, R.; Stevens, E. D.; Scott, N. M.; Costabile, C.; Cavallo, L.; Hoff, C. D.; Nolan, S. P. *J. Am. Chem. Soc.* **2005**, *127*, 2485-2495.
- (13) Kelly III, R. A.; Clavier, H.; Giudice, S.; Scott, N. M.; Stevens, E. D.; Bordner, J.; Samardjiev, I.; Hoff, C. D.; Cavallo, L.; Nolan, S. P. *Organometallics* **2008**, *27*, 202-210.
- (14) Allen, D. P.; Crudden, C. M.; Calhoun, L. A.; Wang, R. *J. Organomet. Chem.* **2004**, *689*, 3203-3209.
- (15) Allen, D. P.; Crudden, C. M.; Calhoun, L. A.; Wang, R. Y.; Decken, A. *J. Organomet. Chem.* **2005**, *690*, 5736-5746.

APPENDIX 1. METALLACYCLOBUTANE STRUCTURE

Appendix 1.1. Introduction

Ruthenium-catalysed olefin metathesis (Scheme 1.2) proceeds through a metallacyclobutane structure (see also Section 1.2.11).¹ The first experimental observation of a ruthenacyclobutane was in 2005 by the Piers group.² They found that at -50°C the reaction (Scheme A1.1) of the second-generation Piers catalyst (**4**)³ with ethene gas generates a ruthenacyclobutane complex (**15**).² The product was identified and studied by multinuclear NMR spectroscopy. It was found to be C_{2v} symmetric and stable for several hours at temperatures below -40°C .²

Scheme A1.1 Synthesis of ruthenacyclobutane complex



Although it is not certain that this complex represents the metallacycle formed in standard ruthenium-catalysed olefin metathesis, it is the best-available model. Promising recent experimental studies have shown that **15** undergoes intermolecular olefin exchange, which is related to the metallacycle formation and cycloreversion steps required in the metathesis mechanism.⁴ Accordingly, information obtained through investigations of this complex should be relevant to understanding the mechanism and improving catalyst design. Because this species is only stable in cold or frozen solutions, not many traditional

characterisation techniques are available. NMR spectroscopy has been very useful in determining some of the properties of the metallacycle, but is inconclusive on several other issues.

X-ray absorption spectroscopy (see also Section 1.4) can be employed for frozen solutions at a wide range of temperatures and concentrations.⁵ This technique provides both electronic and geometric information about the species analysed. X-ray absorption near-edge structure (XANES) is indicative of coordination number and geometry as well as charge on the metal,⁵ whereas extended X-ray absorption fine structure (EXAFS) affords structural information including very accurate bond distances.⁶ Of particular interest for this complex is the experimental Ru-C_β distance (see Scheme A1.1), which could substantiate the proposal that M^{···}(C_α-C_β-C_α) agostic interactions stabilise the metallacyclobutane structure.^{4,7} Given the importance of this species in olefin metathesis, we, in collaboration with the Piers group, have endeavoured to characterise complex **15** using XAS. The first step toward this goal is to prepare suitable samples for data collection and then to collect data of sufficient quality for analysis; both of these tasks have proven to be quite challenging.

Appendix 1.2. Results and Discussion

A1.2.1. Synthesis in Dichloromethane

The syntheses of ruthenacyclobutane **15** and related species have typically been carried out in NMR tubes in temperature-controlled NMR probes. The ruthenium phosphonium alkylidenes are not soluble in most solvents; thus,

dichloromethane (usually dichloromethane- d_2) has always been the solvent in the syntheses of these ruthenacycles.^{2,4,8} In preparing samples for XAS, only a small volume (~ 200 μ L) is required, but it must be contained in a specific type of sample cell. Additionally, at least two samples should be examined by XAS to ensure consistency of the run time, and the data should be confirmed in at least two separate run times at a synchrotron facility.

With the experimental requirements in mind, a procedure was developed in collaboration with the Piers group. In a small Schlenk flask, a 10-15 mM solution of complex **4**^{*9} in dichloromethane is placed in a -78°C cold bath on a Schlenk line. Ethene gas is then admitted to the cold solution and a colour change occurs within ~30 minutes, indicating the presence of **15**. The reaction is allowed to proceed for at least an hour and then XAS sample cells are filled and quickly frozen in liquid nitrogen. Transferring the solution into XAS cells is challenging due to the temperature restrictions. I have tried placing the cells directly in the solution as well as filling the cells with a cold needle and syringe.

The prepared cells can be placed into the flask with the cold solution and then removed once full; however, the narrow opening on the top of the cells makes filling the cells a slow and laborious process. The large opening on the side of the cells is covered with polypropylene film affixed by tape, and the adhesive degrades in solution; thus, if a cell does not fill within about two minutes, the film loosens and the solution cannot be contained in the cell. A new

* The anion in complex **4** is tetrakis(pentafluorophenyl)borate ($B(C_6F_5)_4^-$); the phosphonium alkylidene cation with the commercially-available triflate anion (trifluoromethanesulfonate; OTf; $CF_3SO_3^-$) was sometimes used in the synthesis of **15**. Piers and coworkers have shown that the cation in **4** is unchanged when this anion is employed.

cell must be used, and some of the solution is lost in this process. Additionally, some of the adhesive is presumably dissolved in the solution with the potential to react with other components.

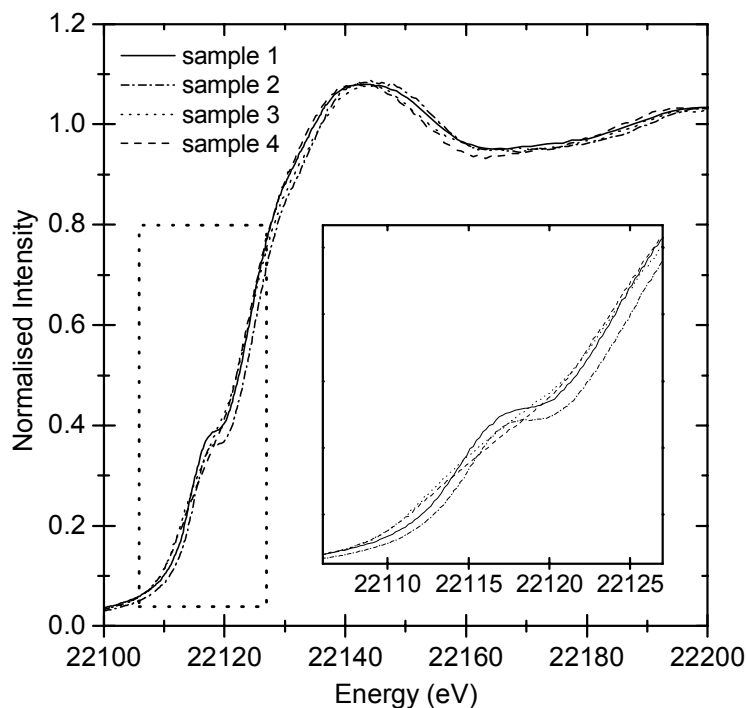
Alternatively, the cells can be filled via cold needle and syringe; however, most syringes do not work well at low temperatures making it difficult to withdraw and dispense the appropriate amount of solution. Furthermore, the transfer must be very fast to avoid degradation upon warming. A syringe constructed for low-temperature work may improve this procedure substantially. A micropipette with a tip small enough to fit in the hole of the XAS cell could also work well because only the tip would require cooling, which should allow the pipette to function normally.

The syntheses and characterisation of ruthenacyclobutanes have previously been carried out in NMR tubes and, largely, in the darkness of an NMR probe; therefore, light sensitivity has not been a concern. In the course of XAS experiments on frozen solutions of complex **15**, I observed that samples exposed to ambient light changed from a red-purple colour to orange even though they were frozen in liquid nitrogen. The light exposure was amplified because the samples were in a bowl shaped Dewar flask with a polished metallic finish, large opening, and shallow depth. This colour change is probably due to degradation of the sample[†] and can be prevented by maintaining samples in darkness; for example, by covering the Dewar flask with aluminum foil. This light sensitivity is also a concern during synthesis and sample preparation; thus, care must be taken to limit light exposure by covering the reaction vessel with

[†] Upon warming to room temperature, samples rapidly turn brown and then black.

aluminum foil and working in darkened conditions. Samples in reflective Dewar flasks are particularly prone to photodamage, so they should be covered as much as possible. It is suspected, based on sample colour and XAS spectra, that photodamage has been a recurrent problem during synthesis and sample preparation. The Ru K-edge XAS spectra of the first sweep for four different samples of **15** are shown in Figure A1.1. It is clear that the data are not similar enough to correspond to the same chemical species. Most notably, two spectra exhibit a substantial pre-edge feature whereas the remaining two spectra show only a low intensity pre-edge peak. It is currently unclear which samples, if any, contain pure complex **15**.

Figure A1.1 Ru K-edge XAS spectra of four separate samples of complex **15**



The reaction mixtures of samples prepared for XAS have not been verified by NMR spectroscopy because the preparation challenges were not fully

recognised until recently. Although it is possible for photodamage to take place after samples are made, it would be useful to collect an NMR spectrum to confirm that the reaction has reached completion with a pure product and that no degradation has occurred. Some uncertainty may remain due to the difficulty of keeping the solution cold during transfers. It would be most appropriate to collect NMR data on the remaining solution after the XAS cells have been prepared. All of these considerations are being incorporated in a new methodology that will allow for rapid and efficient sample preparation followed by adequate sample preservation for XAS analysis.

A1.2.2. Synthesis in Other Solvents

Our work on ruthenium-based complexes includes the investigation of the metal centre as well as the surrounding ligands via XAS. My coworker Mario Delgado-Jaime is continuing his study of the Cl K-edges in collaboration with the Fogg group.¹⁰ As such, it would be useful to study the ruthenacyclobutane structure at the Cl K-edge; this requires the use of a non-chlorinated solvent.

Although the starting ruthenium complex, **4**, is not soluble in toluene or ether, it was suggested by Edwin van der Eide of the Piers group that the ruthenacycle product, **15**, might be soluble in one of these solvents, which could drive the reaction forward. Both toluene and ether can also be used at the low temperatures required for synthesis, so the reaction was attempted, first in toluene and then in ether. Neither of these was successful because complex **4** is completely insoluble in these solvents and the presence of large amounts of ethene was not sufficient to force the reaction. The toluene reaction was

monitored by NMR spectroscopy and showed very little change over time, and even at room temperature.

Dibromomethane is expected to have similar solubilising properties as dichloromethane.^{‡11} This solvent has a very high density (2.5 g/mL) and a melting point of -52.5°C.¹¹ Complex **4** is indeed soluble in dibromomethane and the synthesis of complex **15** was carried out in a similar fashion to that in dichloromethane. An analogous colour change was observed and likely indicates the formation of **15**; however, this product has not been characterised by NMR spectroscopy due to time constraints and a lack of deuterated solvent. This characterisation is necessary to ensure the formation and purity of the desired product. Interestingly, it was noted that when the solution is warmed to room temperature, colour changes due to decomposition occur much slower than when dichloromethane is the solvent.

It is essential that the goal of using a non-chlorinated solvent for this reaction is achieved. XAS is an extremely sensitive technique and even minor chlorine contamination in the solvent could alter the data. To test this concern, Cl K-edge XAS spectra of a pure sample of dibromomethane were collected; preliminary analysis indicates that the solvent is free of chlorine. The Cl K-edge spectra were then collected for samples of **15** in dibromomethane, however, these data appear to be of poor quality due to diffraction and have not been analysed.

[‡] The dipole moments (μ) and dielectric constants (ϵ_r) are very similar for dichloromethane ($\mu = 1.60$ D; $\epsilon_r = 8.93$) and dibromomethane ($\mu = 1.43$ D; $\epsilon_r = 7.77$) compared to, for example, toluene ($\mu = 0.38$ D; $\epsilon_r = 2.38$).

A1.2.3. Photodegradation in the X-ray Beam

Despite the obvious photodegradation in ambient light, samples of the ruthenacyclobutane do not appear to degrade rapidly when exposed to hard X-rays.[§] This observation is based on visual inspection of the colour change, which can be seen on samples after the XAS experiment and on the XAS data, which exhibit only slight differences from sweep-to-sweep^{**}. Figure A1.2 depicts the Ru K-edge XAS spectra of consecutive sweeps at the same position on a sample of **15**. The inset is an expanded view of the pre-edge region in which a progressive change with increasing X-ray exposure time is apparent. By contrast, no significant change in the EXAFS region is visually observable as illustrated in Figure A1.3.

[§] Because of the challenging sample preparation for complex **15**, we are not actually certain that we have data for this species; therefore, its X-ray photosensitivity remains unclear.

^{**} Each sweep takes 20 to 35 minutes, depending on the collection set-up. For some experiments, the sample is protected from the X-ray beam whenever data collection is not occurring.

Figure A1.2 XANES region of the Ru K-edge XAS spectra of complex **15** for six consecutive sweeps with pre-edge feature expanded (inset)

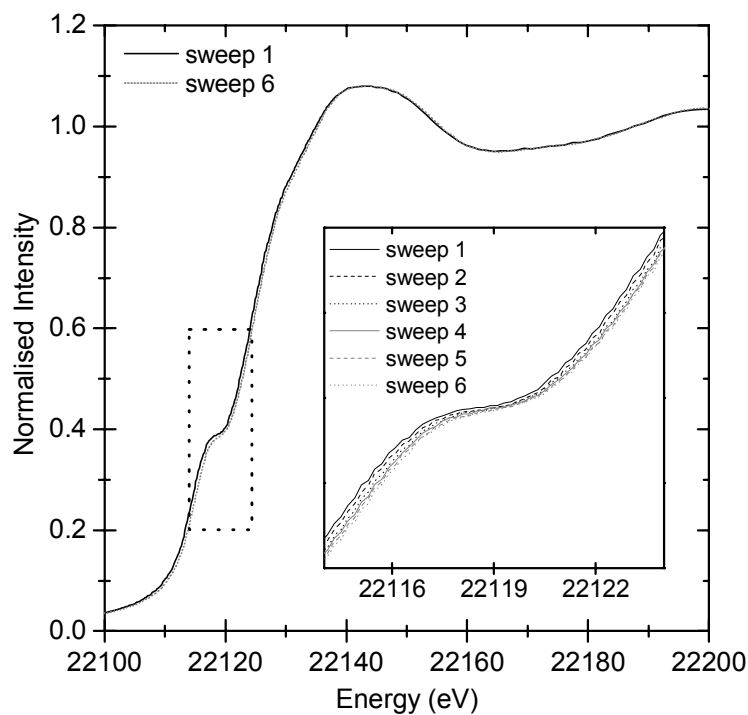
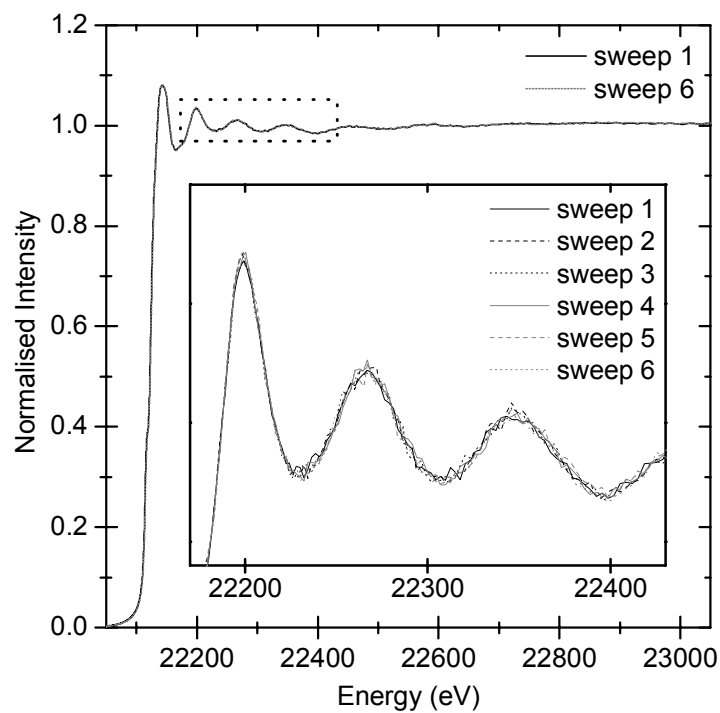


Figure A1.3 EXAFS region of the Ru K-edge XAS spectra of complex **15** for six consecutive sweeps with oscillations expanded (inset)



Several sweeps of a solution sample are required to ensure that the averaged spectra will have sufficient quality for analysis. When photodegradation is occurring in the X-ray beam, only one, or possibly two, sweeps of a particular spot on the sample can be averaged together. In order to obtain a sufficient number of sweeps, data must be acquired for several spots on the same sample and possibly for more than one sample. As a result of the difficulties with sample preparation and photodegradation, we have not yet successfully collected data sufficient for the analysis of the ruthenacyclobutane (**15**) XAS spectra.

Appendix 1.3. Conclusions

The ruthenacyclobutane complex formed at low temperature from the reaction of Piers phosphonium alkylidene and ethene is of significance to the ruthenium-catalysed olefin metathesis mechanism. XAS is one of few characterisation techniques suitable for further analysis of this complex; however, the synthesis and XAS sample preparation are complicated by the temperature and light sensitivity of **15**. Additionally, photodegradation in the X-ray beam renders more than two consecutive sweeps unfit for analysis. From these preliminary investigations, it is feasible that, with proper attention to these challenges, suitable samples can be obtained and satisfactory XAS data can be acquired for the ruthenacyclobutane species.

Appendix 1.4. Experimental

A1.4.1. General Considerations

All storage and manipulations of compounds were carried out under an inert atmosphere of nitrogen using standard Schlenk line or glove box techniques.

A1.4.2. Materials

Dichloromethane, toluene, and ether were dried by passage through solvent purification columns. Ampoules of toluene- d_8 were purchased from Cambridge Isotope Laboratories and used as received. Dibromomethane was purchased from Sigma-Aldrich, degassed, and dried over 4 Å molecular sieves. Ethene gas was purchased from Praxair and used as received. Complex **4** was synthesised as described elsewhere³ and obtained from the Piers group.

A1.4.3. Representative Synthesis of Complex **15** in Dichloromethane

In a glove box, **4** (OTf⁻ anion; 21 mg; 0.023 mmol) was placed in a small Schlenk flask.^{††} 2 mL dichloromethane was added to form an 11 mM solution. A stir bar was added and the flask was sealed with a septum. The flask was connected to a Schlenk line and cooled in a CO₂/acetone bath (-78°C). The vacuum line was evacuated and purged with ethene gas twice. The flask containing a solution of **4** was opened to the flow of ethene gas while stirring. Under high pressure of ethene, the septum was pierced with a needle to allow

^{††} A round-bottom Schlenk flask can be used, especially if the cells are filled via syringe; however, a customised Schlenk flask with a narrow-tube shape allows for easier filling of the cells when they are placed directly in the flask, while also using a minimal amount of material.

the gas to flow through for ~5 minutes. The needle was removed and the flow of ethene gas reduced. The flask was covered with aluminum foil and left under low flow of ethene gas for ~75 minutes at -78°C . The colour changed from very light brown to dark red-purple within 30 minutes indicating the presence of **15**.

A1.4.4. Synthesis of Complex 15 in Dibromomethane

The synthesis was similar to that using dichloromethane except that the melting point of dibromomethane is -52°C ; hence, the experiment was performed in a CO_2 /acetonitrile bath (-42°C).[‡]

A1.4.5. XAS Sample Preparation of Complex 15

The pressure of ethene gas was increased and the septum removed from the Schlenk flask containing a cold solution of **15**. An XAS solution cell with polypropylene film covering the open window was pre-cooled in liquid nitrogen, placed in the solution, and agitated to promote filling through the hole on the top. Once the cell was filled or partially-filled, it was removed and immediately frozen in liquid nitrogen. If a cell did not fill quickly, the adhesive could be seen to detach and the cell was removed empty.

An alternate method for filling the XAS cells has been used and further development of this will likely improve the procedure. A 1-mL disposable syringe and needle were cooled in liquid nitrogen, allowed to warm slightly, and used to draw up a small amount of the cold solution of **15**. The solution was then injected into the opening of a cell and the cell was frozen in liquid nitrogen. This method

[‡] The dichloromethane reaction can also be performed at the higher temperature (-42°C).

has the advantage that it can be performed without removing the septum from the Schlenk flask; however, the function of the syringe is impaired at low temperatures.

Samples were stored and transported to the synchrotron facility in a Dewar container filled with liquid nitrogen. They remained frozen during sample changes and data acquisition. Because the samples are sensitive to ambient light, they were protected with aluminum foil as much as possible whenever they were out of the transport Dewar container.

A1.4.6. XAS Data Acquisition

Acquisition details are similar to those for solid samples as described in Section 3.4.4. Data were collected on beamlines 7-3 and 9-3.

A1.4.7. XAS Data Processing

Processing details are similar to those for solid samples as described in Section 3.4.5, except that fluorescence rather than transmission data are shown.

Appendix 1.5. References

- (1) *Handbook of Metathesis*; Grubbs, R. H., Ed.; Wiley-VHC: Weinheim, 2003.
- (2) Romero, P. E.; Piers, W. E. *J. Am. Chem. Soc.* **2005**, *127*, 5032-5033.
- (3) Romero, P. E.; Piers, W. E.; McDonald, R. *Angew. Chem. Int. Ed.* **2004**, *43*, 6161-6165.
- (4) Romero, P. E.; Piers, W. E. *J. Am. Chem. Soc.* **2007**, *129*, 1698-1704.
- (5) Penner-Hahn, J. E. *Coord. Chem. Rev.* **2005**, *249*, 161-177.
- (6) Zhang, H. H.; Hedman, B.; Hodgson, K. O. In *Inorganic Electronic Structure and Spectroscopy, Volume I: Methodology*; Solomon, E. I., Lever, A. B. P., Eds.; John Wiley & Sons: New York, 1999, p 513-554.
- (7) Suresh, C. H.; Baik, M.-H. *Dalton Trans.* **2005**, 2982-2984.
- (8) Wenzel, A. G.; Grubbs, R. H. *J. Am. Chem. Soc.* **2006**, *128*, 16048 -16049.
- (9) Dubberley, S. R.; Romero, P. E.; Piers, W. E.; McDonald, R.; Parvez, M. *Inorg. Chim. Acta* **2006**, *359*, 2658-2664.
- (10) Delgado-Jaime, M. U.; Conrad, J. C.; Fogg, D. E.; Kennepohl, P. *Inorg. Chim. Acta* **2006**, *359*, 3042-3047.
- (11) *Handbook of Chemistry and Physics*; 88 ed.; Lide, D. R., Ed.; CRC: Boca Raton, 2007.

APPENDIX 2. INVESTIGATIONS OF LOW-TEMPERATURE REACTIONS WITH CO

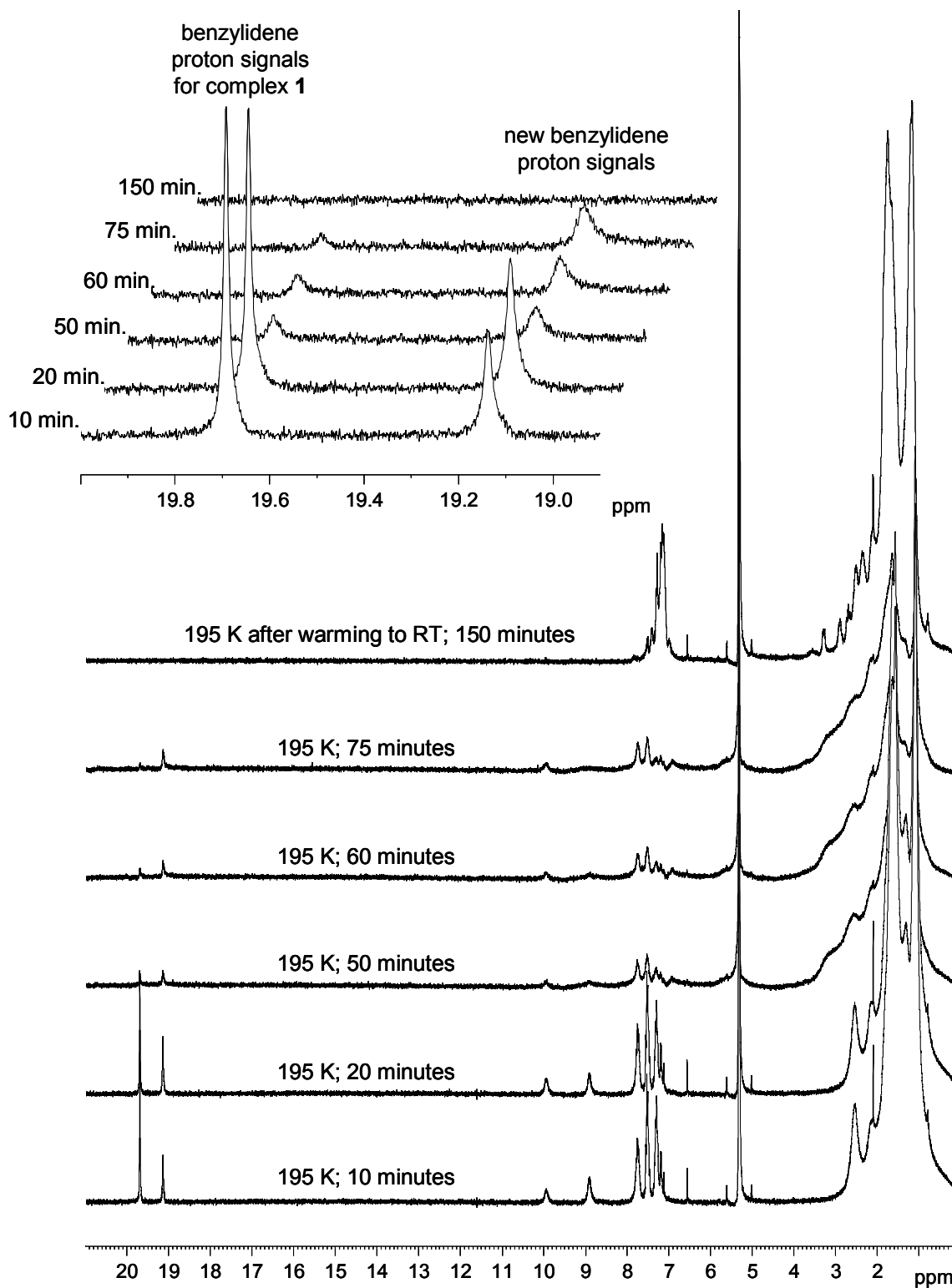
The synthesis of modified ruthenium benzylidenes through ligand substitution of small-molecules (NO, CO, and N_3^-) has been briefly explored. We expect that these ligands would be easily photodissociated, resulting in a precatalyst that can be photoactivated. These complexes could be useful for specialised applications of olefin-metathesis although our interest is primarily to find ways to trap reactive intermediates in the metathesis mechanism. For instance, the generation of a four-coordinate intermediate that is photochemically controlled could allow us to trap the intermediate or follow its production spectroscopically.

As an initial study, I have investigated the reaction of ruthenium-benzylidene complexes with carbon monoxide gas. We anticipated that exposure to CO at room temperature would cause decomposition of the benzylidene; thus, I have studied the addition of CO(g) to solutions of ruthenium complexes at 195 K. The reactions were performed under inert conditions in NMR tubes and followed with low- or variable-temperature NMR spectroscopy. Reactions with bispyridine ruthenium benzylidenes (**7** and **8**) led to rapid decomposition of the benzylidene fragment. Reactions with complex **1** have been somewhat more promising, although degradation is occurring quickly, even at constant temperature of 195 K.

In one experiment, CO gas was admitted to a cold solution of **1** (~3 mg) in dichloromethane (1 g). The NMR tube was quickly placed in a precooled NMR

probe and data acquisition began in the 0 to 30 ppm region for ^1H NMR. The position of the benzyldiene proton peak for complex **1** is 19.7 ppm at this temperature. By the time the first spectrum is recorded (approximately 10 minutes after CO was introduced to the tube), there is a second benzyldiene signal present at 19.1 ppm and that signal increases over time relative to the signal for **1** (Figure A2.1). However, both benzyldiene signals are decreasing, indicating rapid decomposition of the benzyldiene fragment. Other features in the spectrum are clearly changing, but at this point the products are not known and further study is required. The analogous reaction with complex **2** may generate more stable products due to the presence of an NHC ligand.

Figure A2.1 NMR spectra of reaction of complex **1** and CO(g) with an expanded view of the benzylidene region (inset)^a



^a NMR spectra were collected at 195 K in dichloromethane-*d*₂ at 300 MHz.

APPENDIX 3. COMPUTATIONAL DETAILS

All of the computations used in this thesis and their analyses were performed by Mario Ulises Delgado-Jaime or Pierre Kennepohl.

Geometry optimisations followed by ground state DFT calculations were performed using the Vosko-Wilk-Nusair local density approximation with exchange and correlation corrections from Becke¹ and Perdew^{2,3}, respectively (BP86). Slater-type orbitals⁴ (STOs) were used for the triple zeta basis set with an additional set of polarization functions (TZP). The $[\text{Ar}]^{18}3d^{10}$ core electrons of ruthenium were treated by the frozen core approximation.⁵ The calculations were carried out with the program package ADF2005.⁶⁻⁸ The run files corresponding to the ground state calculations can be found in the supplementary information of references 9 and 10.

Appendix 3.1. References

- (1) Becke, A. D. *Phys. Rev. A* **1988**, *38*, 3098-3100.
- (2) Perdew, J. P. *Phys. Rev. B* **1986**, *34*, 7406.
- (3) Perdew, J. P. *Phys. Rev. B* **1986**, *33*, 8822-8824.
- (4) Snijders, J. G.; Baerdens, E. J. *At. Data Nucl. Data Tables* **1982**, *26*, 483-509.
- (5) Baerdens, E. J.; Ellis, D. E.; Ros, P. *Chem. Phys.* **1973**, *2*, 41-51.
- (6) Fonseca Guerra, C.; Snijders, J. G.; te Velde, G.; Baerdens, E. J. *Theor. Chem. Acc.* **1998**, *99*, 391-403.
- (7) te Velde, G.; Bickelhaupt, F. M.; Baerends, E. J.; Fonseca Guerra, C.; van Gisbergen, S. J. A.; Snijders, J. G.; Ziegler, T. *J. Comp. Chem.* **2001**, *22*, 931-967.
- (8) ADF2005.01; Theoretical Chemistry, Vrije Universiteit: Amsterdam, The Netherlands, 2005.
- (9) Getty, K.; Delgado-Jaime, M. U.; Kennepohl, P. *Inorg. Chim. Acta* **2008**, *361*, 1059-1065.
- (10) Getty, K.; Delgado-Jaime, M. U.; Kennepohl, P. *J. Am. Chem. Soc.* **2007**, *129*, 15774-15776.